UC Berkeley
UC Berkeley Electronic Theses and Dissertations

Title
Interactions between Biomaterials and the Sclera: Implications on Myopia Progression

Permalink
https://escholarship.org/uc/item/7kn9v5cw

Author
Su, James

Publication Date
2009

Peer reviewed|Thesis/dissertation

eScholarship.org Powered by the California Digital Library
University of California

Interactions between Biomaterials and the Sclera:

Implications on Myopia Progression

by

James Su

A dissertation submitted in partial satisfaction of the

requirements for the degree of

Doctor of Philosophy

in

Vision Science

in the

Graduate Division

of the

University of California, Berkeley

Committee in charge:

Professor Christine F. Wildsoet, Chair

Professor Kevin E. Healy

Professor Xiaohua Gong

Fall 2009

Interactions between Biomaterials and the Sclera:

Implications on Myopia Progression

© 2009

by

James Su

University of California, Berkeley

Abstract

Interactions between Biomaterials and the Sclera:

Implications on Myopia Progression

by

James Su

Doctor of Philosophy in Vision Science

University of California, Berkeley

Professor Christine F. Wildsoet, Chair

Myopia prevalence has steadily climbed worldwide in recent decades with the most dramatic impact in East Asian countries. Treatments such as eyeglasses, contact lenses, and laser surgery for the refractive error are widely available, but none cures the underlying cause. In progressive high myopia, invasive surgical procedures using a scleral buckle for mechanical support are performed since the patient is at risk of becoming blind. The treatment outcome is highly dependent on the surgeon's skills and the patient's myopia progression rate, with limited choices in buckling materials. This dissertation, in four main studies, represents efforts made to control high myopia progression through the exploration and development of biomaterials that influence scleral growth.

First, mRNA expression levels of the chick scleral matrix metalloproteinases, tissue-inhibitor of matrix metalloproteinases, and transforming growth factor-beta 2 were assessed for temporal and defocus power effects. The first study elucidated the roles that these factors play in scleral growth regulation and suggested potential motifs that can be incorporated in future biomaterials design. Second, poly(vinyl-pyrrolidone) as injectable gels and poly(2-hydroxyethyl methacrylate) as solid strips were implanted in chicks to demonstrate the concept of posterior pole scleral reinforcements. This second study found that placing appropriate biomaterials at the posterior pole of the eye could directly influence scleral remodeling by interacting with the host cells. Both studies advanced the idea that scleral tissue remodeling could be potentially controlled by well-designed biomaterials.

These findings led to the exploration of biomimetic hydrogels comprising enzymatically-degradable semi-interpenetrating polymer networks (edsIPNs) to determine their biocompatibility and effects on the chick posterior eye wall. This third study demonstrated the feasibility of stimulating scleral growth by applying biomimetic injectable materials. Fourth, the muscarinic antagonist drug, atropine, was encapsulated within the edsIPNs and delivered to the chick eye posterior pole to evaluate the local effect of atropine release. This fourth study offered an alternative method of ocular drug delivery for treatment of myopia, with the potential to

elucidate the actual location of the inhibitive effect of atropine on myopia progression. In summary, this dissertation contributes to the design and use of biomaterials specific to myopia therapy and adds novel insights to scleral tissue engineering.

To my dearest great-grandmother

蘇楊金葉

Su Yang Jin Ye

For her everlasting love

TABLE OF CONTENTS

DEDICATION i
TABLE OF CONTENTS ii
LIST OF FIGURES iv
LIST OF TABLES v
LIST OF ABBREVIATIONS vi
ACKNOWLEDGEMENTS viii

CHAPTER I: INTRODUCTION – TOWARD A BIOINSPIRED THERAPY FOR MYOPIA

Abstract 1
1. Myopia & Eye Growth Regulation 2
2. History of Scleral Biomaterials 13
3. General Experimental Approach & Methods 14
4. Dissertation Outline 17

CHAPTER II: EFFECTS OF POLY(2-HYDROXYETHYL METHACRYLATE) AND POLY(VINYL-PYRROLIDONE) HYDROGEL IMPLANTS ON MYOPIC AND NORMAL CHICK SCLERA

Abstract 19
1. Introduction 20
2. Materials & Methods 22
3. Results 25
4. Discussion 37
5. Conclusion 40

CHAPTER III: DEFOCUS DURATION AND POWER DEPENDENCE OF CHICK SCLERAL MMP-2, MMP-13, TGF-β2, AND TIMP-2 MRNA EXPRESSION

Abstract 42
1. Introduction 43
2. Materials & Methods 44
3. Results 49
4. Discussion 57
5. Conclusion 58

CHAPTER IV: SCLERAL REINFORCEMENT THROUGH HOST TISSUE INTEGRATION WITH BIOMIMETIC ENZYMATICALLY-DEGRADABLE SEMI-INTERPENETRATING POLYMER NETWORK

Abstract 60
1. Introduction 61
2. Materials & Methods 62
3. Results 67
4. Discussion 74
5. Conclusion 76

CHAPTER V: POLYMERIC DRUG DELIVERY VEHICLES FOR THE DELIVERY OF ATROPINE AT POSTERIOR SCLERA FOR THE INHIBITION OF MYOPIA PROGRESSION

Abstract 77
1. Introduction 78
2. Materials & Methods 79
3. Results 82
4. Discussion 86
5. Conclusion 88

CHAPTER VI: DISSERTATION SUMMARY AND DISCUSSION

1. Major Findings of the Dissertation 89
2. Discussion 90
3. Future Work 91

BIBLIOGRAPHY 93

LIST OF FIGURES

Figure 1-1	Diagram illustrating the visually driven signaling pathway ……	3
Figure 1-2	Transmission electron microscopy image of chick fibrous sclera ……	8
Figure 1-3	Image of chick wearing a negative lens and illustration of LIM ……	15
Figure 1-4	Sample ultrasonography trace taken during measurement ……	15
Figure 1-5	Images of gold beads on scleral surface taken by X-ray ……	16
Figure 2-1	Mean scleral thickness, scleral cup depth, & axial length (pHEMA)……	27
Figure 2-2	Mean scleral thickness, scleral cup depth, & axial length (PVP) ……	29
Figure 2-3	Toluidine blue-stained sections of sclera with pHEMA implant ……	32
Figure 2-4I	Masson's Trichrome of posterior sclera with PVP injection ……	33
Figure 2-4II	Masson's Trichrome of posterior sclera with PVP + form deprivation …	34
Figure 2-4III	Masson's Trichrome of posterior sclera with PVP + (-)10 D lens ……	35
Figure 2-5	Mean scleral chondrocyte densities at posterior chick sclera ……	36
Figure 3-1	Choroidal thickness and axial lengths of different treatment groups ……	50
Figure 3-2	Diagrams of agarose gel electrophoresis and melt curve analysis ……	51
Figure 3-3	Threshold cycle values for all genes measured in scleral layers ……	52
Figure 3-4	Mean normalized expressions in the fibrous sclera ……	53
Figure 3-5	Mean normalized expressions in the cartilaginous sclera ……	55
Figure 3-6	Percent differences of mean normalized expressions of TGF-β2 ……	56
Figure 4-1	Cross-sectional and posterior view of chick eye and edsIPNs ……	61
Figure 4-2	Schematics illustrating edsIPNs reaction, structure, and SEM ……	63
Figure 4-3	Rheological measurements of edsIPN showing complex modulus ……	68
Figure 4-4	Phase contrast images of scleral fibroblasts on TCPS and edsIPN ……	69
Figure 4-5	Sample ultrasonography data taken on chick eye with edsIPN ……	71
Figure 4-6	H&E stain of scleras with edsIPN injection over 4 weeks ……	72
Figure 4-7	H&E and Masson's Trichrome stain of edsIPN on sclera at 4 wks ……	73
Figure 5-1	Release of atropine from preloaded edsIPN ……	82
Figure 5-2	Ultrasonography measurements of vitreous chamber depths ……	83
Figure 5-3	Ultrasonography measurements of SCD and AL ……	84
Figure 5-4	Interocular differences in SCD and AL ……	84
Figure 5-5	Mean endpoint refractions represented by box plot ……	85
Figure 5-6	Endpoint refraction versus vitreous chamber depth ……	86

LIST OF TABLES

Table 2-1 Treatments and animal numbers for each experiment in study …… 22
Table 2-2 Mean ocular dimensions ± standard error of pHEMA group …… 26
Table 2-3 Mean ocular dimensions ± standard error of PVP group …… 28
Table 2-4 Mean ocular dimensions ± standard error of PVP + lens groups …… 30
Table 2-5 Mean interocular difference data normalized to baseline values …… 31
Table 3-1 Experimental setup describing lens treatments and time groups …… 45
Table 3-2 Accession numbers of genes investigated with primer pairs …… 47
Table 4-1 Mean endpoint refraction ± standard error of edsIPN-injected eyes …… 72
Table 5-1 Treatment groups for *in vivo* assessment of atropine delivery …… 81
Table 5-2 Summary of endpoint refraction data for all treatment groups …… 85

LIST OF ABBREVIATIONS

AAc	acrylic acid
ANOVA	analysis of variance
AP	ammonium persulfate
ASTM	American Society for Testing and Materials
bp	base pairs
bsp	bone sialoprotein
cDNA	complementary deoxyribonucleic acid
CT	threshold cycle
D	diopters
DMEM	Dulbecco's modified Eagle medium
DNA	deoxyribonucleic acid
dNTP	deoxyribonucleotide triphosphate
E	efficiency of primer amplification
ECM	extracellular matrix
edsIPN	enzymatically degradable semi-interpenetrating polymer network
EG	ethylene glycol
EGDMA	ethylene glycol dimethacrylate
e-PTFE	expanded polytetrafluoroethylene
FITC	fluorescein isothiocyanate
H&E	hematoxylin and eosin
HEMA	2-hydroxyethyl methacrylate
IGF	insulin-like growth factor
IOP	intraocular pressure
LCST	lower critical solution temperature
MMP	matrix metalloproteinase
MNE	mean normalized expression
mRNA	messenger ribonucleic acid
NADPH	reduced nicotinamide adenine dinucleotide phosphate
NIPAAm	*N*-isopropylacrylamide
NMDA	*N*-methyl *D*-aspartate
NO	nitric oxide
NOS	nitric oxide synthase
OD	optical density
PBS	phosphate buffered saline
PCR	polymerase chain reaction
pHEMA	poly(2-hydroxyethyl methacrylate)
PVP	polyvinylpyrrolidone
RGD	arginine-glycine-aspartic acid
RNA	ribonucleic acid
RPE	retinal pigment epithelium
ScC	scleral chondrocytes
ScF	scleral fibroblasts
SE	standard error
sIPN	semi-interpenetrating polymer network

TCPS	tissue culture polystyrene
TEMED	*N,N,N',N'*-tetramethylenediamine
TGF-β	transforming growth factor-beta
TIMP	tissue inhibitor of metalloproteinase
VEGF	vascular endothelial growth factor
ZENK	*Z*if268, *E*gr-1, *N*GFI-A, and *K*rox-24

Acknowledgements

I would like to thank all of my PhD dissertation committee members, Professors Christine F. Wildsoet, Kevin E. Healy, and Xiaohua Gong for their continual guidance and support. I would like to thank all of my research collaborators, Drs. Elena Iomdina, Elena Tarutta, Jie Song, Brian Ward, Zhan Zhang, and Samuel T. Wall for providing research insights, advice, and assistance. I would like to thank Professor Vivian Choh, currently at the University of Waterloo, Canada, for providing me invaluable training and assistance at the start of my PhD research. I would like to thank all members of the Wildsoet Lab for working together and creating an unforgettable experience throughout my graduate study. I would like to thank all members of the Healy Lab for graciously providing research advice and support, and welcoming someone from a completely different field of study. I would like to thank all the endearing undergraduate mentees who have crossed paths with me at Cal, for they have always asked some of the most interesting questions. Finally, I would like to thank my whole family for their love and support. In particular, I am grateful to my dearest fiancée, Judy S. Hwang, for her unlimited love to the person that I am.

Chapter I

Introduction – Toward a Bioinspired Therapy for Myopia

Abstract

High axial myopia (defined as extreme near-sightedness of -6 diopters or worse) is the result of excessive eye elongation that leads to a significant mismatch between ocular axial length and focal power. Blinding complications, such as retinal detachment and glaucoma, combined with increasing prevalence worldwide, particularly in parts of Asia, have led myopia to become a significant public health problem for which optometrists simply prescribe optical appliances and refractive surgeries that treat the focusing error but not the axial elongation. Although efforts have been spent to elucidate the mechanisms behind myopia progression and develop treatment methods based on optical and pharmacological interventions, there has been little success in developing a treatment regime that effectively stops the elongation process. Previous research has shown that emmetropization, i.e. the reduction of refractive error during development, is an active and visually guided process, suggesting the utilization of visual cues as a local error signal to regulate eye growth that begins at the retina and ends at the sclera, the outer fibrous wall of the eye. As a treatment target, the sclera is favored over other ocular tissues due to its avascular nature and scarcity of sensory cells. These are significant advantages, particularly for the progressing myopes in the pediatric population. Recent animal studies that measured changes in scleral cells and proteins show tight regulation of scleral remodeling throughout induced myopia progression. A look into how the sclera remodels during axial elongation can significantly increase our understanding of the mechanisms underlying myopia and offer design parameters for potential bioinspired therapies that can take advantage of the native scleral response during myopia development.

1. Myopia & Eye Growth Regulation

Myopia is the most common refractive error and one of the top five major diseases causing blindness in humans (McCarty and Taylor, 2000). Despite the effectiveness of eyeglasses, contact lenses, and laser eye surgery in correcting refractive errors, there is no current treatment that targets the underlying cause. Understanding the biological mechanisms that cause myopia requires elucidating what factors cause the changes that lead to a mismatch between the eye's refractive power and its axial length. What is telling the eye to grow too long for its refractive power? Both genetic and environmental factors are now generally accepted to play important roles in myopia development, but the "nature versus nurture" debate continues over the relative contribution of each factor (Morgan, 2003; Mutti et al., 1996; Wallman, 1994). The increasing worldwide myopia prevalence (Park and Congdon, 2004) and well-known dependence of myopia development on visual near work (Rosenfield and Gilmartin, 1998) and level of education (Curtin, 1985; Morgan and Rose, 2005) suggest a strong environmental influence. However, common familial patterns of inheritance (Klein et al., 2005), twin studies (Dirani et al., 2006), and multiple identified genetic loci (Hornbeak and Young, 2009) lends support to the inheritability of myopia. Due to its multifactorial etiology, myopia has largely eluded the establishment of a clear developmental mechanism upon which an effective treatment or cure could be designed.

High myopia (defined as refractive error of -6 diopters, D, or worse), once considered rare, is also increasingly common (Lin et al., 1999; Saw et al., 1996). A seemingly small, 1 mm increase in ocular axial length of the eye corresponds to an additional refractive error of -3 D in humans. With longer axial lengths and associated stretching of the inner layers of the eye, high myopes are at increased risk of retinal detachment, glaucoma, macular degeneration and other central retinal complications that may lead to blindness (Curtin, 1985). Even moderate myopes are four times more likely than normal to suffer retinal detachment (Chou et al., 2006). So called "lacquer cracks" in Bruch's membrane (supporting structure of the retinal pigment epithelium), retinoschisis (retinal splitting), widespread atrophy of the retinal pigment epithelium and choroidal neovascularization (called "Fuch's spot" in the macular region), are other causes of visual impairment associated with high myopia (Saw et al., 2005; Tano, 2002). Both optical and surgical corrections do not alter posterior eye size, thus the risks of pathological complications remain in highly myopic patients. Apart from the direct risks to vision, myopia has a significant worldwide economic impact on health budgets due to costs associated with its correction. More than $5 billion annual burden in direct medical costs to the U.S. economy has been associated with refractive error (Frick and Rein, 2007). The ever-increasing worldwide prevalence, risk of complications, and high economic costs not only warrant the attention and concern of the general public, but also add to the motivation behind myopia research.

At the biological level, measuring changes that occur at each individual ocular layer during myopic eye growth can help to identify factors involved in myopia development and progression. The refractive state of the eye is actively adjusted during growth based on visual information received by the retina, a finding that has been substantiated by numerous myopia studies involving animal models (Choh et al., 2006; Howlett and McFadden, 2006; Kee et al., 2001; Shaikh et al., 1999; Smith et al., 1999). This process is termed active emmetropization and strongly evidenced by compensatory eye growth responses to focusing errors imposed on animal

subjects by attached lenses (Wildsoet, 1997). Optical manipulations, such as form deprivation by lid-suturing or wearing translucent occluders (diffusers), and wearing positive- or negative-powered spectacle lenses on growing chick eyes, can disrupt normal ocular growth as the eyes compensate for the imposed defocus by either shortening (with imposed myopia) or lengthening (with imposed hyperopia) the vitreous chamber depth (Sivak et al., 1990). Form deprivation imposes open loop conditions that also lead to lengthening of the vitreous chamber depth (Smith et al., 1999). This compensatory eye growth response occurs even after optic nerve section, in other words, without any input from the brain, suggesting local control of active emmetropization (Wildsoet and Wallman, 1995; Wildsoet, 2003; Wildsoet and Pettigrew, 1988). Separated from the central nervous system, active emmetropization most likely relies on the effects that the neural retina imposes on the subsequent layers, including retinal pigment epithelium, choroid, and sclera in the posterior segment of the eye. A diagram illustrating the visually driven signaling pathway is presented in Figure 1-1. Each layer, starting with the retina, is composed of distinctive cell types generating unique signaling molecules, and plays different but equally important roles in determining eye growth.

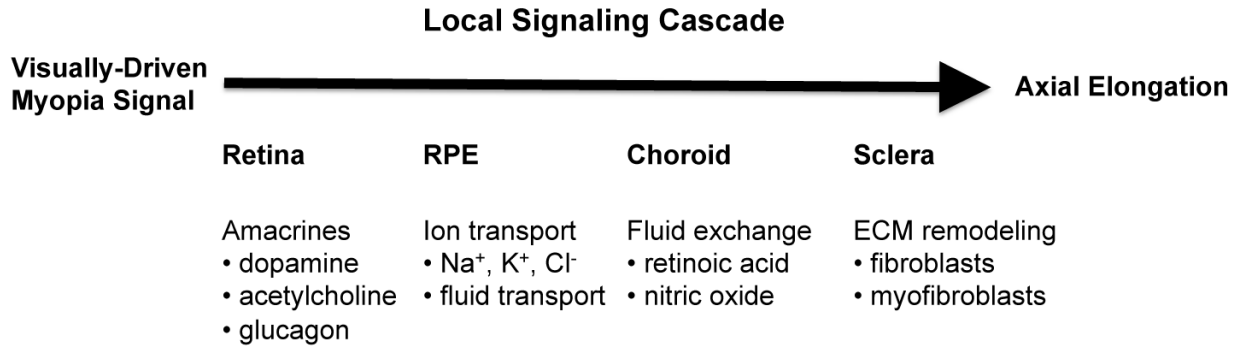

Figure 1-1. Diagram illustrating the visually driven signaling pathway from the retina to the sclera with list of major potential contributors involved. This represents a local signaling cascade effective without input from the central nervous system, leading to axial elongation as seen with induced myopia progression. RPE = retinal pigment epithelium. ECM = extracellular matrix.

1.1 Retina: Origin of the myopia signaling cascade

As retina is the first layer of the eye that processes visual information, it is also the most likely candidate to generate the primary signal for myopia development (Wallman, 1993). The retina's foremost function is to sense light, with neural pathways proceeding in a serial fashion from the photoreceptors to the bipolar cells to the ganglion cells and ultimately to the visual cortex. However, nestled in between the bipolar and ganglion cells at the inner plexiform layer are interneurons known as amacrine cells. These retinal cells and their respective neurotransmitter molecules have been implicated as potential contributors to myopia development (Wallman, 1993), with dopaminergic amacrine cells (Schaeffel et al., 1995), muscarinic cholinergic amacrine cells (McBrien et al., 2001b), and glucagonergic amacrine cells (Fischer et al., 1999a) being prevailing retinal cell populations that have repeatedly demonstrated influence in eye growth regulation.

1.1.1 Dopaminergic amacrine cells

Any signaling molecule found to be the principal retinal output controlling emmetropization would be expected to have its concentration change in opposite directions in response to opposite defocus signs (Simon et al., 2004), and affect downstream signaling in a matter of minutes (Zhu et al., 2005). The concept that eyes can encode the sign of defocus by varying the concentration levels of signaling molecules is the basis upon which many pharmacological studies are conducted. Substantial evidence exists for a role of dopamine in form deprivation myopia. Retinal levels of dopamine are decreased during the day in form deprived monkey eyes (Iuvone et al., 1989) and chick eyes (Stone et al., 1989). The application of dopamine agonists, such as apomorphine, reduces form deprivation myopia in both monkeys and chicks (Iuvone et al., 1991; Stone et al., 1989), most likely through a D2 dopamine receptor mechanism (Rohrer et al., 1993). On the other hand, the application of 6-hydroxy dopamine (Li et al., 1992) and continuous light (Bartmann et al., 1994), both lower retinal dopamine levels and reduce form deprivation myopia, but not lens-induced myopia (Schaeffel et al., 1994). After removal of form deprivation, dopamine levels slowly return to normal, but the rate of ocular elongation abruptly drops below normal, showing that dopamine's action is not bidirectional (Schaeffel et al., 1995), although evidence exists that show dopamine levels respond to lens-induced myopia (Guo et al., 1995). These results, taken together, suggest that retinal dopamine is involved in the control of eye growth, but is not likely to be the only retinal output controlling emmetropization.

1.1.2 Muscarinic cholinergic amacrine cells

The use of muscarinic receptor antagonists such as atropine to inhibit myopia progression started as a belief that too much near work leads to heavy eyestrain from frequent and sustained accommodation. As this was the primary suspect in the cause of functional or physiologic myopia, it was thought that cycloplegia, i.e. paralysis of the ciliary muscles of the eye that controls accommodation, should be employed as part of myopia management (Bedrossian, 1971; Sampson, 1979). However, this theory was shown to be fallible as the cycloplegic agents such as muscarinic receptor antagonists were determined to reduce experimental myopia via a nonaccommodative mechanism in chicks and tree shrews (Cottriall and McBrien, 1996; McBrien et al., 1993). Chicks do not have muscarinic receptors on their ciliary muscles, and thus the ability of muscarinic receptor antagonists to reduce myopia progression in chicks points to other target sites of action. Still, large amounts of evidence from both animal and human studies exist that demonstrate the effectiveness of muscarinic receptor antagonists in controlling myopia (Chua et al., 2006; Lee et al., 2006; Luft et al., 2003; Schmid and Wildsoet, 2004; Siatkowski et al., 2008), even though the target site of action that inhibits ocular elongation remains unclear. In addition to atropine, pirenzepine is another muscarinic receptor antagonist that has been researched extensively as a myopia treatment (Bartlett et al., 2003; Siatkowski et al., 2008). However, unlike atropine, pirenzepine is selective for M1 receptors only (Cottriall and McBrien, 1996). Not all muscarinic receptor antagonists are effective against myopia, as the only ones shown to effectively reduce myopia are atropine, pirenzepine (M1 specific), himbacine (M2 specific), and oxyphenonium (Luft et al., 2003), and at least for atropine, its effectiveness is

lessened after extended application (Tong et al., 2009). The ineffectiveness of other muscarinic receptor antagonists suggests that muscarinic antagonists act only through specific types of receptors or a combination thereof, or through a non-muscarinic mechanism on which only some of these drugs act.

There is accumulating evidence against a retinal site of action for the anti-myopia effects of muscarinic receptor antagonists. When retinal cholinergic amacrine cells were selectively destroyed by ethylcholine mustard aziridinium ion (ECMA), chick eyes remained emmetropic and susceptible to form-deprivation myopia, which could still be blocked by atropine (Fischer et al., 1998b). In the use of quisqualate to kill amacrine cells but leaving photoreceptors untouched, the emmetropization process was demonstrated to be still functional, supporting the idea that the outer retina is a likely site of form-deprivation detection (Diether and Schaeffel, 1999; Fischer et al., 1998c), without the need for amacrine cells. Other identified sites of action of muscarinic receptor antagonists include the retinal pigment epithelium, choroid, ciliary body, and the sclera (Fischer et al., 1998a; Lind et al., 1998; McBrien et al., 2009b). Recent strong evidence supports the idea of a scleral site of action, mostly due to influences of muscarinic receptor antagonists on scleral cells (Casanova et al., 2006; Lind et al., 1998). However, comprehensive profiling of muscarinic receptor gene and protein expression in tree shrew ocular tissues demonstrated that the genes of the muscarinic receptor subtypes M1 thru M5 are not altered in their expression levels both early in myopia development and after significant structural change with measurable axial elongation (McBrien et al., 2009b). There was no change in retinal acetylcholine concentration of chick or tree shrew due to form-deprivation myopia (McBrien et al., 2001b). Additional support for a scleral site of action comes from the demonstration that guinea pig scleras express muscarinic subtypes M1 to M5 (Qu et al., 2006), and particularly in the posterior sclera, expression of the M1 and M4 subtypes was significantly increased in form-deprived guinea pig eyes (Liu et al., 2007). Overall, these results point to a high likelihood that effective muscarinic receptor antagonists inhibit myopia through a different target away from the neural retina, with strong support for developing a new myopia control treatment targeting other ocular tissues such as the sclera.

1.1.3 Glucagonergic amacrine cells

In the chicken myopia model, form-deprivation myopia can be suppressed by antagonists to NMDA-type glutamate receptors (Fischer et al., 1998c; Vessey et al., 2005), while stimulation of NMDA receptors activates immediate-early gene expression of the transcription factor known as ZENK (an acronym for *Z*if268, *E*gr-1, *N*GFI-A, and *K*rox-24) in glucagonergic amacrine cells (Fischer et al., 1999a). ZENK expression is stimulated by conditions that inhibit ocular elongation such as imposed by plus-lens treatments and recovery from form-deprivation myopia, but not by conditions that induce ocular elongation such as minus-lens treatments and form-deprivation (Bitzer et al., 2006; Fischer et al., 1999a). The release of glucagon during plus-lens treatments is coupled to induction of ZENK, and the absence of immediate-early gene expression during minus-lens treatments and form-deprivation suggest that lack of glucagon is responsible for the development of experimental myopia in chickens (Feldkaemper and Schaeffel, 2002; Fischer et al., 1999a). Further evidence supporting the notion that glucagon may act as regulator of eye growth comes from the observation that retinal glucagon receptor mRNA levels follow the ZENK bidirectional expression pattern (Buck et al., 2004). With the application of muscarinic

cholinergic antagonists and dopamine agonists, both of which are known to block myopic eye growth, the down-regulation of retinal ZENK mRNA is reversed and the measured mRNA expression is higher than in control eyes (Ashby et al., 2007). However, no evidence has yet been found to indicate that the same signals occur in the mammalian model, as the expression patterns of several glucagon super-family members in the mouse retina do not appear to be visually regulated (Mathis and Schaeffel, 2007), and glucagon itself has not been found. While ZENK gene knockout mice exhibit axial myopia, it is still unclear whether the observed effect of deleting Egr-1 is due to altered retinal function or changes in other systems that may affect ocular growth (Schippert et al., 2007). Although ZENK expression responds in a bidirectional manner in correlation with the sign of imposed defocus, the glucagonergic control pathway still requires additional studies, particularly in mammalian animal models, to elucidate the role that glucagon plays in eye growth regulation.

1.2 Retinal pigment epithelium: Information gateway in myopia

Given that there is strong support for visually guided local eye growth control and by being situated between the retina and the adjacent choroidal and scleral layers, the retinal pigment epithelium (RPE) must play a critical role in relaying growth modulatory signals between the retinal source and its targets. The RPE forms a polarized tight barrier between the outer segment of photoreceptor cells and the choroidal vasculature, and traditionally is thought to mainly function to recycle the outer segment of photoreceptors, isomerize all-*trans*-retinol to 11-*cis*-retinal in the visual cycle, and generally maintain the composition of subretinal space by regulating metabolites and fluid transport (Strauss, 2005). The RPE has not been a major focus in myopia research, although during eye enlargement, while cell numbers remain unaltered, passive spreading and consequent flattening of retinal pigment epithelial cells has been reported (Lin et al., 1993). However, recent studies on retinal neurotransmitters have called for closer look into RPE fluid transport, growth factor secretion, and their possible roles in eye growth regulation.

The fluid transport capacity of the RPE is closely regulated by tight-junctions between epithelial cells and a plethora of ion transporters on both the apical (facing subretinal space) and the basal (facing choroid) membranes (Rymer and Wildsoet, 2005). During chick eye recovery from form-deprivation myopia, concentrations of sodium (Na) and chloride (Cl) ions in RPE-photoreceptor outer segments and extravascular choroid decrease over time, returning to normal after 48 h (Liang et al., 2004). Involvement of fluid exchange during form deprivation recovery suggests that fluid exchange and its corresponding transporters, which are responsive to pharmacological manipulations, may play significant roles in eye growth regulation. Ion movement involving apical Na-K-Cl cotransporters and basal Cl channels has been directly linked to fluid movement from the subretinal space to the choroid during light and dark adaptation (Li et al., 1994).

Growth factor secretion in the RPE as an alternative mechanism in eye growth regulation is supported by various studies, including findings that insulin-like growth factor (IGF) and its receptors function as an autocrine/paracrine signaling system in the monkey RPE (Waldbillig et al., 1992), that somatostatins inhibit IGF-1 mediated induction of vascular endothelial growth factor (VEGF) in human RPE cells (Sall et al., 2004), and that transforming growth factor-beta (TGF-β) blocks nitric oxide production in the murine RPE (Goureau et al., 1997). Furthermore,

the mRNA expression patterns of insulin-like growth factor 1 receptor (IGF-1R) and somatostatin receptor 2 have bidirectional modulation in the chick RPE, while TGF-β2 and transforming growth factor beta receptor 1 (TGFβR1) are unidirectionally modulated (Zhan et al., 2008). Adding to the evidence that growth factors have an active role in the RPE is the finding that apomorphine, a dopamine receptor agonist, regulates the expression of TGF-β1 and TGF-β2 in human fetal retinal pigment epithelial cells (Zhang et al., 2009).

Using isolated retina-RPE-choroid complex of the chick eye, it was shown that muscarinic antagonists cause spreading depression, a wave of hyperactivity followed by a wave of inhibition, of the isolated complex, and that in turn boosts the neurotransmitter release from cellular stores, which could potentially be the mechanism behind the eye growth inhibiting effect of atropine (Schwahn et al., 2000). Retinal dopamine content was elevated with the application of atropine, with subsequent damped oscillations of RPE potentials. Furthermore, atropine suppressed myopia only at sufficiently high doses that had observable toxic effects in the retina. In addition to dopamine, other neurotransmitters that have been shown to modulate RPE physiology to potentially influence eye growth include glucagon and vasoactive intestinal peptide (Koh and Chader, 1984; Rymer and Wildsoet, 2005; Seko et al., 1997). Each of these neurotransmitters present in the retina influences RPE physiology through different pathways, but the major contributor to eye growth regulation must ultimately influence immediate fluid movement into and out of the adjacent choroid, either through ion transport or growth factor secretion.

1.3 Choroid: Intermediate response against induced defocus

The choroid is a highly vascular tissue consisting of Bruch's membrane adjacent to the RPE, followed by an inner layer known as the choriocapillaris (a dense network of fenestrated capillaries), and lastly an outer layer neighboring the sclera that contains numerous larger diameter blood vessels and in the avian choroid, lymphatic vessels known as lacunae (De Stefano and Mugnaini, 1997). The main functions of the choroid include supplying the outer retina with oxygen and nutrients under highly regulated blood flow, and acting as a heat sink to regulate ocular temperature (Bill, 1985; Parver et al., 1980). The regulatory functions are made possible by dense innervation from the autonomic nervous system, and part of the autonomic control may be accomplished by intrinsic choroidal neurons residing within the choroid (Schrödl, 2009). These neurons most likely innervate extravascular smooth muscle cells that stain positive for α-smooth muscle actin, providing the choroid with contractile properties in response to neural innervation (Poukens et al., 1998). In addition, the fenestrated choriocapillaris is highly permeable to low molecular weight substances, allowing rapid fluid exchange in the choroid that could influence smooth muscle tone (Törnquist et al., 1990). It is possible that choroidal blood flow may also be regulated by retinal image defocus, via signals released from the RPE (Wallman et al., 1995). Changes in choroidal blood flow was observed to precede changes in choroid thickness following form-deprivation or recovery (Fitzgerald et al., 2002). Indeed, the choroid has been found to thicken with plus lens treatment, or thin with minus lens treatment or form-deprivation (Wallman et al., 1995; Wildsoet and Wallman, 1995). The debate remains open on which molecules are ultimately responsible for causing the thinning and thickening responses of the choroid, presumably as a result of the eye growth signals that come from the RPE with

lens-induced defocus or form-deprivation. A number of signaling molecules have been localized in the choroid that could potentially influence myopic eye growth, but two molecules in particular, retinoic acid and nitric oxide, have strong support for being the major contributors to the observed choroidal blood flow changes.

A large amount of retinoic acid is produced in the choroid (Fischer et al., 1999b), and the production is differentially affected by lens-wear (Bitzer et al., 2000; Simon et al., 2004). In the chick, positive lens wear, which inhibits ocular elongation, increases retinoic acid production by more than 4-fold, while negative lens wear, which promotes ocular elongation, sharply decreases retinoic acid synthesis (Mertz and Wallman, 2000), and similar findings have been found in the guinea pig (McFadden et al., 2004). Physiological concentrations of retinoic acid added to *in vitro* scleral fibroblast cultures inhibited proteoglycan synthesis (Mertz and Wallman, 2000). Together with the finding that scleral fibroblasts have retinoic acid receptors (Fischer et al., 1999b), retinoic acid could be used by the eye growth regulation system to modulate proteoglycan synthesis and cell division in the sclera.

The choroid have been associated with rich parasympathetic innervation, with findings of NADPH-positive nerve terminals within the extravascular smooth muscle cells, from nonadrenergic, noncholinergic intrinsic choroidal neurons that utilize nitric oxide (NO), a gaseous neurotransmitter (Poukens et al., 1998). Ocular NO may be involved in the visually induced choroidal thickness change. For example, inhibition of nitric oxide synthesis using N^G-nitro-L-arginine methyl ester inhibits choroidal thickening due to myopic defocus (Nickla and Wildsoet, 2004). On the other hand, intravitreal injections of the NO precursor L-arginine caused transient increases in choroidal thickness, adding support to a modulatory influence of NO on the choroid (Nickla et al., 1999b). Studies using additional specific NO synthase (NOS) inhibitors such as nNOS inhibitor N^W-propyl-L-arginine suggest that the source of NO is most likely the intrinsic choroidal neurons or the parasympathetic innervation from the ciliary and/or pterygopalatine ganglia (Nickla et al., 2009). NO may also play a significant role in regulating the scleral response to visual manipulations by targeting a sparse cell population known as myofibroblasts in the posterior region of the sclera (Poukens et al., 1998). The properties and functions of scleral myofibroblasts are not well characterized, but these cells possess contractile abilities similar to choroidal smooth muscle cells, and may be key in sensing changes in intraocular pressure and in initiating scleral remodeling during compensatory eye growth.

1.4 Sclera: Controller of eye dimensions

As the outermost layer of the eye, the sclera not only determines eye size, but also serves to protect the sensitive neural retina from the external environment. Anatomically, the avascular sclera is adjacent to the vascular-rich choroid on its inner surface, and is sheathed by Tenon's capsule, a thin hypocellular membrane structure, and extraocular muscle insertions on its outer surface (Trier, 2005; Watson and Young, 2004). The mammalian sclera is made up of extensive fibrous connective tissue, with fibroblasts comprising the main cellular component, enmeshed in extracellular matrix (ECM) material that includes collagen and proteoglycans (McBrien and Gentle, 2003). A transmission electron microscopy image of the sclera is shown in Figure 1-2, where the collagen fibers are visible around scleral fibroblasts.

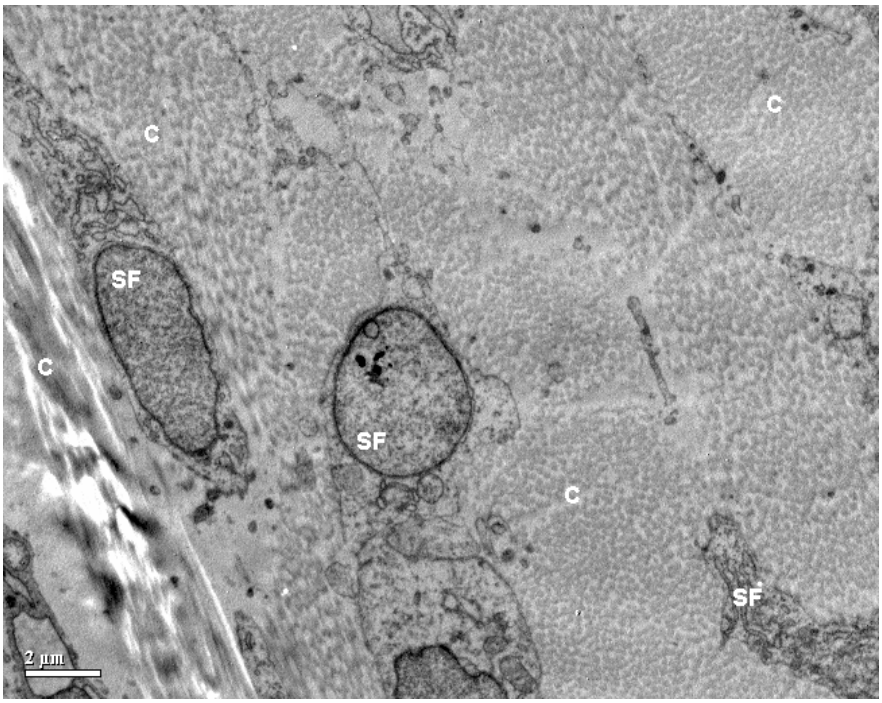

Figure 1-2. Transmission electron microscopy image of chick fibrous sclera. C = collagen fibers, SF = scleral fibroblasts. Note the different orientations of the collagen fibers organized into stacked layers called lamellae. Bar = 2 µm.

Scleral myofibroblasts expressing α-smooth muscle actin have been identified at the scleral spur and inner posterior sclera (Tamm et al., 1995), and found to increase in numbers with increasing age (Poukens et al., 1998). Adult human scleral thickness ranges from 1-1.35 mm at the posterior pole, and decreases gradually to 0.4-0.6 mm at the equator, and increases to about 0.8 mm at the limbus, where the anterior sclera meets the cornea (Norman et al., 2009; Olsen et al., 1998; Trier, 2005). Within the mammalian sclera, collagen types I, III, V, and VI comprise 90% of the total ECM dry weight (Edelhauser and Ubels, 2003), with type I being the predominant type followed by type III, and only minute amounts of other collagen types (Watson and Young, 2004). Other components that comprise the scleral ECM include elastic fibers such as elastin (Marshall, 1995), proteoglycans such as aggrecan, decorin, and biglycan (Rada et al., 2000; Siegwart Jr and Strang, 2007), and glycosaminoglycan side-chains such as chondroitin sulfate, dermatan sulfate, heparin sulfate, and hyaluronan (Moring et al., 2007). Glycoproteins that are important for cellular attachment such as fibronectin and laminin have also been identified in the sclera (Chapman et al., 1998; Marshall, 1995). Due to its major role in determining eye size, scleral growth is presumed to be under tight regulation through various signaling pathways that affect its biomechanical properties.

1.4.1 Modulation of scleral growth

Scleral growth is an active process that involves visually induced signals in the retina, which are relayed to the sclera through intervening ocular tissue layers. Observations from animal models of myopia indicate scleral growth changes are likely to reflect the product of a remodeling process that also underlies normal (developmental) eye enlargement, but exaggerated

in the case of myopia. Myopia-associated changes in the activity levels of matrix metalloproteinases (MMPs) and tissue inhibitors of metalloproteinases (TIMPs) in the sclera are consistent with this interpretation (Jones et al., 1996; Siegwart and Norton, 2005). Intraocular pressure (IOP) is likely to play a critical role, providing the inflationary force for normal eye enlargement (Friedman, 1966). If the sclera becomes at least transiently weaker during remodeling, the influence of even normal IOP is expected to lead to further eye enlargement. The scleral ECM remodeling process is highly active; response to visual manipulations leads to significant changes within the scleral ECM, most likely through activation of fibroblasts and myofibroblasts that are also known to be responsive to select pharmacological treatments.

In the chick eye model, the synthesis of proteoglycans changes in opposite directions in the fibrous and cartilage scleras (Marzani and Wallman, 1997). Negative lens and form-deprivation by diffusers accelerate scleral growth, with increased ECM synthesis thickening the cartilage layer, and decreased ECM synthesis thinning the fibrous layer. On the other hand, positive lens wear decelerates scleral growth, with decreased ECM synthesis thinning the cartilage layer, and increased ECM synthesis thickening the fibrous layer (Gottlieb et al., 1990; Marzani and Wallman, 1997; Rada et al., 1998). However, the combined chick sclera does not change thickness overall in either case, likely due to the transdifferentiation of scleral fibroblasts into chondrocytes and vice versa during eye growth changes (Kusakari et al., 2001). The fibrous sclera in mammalian models responds to visual manipulations in the same manner as the fibrous sclera in the chick model, with reduced ECM synthesis with induced myopia (negative lens or diffuser wear), and increased ECM synthesis with induced hyperopia (positive lens wear) (McBrien and Gentle, 2003; Norton and Rada, 1995).

Many proteins related to ECM remodeling are differentially regulated during visual manipulations. In monocular form-deprivation in tree shrews, MMP-2 mRNA level becomes higher, while collagen mRNA level becomes lower than in control eyes (Siegwart and Norton, 2002). These differential effects reverse during recovery, i.e. when monocular form-deprivation is removed. Treatment with intraperitoneal injections of β-aminoproprionitrile or D-penicillamine, agents that block collagen crosslinking, increases the effects of form-deprivation myopia in tree shrews but not chickens (McBrien and Norton, 1994), underscoring differences in scleral responses of the avian versus the mammalian sclera. The fact that fellow eyes without form-deprivation do not show greater elongation although they were exposed to the same amount of drug suggests that in normal eyes collagen crosslinking does not provide the only resistance to expansion of the eye by IOP.

Residing in the mammalian sclera are scleral myofibroblasts (Poukens et al., 1998), cells that have the ability to contract to resist applied forces, and may account for observed shrinking of the tree shrew eyes under elevated IOP (Phillips and McBrien, 2004). Scleral myofibroblasts have not been well characterized for their role in myopia progression, but several studies have already shown the ability of fibroblasts to transdifferentiate into myofibroblasts, including the finding that sphingosine 1-phosphate induces α–smooth muscle actin expression in lung fibroblasts (Urata et al., 2005), TGF-β1 induces transdifferentiation through integrin-mediated signaling and focal adhesion kinase (Ding et al., 2008), and growth factors such as connective tissue growth factor promotes myofibroblast differentiation and collagen synthesis (Grotendorst and Duncan, 2005). On the other hand, prostaglandin E2 inhibits fibroblast to myofibroblast

transition in human lung fibroblast cultures (Kolodsick et al., 2003). Scleral myofibroblasts could have a function similar to the avian scleral cartilage layer in providing the necessary biomechanical resistance against IOP, especially during periods of accelerated eye growth. Adding the fact that scleral myofibroblasts may be innervated in the mammalian eye (Tamm et al., 1995), this cell population warrants further study to shed light on its involvement in scleral biomechanics as part of eye growth regulation.

1.4.2 Scleral biomechanics

Changes in scleral biomechanics during myopia development have largely been attributed to changes in matrix composition (McBrien et al., 2000; Norton and Rada, 1995), but cellular contributions have also been recently explored (McBrien et al., 2009a; Shelton and Rada, 2007). Scleral collagen fibers exhibit large variations in diameters, and are arranged irregularly in multi-layered lamellae of varying thickness (Curtin et al., 1979). The collagen fibers run tangential to the scleral shell surface, with a preferred direction of orientation within individual lamellae (Watson and Young, 2004). In normal sclera, the collagen fibers show a gradient in fiber diameters from smaller diameters in the inner sclera towards larger diameters in the outer sclera. However, in myopic sclera, the collagen fiber diameter gradient is lost and replaced by more uniformly sized collagen fibers of smaller diameter (McBrien et al., 2001a). With increasing age, natural collagen crosslinking in the body is a characteristic of soft tissues (Bailey et al., 1998), which results in an increase of tissue stiffness, a property that was also observed in the human sclera (Friberg and Lace, 1988). In highly myopic human or animal eyes with experimentally induced myopia, reductions in both collagen content and fiber diameters have been linked to decreased creep resistance (McBrien et al., 2001a; Norton and Rada, 1995). Form-deprivation myopia in both the chick and tree shrew has been associated with increased creep rate of posterior and equatorial sclera (Phillips et al., 2000), with creep rate being directly related to the change in axial elongation rate (Siegwart and Norton, 1999). Furthermore, scleral tissue modulus has been measured and reported to characterize scleral biomechanics. Normal chick scleral elastic modulus is around 15.38 MPa, tree shrew scleral elastic modulus is around 2.72 MPa (Phillips and McBrien, 1995; Phillips et al., 2000), and human scleral elastic modulus is on the order of 1.8-2.9 MPa (Battaglioli and Kamm, 1984; Friberg and Lace, 1988). Comparison between chick and tree shrew normal and myopic eyes demonstrated that there was no significant difference in mean values of posterior scleral elastic modulus or failure load (Phillips and McBrien, 1995; Phillips et al., 2000). These findings imply that most differences found in load versus extension behavior can be attributed to differences in scleral thickness changes, and not structural changes within the scleral matrix.

Another consideration in scleral biomechanics for high axial myopia is that any reinforcement strategy must be able to withstand the forces acting on the scleral shell. A well-known relationship between pressure and wall tension for a sphere is the Law of Laplace (Berne and Levy, 2001). When applied to the eye, assuming spherical shape with uniform ocular shell thickness, Laplace's law states that:

$$T = \frac{\Delta P \times r}{h} \quad \text{(Equation 1-1)},$$

where scleral wall tension T is the product of trans-scleral pressure gradient ΔP and the spherical radius r, and inversely proportional to scleral wall thickness h (Davanger, 1971). This model has limitations in describing the eye, including the assumption that the eye wall structure is homogeneous and isotropic. In a simplified myopia model, assuming no change in the trans-scleral pressure gradient as myopia progresses, the spherical radius is increased (axial length increase) while the scleral wall thickness decreases. Both of these changes contribute to an increased wall tension, and any reinforcement strategy should take into account the significantly increased wall tension due to myopia progression. In addition, the effect of eye wall tension on scleral cell viability is an area that needs further investigation.

The sclera is normally subject to cyclic strain from extraocular muscle and lid movements, i.e. blinking, that applies pressure to the eye. Furthermore, underlying changes in scleral biomechanics might be the remodeling of scleral extracellular matrix by native scleral cells due to mechanical strains imposed by variations in IOP. A wide range of mechanical strain levels on scleral fibroblasts has been found to trigger remodeling of the ECM, including 0.45% cyclic strain with suppression of TIMP-1 (Yamaoka et al., 2001) to 15% cyclic strain with production of MMP-2 and suppression of TIMP-2 (Shelton and Rada, 2007). However, further cellular work may need to narrow the range for appropriate physiological strain levels, as recent study in monkeys show highest physiological peak strain at 2.4% (Girard et al., 2009). Although the role of cyclic strain in the maintenance of sclera is unknown, these results point to the establishment of targets, namely the MMPs and TIMPs, to measure cellular response in the sclera. Without a doubt, the scleral extracellular matrix and native cellular populations play significant roles in the control of scleral biomechanics, which in turn influences axial elongation rate during eye growth regulation.

1.5 Sclera as a safe potential target for myopia treatment

Having a multitude of neural synapses makes the retina a difficult site to develop a highly specific treatment for myopia with well-controlled targets. Adding the fact that the majority of patients developing myopia are young and getting younger (Morgan and Rose, 2005), a retinal treatment could easily lead to the development of unwanted visual side effects due to expected prolonged treatment into early adulthood to prevent myopia. As for RPE, it plays an important role in regulating the transport of biological signals and ions between the retina and the choroid. Any treatment targeting the RPE could be problematic as altering the fluid transport properties could be detrimental to retinal health. Following behind is the choroid, which is influenced by both the RPE and autonomic innervation that regulates the blood flow through its rich vascular network. Any disruption to the regulated blood flow in the choroid could be damaging to retinal health, not to mention the potential immediate changes to optical focus due to the thinning or thickening response. In contrast, the sclera is the endpoint target of myopic eye growth signals. Potential complications in the other layers of the eye support the sclera as the preferred target for potential myopia treatments. With its relatively avascular nature and lack of sensory neural fibers, the sclera actively remodels the ECM through cellular response to eye growth signals, a property that could be exploited to safely intervene in myopia progression. To date, researchers in the field of ophthalmology have explored only materials adapted from different non-medical fields and applied them to the sclera in an attempt to passively prevent further elongation in high axial myopia. However, current advances in biomaterials have made possible the control of

cellular behavior within defined microenvironments, paving the way for the development of novel biomaterials that can actively sense and respond to scleral changes during myopia progression.

2. History of Scleral Biomaterials

The application of various biomaterials to the sclera for treating different ocular conditions such as retinal detachments has been in practice since the 1930s (Schepens and Acosta, 1991). Most of these are shaped into bands known as "scleral buckles", which are typically made from silicone- and hydrogel-based polymers, and used in surgery to close retinal breaks after detachments (Colthurst et al., 2000). In relation to the latter application, there are reports of signs of inflammation after less than one year with silicone materials and hydrogels such as poly(methyl acrylate-*co*-2-hydroxyethyl acrylate) crosslinked with ethylene diacrylate. Some of these scleral buckles, marketed under trade names MAI (Ho et al., 1984) and MIRAgel (D'Hermies et al., 1995; D'Hermies et al., 1998), have been reported to degrade into fragments leading to foreign body giant cell granulomatous reactions, rendering the implants ineffective with respect to their intended functions. In the context of myopia control, a treatment for very high myopia used in the U.S. since the 1950s involves the attachment of scleral strips cut from donor cadaveric eyes, as means of providing at least temporary mechanical support (Borley and Snyder, 1958; Ward et al., 2009). This method has proven to be less than ideal, not only because of limited availability of donor eyes, but also because the diseased eyes are abnormally long, often necessitating splicing donor tissues to completely wrap around the posterior pole. In addition, the host tissue may resorb portions of the donor graft, reducing the surface contact area reinforcing the globe (Curtin and Whitmore, 1987). These procedures focused entirely on mechanically supporting the weakened posterior sclera without much understanding of the biological responses of the host sclera.

More recent studies have been carried out to understand how the sclera responds to different types of implant materials. A practical surgical approach for applying synthetic polymers to the sclera (scleroplasty) for high axial myopia has utilized pre-formed polymer formulations, which are expected to act as scleral bands reinforcing the posterior pole (Jacob-LaBarre et al., 1994; Tarutta et al., 1999). These types of synthetic scleral bands typically induce fibrous encapsulation of the implant, and the fibrous capsule is likely to change in cellular and collagen composition over time, with the shift from an approximately equal mix of type I and III collagen at 3 months to mostly type I collagen by 18 months, observed in a long-term rabbit study (Jacob et al., 1996). The fibrous capsule represents new tissue formation that potentially could mechanically strengthen the sclera, as the native sclera is composed of predominantly type I collagen. Over time, due to constant exposure to stresses from ocular movement and intraocular pressure variations, synthetic scleral bands exhibit changes in their physical properties (Jacob et al., 1997). The changes in physical properties could include material compliance and creep. Material compliance, the reciprocal of Young's modulus, in the diseased sclera is much higher than that of the normal sclera. Similarly, scleral creep rate, the amount of tissue extension under a constant load over time, increases in eyes with developing myopia, and decreases in eyes recovering from myopia. (McBrien et al., 2009a). In order to prevent further scleral distension, the reinforcement materials should have lower compliance than the myopic sclera, yet sufficient

compliance to avoid cutting into the sclera. Porous materials such as polyurethane fabric have been shown to allow additional strength increase after implantation due to cellular in-growth, and expanded polytetrafluoroethylene (e-PTFE) has been shown to be most stable and resistant to creep extension under constant stress in the ocular environment (Jacob et al., 1997). Although these recent studies have started looking at the biological response when studying the effects of synthetic scleral bands, no studies have been conducted where specific design parameters for the scleral bands are introduced to allow controllable biological scleral responses at the cellular and tissue levels.

Other materials that have been applied to the sclera include glaucoma filtration implants (De Feo et al., 2009; DeCroos et al., 2009; Lloyd et al., 2001), for reducing intraocular pressure by creating a direct opening from the intraocular cavity to the extraorbital space, and scleral plugs (Liu et al., 2009; Yasukawa et al., 2001; Zhang et al., 2008), which act to seal scleral incisions after vitrectomy or delivery of drugs to the inside of the eye via a embedded drug depot secured at the scleral wall (Short, 2008). Observed scleral responses to these devices have been relatively similar to what were found for scleral bands. Since these devices are made for the treatment of other ocular conditions and most are implanted at the anterior sclera, in contact with the aqueous humor, readers are directed to the aforementioned references for additional information in regards to their respective performance.

The field of biomaterials has evolved from incorporating materials from various industries, and using them to restore the structure and/or function of tissues and organs, to the modern day use of tailored materials that elicit specific biological responses (Healy et al., 1999; Hubbell, 1995; Kohane and Langer, 2008; Peppas and Langer, 1994). Biomimetic polymers that are environmentally responsive (e.g. pH and temperature responsive) that could be modified to respond appropriately to a disease state in the body are not only possible, but have been extensively investigated for various applications. One class of this type of material is a peptide-modified hydrogel that is thermally responsive to body temperature and is degradable by the body's natural proteases (Stile *et al.*, 2001; Kim *et al.*, 2005), both of which are desirable properties given the need for mechanical support and the heightened protease activities observed during visually guided scleral remodeling. This class of materials would lend itself to the incorporation of specific design parameters where controlled biological responses are needed to halt or even reverse the axial elongation observed during myopia progression.

3. General experimental approach & methods

All of the experimental approach and methods employed in this dissertation work are either described in detail or referenced as appropriate in respective chapters. However, since the chick model and A-scan ultrasonography are both extensively utilized in all studies, the animal model and the ocular dimensions monitoring method are described here in more detail to help with understanding the experiments. A brief description on an X-ray imaging technique is included to demonstrate the localization of polymer implantations at the posterior pole of the eye.

Chicks (*Gallus gallus domesticus*) are chosen as the animal model for this dissertation work since there are reliable established chick protocols for inducing myopia. Although the chick sclera is bi-layered with an inner cartilage layer, it has a fibrous layer that shows similar changes in myopia to the mammalian sclera. Also, because it is fast growing, the chick is suitable for the initial testing of treatment options, acknowledging that further testing in mammalian and/or primate models will probably be required before any use in humans. In addition, the chick model is likely the most economical due to relatively low acquisition and maintenance costs. Finally, the Wildsoet lab has a wealth of experience in working with the chick model, having contributed significantly to chick-based myopia research findings. We use negative defocusing lenses to provoke myopic responses in the chicks. An image of the chick eye wearing a negative defocusing lens is shown in Figure 1-3, with the schematic showing consequent ocular elongation in response to backward shifting of focal plane.

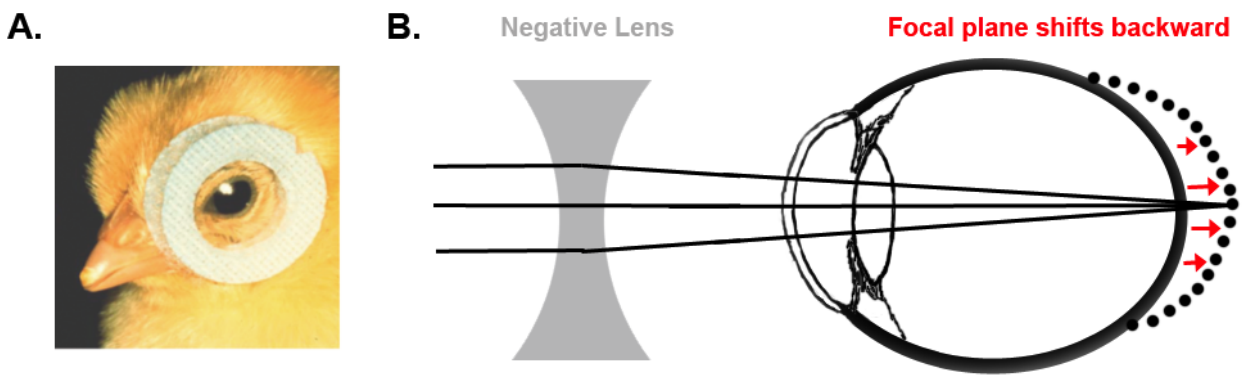

Figure 1-3. A) Image of chick wearing a negative lens. B) Lens-induced myopia (LIM) showing the backward shifting of the focal plane leading to a blurred image on the retina, causing the eye to elongate in order to match the shifted focal plane.

This lens treatment imposes similar visual conditions to those encountered with faulty accommodation, which plays a role in the development of human myopia. Although chicks are small animals, their eyes are relatively large compared to their body size. All polymer formulations were implanted in the orbital space, sandwiched between the posterior pole of the eye where most of the myopic "growth" occurs, and the extraocular muscles.

Outcome measures of all polymer treatments described in this dissertation work include evidence of ocular growth, as measured by high frequency A-scan ultrasonography. Current equipment can measure eye length and scleral thickness to a resolution of 10 μm, with the potential to also detect implanted polymers. Evidence of reduced eye elongation and thickened sclera in response to implantation is detectable by this methodology. The axial dimensions of the principal ocular components (anterior chamber depth, lens, vitreous chamber depth, retina, choroid, and scleral thicknesses) can be derived from the recorded ultrasonography traces. A sample ultrasonography trace is illustrated in Figure 1-4.

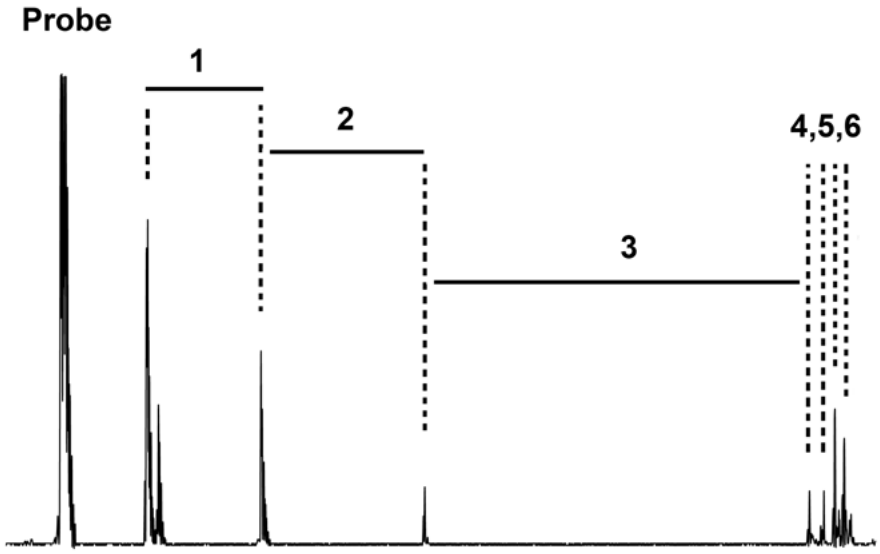

Figure 1-4. Sample ultrasonography trace depicting all principal dimensions of the chick eye. 1 = anterior chamber depth. 2 = lens thickness. 3 = vitreous chamber depth. 4 = retinal thickness. 5 = choroidal thickness. 6 = scleral thickness.

Typically a large number of traces (n > 12) are collected for each measurement. Two major parameters, scleral cup depth and axial length, are presented in many of the studies reported in this dissertation work to describe ocular growth. Scleral cup depth is represented by the sum of vitreous chamber depth, retinal thickness, and choroidal thickness. Axial length is represented by the sum of anterior chamber depth, lens thickness, and scleral cup depth. These two parameters are reported separately to account for potential contribution to ocular growth by the anterior segment of the eye.

An X-ray imaging technique that makes use of fine gold beads can be utilized to visualize polymer location (Hainfeld and Powell, 2000). This method was used to initially demonstrate polyvinylpyrrolidone (PVP) polymer location post-implantation, providing confidence in the reliability of the surgical implantation technique used throughout this dissertation work. Gold beads of approximately 100 µm uniform diameter were physically mixed together inside the PVP polymer gel. A sample image of the X-ray imaging technique in chick eye is shown in Figure 1-5 along with transformed images of the gold beads showing different viewing angles. This imaging method could potentially be utilized to characterize the distribution of injected polymers and also regional changes in scleral growth by tracking the movement of the fine gold beads over time.

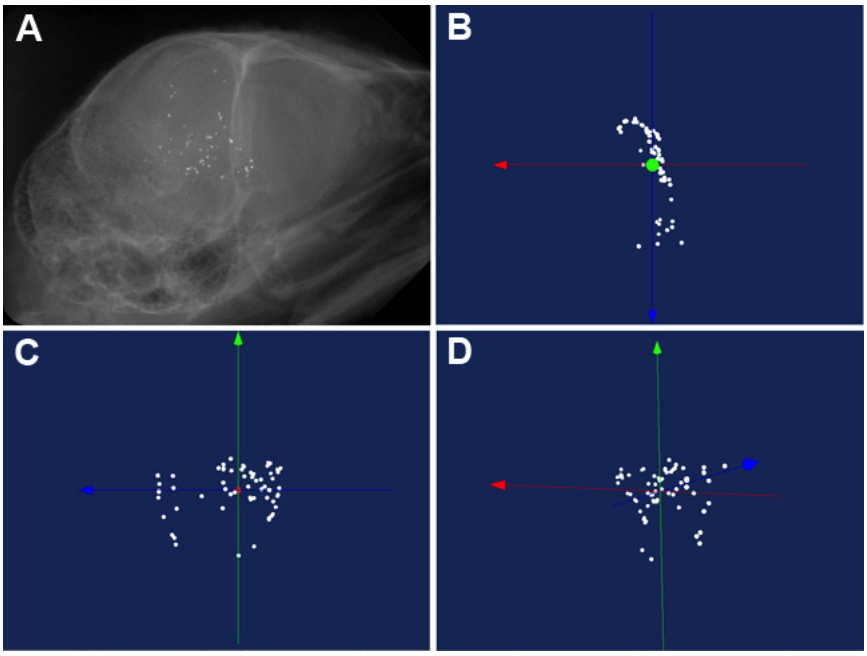

Figure 1-5. Images of gold beads, collected with an X-ray imaging technique, showing localization of the implanted PVP polymer to the outer scleral surface at the posterior pole of the eye. A) Location of gold beads embedded in polymer inside the chick orbit. B) Superior, C) Posterior, and D) Lateral views.

4. Dissertation Outline

In this dissertation, the feasibility and efficacy of using polymer-based implants to slow the remodeling process and/or increase the mechanical strength of the sclera are investigated. A plausible strategy for arresting myopic eye growth put forward by this dissertation work involves understanding the biological changes that occur in the myopic sclera, and utilizing that information to design biomimetic materials that can actively respond to the cellular and tissue demands of the sclera during myopic growth.

3.1 Specific aims

Chapters II, III, IV, and V of this dissertation are divided and organized according to the specific aims in the following order:

1. To evaluate the scleral responses to two different polymer formulations, poly(2-hydroxyethyl methacrylate) (pHEMA) and poly(vinyl-pyrrolidone) (PVP), implanted adjacent to the outer scleral surface of normal chick eyes, as well as form-deprived and lens-induced myopic chick eyes for the latter formulation. Both polymer systems are formulated to strengthen the sclera, although the underlying mechanisms are expected to be different, and to assess the practical (surgical) implications in pre-molded (pHEMA) versus injectable (PVP) polymer systems. This work was published in the journal of Experimental Eye Research.

2. To investigate the temporal and magnitude effects of myopic and hyperopic defocus on the mRNA expression levels of geltinase-A (MMP-2), collagenase 3 (MMP-13), transforming growth factor beta-2 (TGFβ-2), and tissue inhibitor of matrix metalloproteinase-2 (TIMP-2), which are implicated in scleral remodeling and have the potential to be applied to tailor novel biomaterials for the treatment of high axial myopia.

3. To develop and characterize an implantable synthetic biomimetic hydrogel that is capable of inducing new tissue growth by allowing cellular in-growth and degradation through protease activities. The goal is to prevent excessive eye enlargement by effectively increasing the scleral wall thickness in the chick eye model. A biomaterial could achieve that goal by serving as a tissue scaffold that can attract native scleral cells to migrate and proliferate inside the synthetic ECM. This work was published in the journal of Tissue Engineering.

4. To characterize the developed biomimetic hydrogel formulation for delivering atropine in chick eyes. Atropine has been shown to have the potential to control myopia progression, and the development of a sustained release formulation could allow the drug to be applied at the posterior segment, avoiding complications such as photophobia in the anterior segment of the eye. Depending on the intended treatment duration, the polymer will need to possess predictable degradation profile over time. The drug release profile also has the potential to be controlled by the inclusion of degradable nanoparticles that encapsulate the drug at the core of the nanoparticles.

These individual specific aims are expanded and discussed in further detail in the subsequent chapters II-V. In chapter VI, the major findings of the dissertation work are summarized with a discussion of its contributions to the various interdisciplinary fields in general, including myopia, ocular therapies, and biomaterials research. Lastly, a discussion on future directions and potential further developments is included.

Chapter II

Effects of Poly(2-hydroxyethyl methacrylate) and Poly(vinyl-pyrrolidone) Hydrogel Implants on Myopic and Normal Chick Sclera

Abstract

There has been generally little attention paid to the utilization of biomaterials as anti-myopia treatments. The purpose of this study was to investigate whether polymeric hydrogels, either implanted or injected adjacent to the outer scleral surface, slow ocular elongation. White Leghorn (*Gallus gallus domesticus*) chicks were used at 2 weeks of age. Chicks had either (1) strip of poly(2-hydroxyethyl methacrylate) (pHEMA) implanted monocularly against the outer sclera at the posterior pole, or (2) an in situ polymerizing gel [main ingredient: poly(vinyl-pyrrolidone) (PVP)] injected monocularly at the same location. Some of the eyes injected with the polymer were fitted with a diffuser or a -10D lens. In each experiment, ocular lengths were measured at regular intervals by high frequency A-scan ultrasonography, and chicks were sacrificed for histology at staged intervals. No *in vivo* signs of either orbital or ocular inflammation were observed. The pHEMA implant significantly increased scleral thickness by the third week after implantation, and the implant became encapsulated with fibrous tissue. The PVP-injected eyes left otherwise untreated, showed a significant increase in scleral thickness, due to increased chondrocyte proliferation and extracellular matrix deposition. However, there was no effect of the PVP injection on ocular elongation. In eyes wearing optical devices, there was no effect on either scleral thickness or ocular elongation. These results represent "proof of principle" that scleral growth can be manipulated without adverse inflammatory responses. However, since neither approach slowed ocular elongation, additional factors must influence scleral surface area expansion in the avian eye.

Chapter III was reproduced with modification from the following published paper:

Su J, Iomdina E, Tarutta E, Ward B, Song J, Wildsoet CF, 2009. Effects of poly(2-hydroxyethyl methacrylate) and poly(vinyl-pyrrolidone) hydrogel implants on myopic and normal chick sclera. *Experimental Eye Research* 88(3): 445-57.

1. Introduction

Anti-myopia treatments are still limited, and indeed controversial, despite increased research efforts directed towards this need and an overall increase in the prevalence of myopia worldwide, currently estimated at between 10-25% in the western countries and 60-80% in the eastern countries (Gilmartin, 2004; Saw, 2003).. To slow myopia progression, there is only one pharmacological treatment currently in use - topical atropine (Fan et al., 2007; Shih et al., 2001), whose use is accompanied by numerous side effects and offers little benefit for already highly myopic eyes. For these high-risk eyes, the only available treatment is donor scleral graft reinforcement surgery (Avetisov et al., 1997; Thompson, 1978), which is reserved for eyes exhibiting scleral creep, and is limited by access to suitable donor tissue. While a limited range of synthetic polymer scleral reinforcement materials have been developed (Jacob et al., 1997; Tarutta et al., 1999), they have not yet seen widespread clinical use. Ways of promoting collagen crosslinking to strengthen the sclera and so prevent eye elongation have also been explored (Paik et al., 2008; Wollensak and Spoerl, 2004), but there remain obstacles to their clinical application. Specifically, the chemical cross-linking agents typically used, e.g., glutaraldehyde, are highly toxic and radiation alternatives, e.g., riboflavin-UVA irradiation, may elicit cellular reactions, potentially leading to local photoreceptor death (Wollensak et al., 2005).

The chick was chosen here as the animal myopia model for testing the notion that biocompatible synthetic hydrogel polymers can be used to reinforce and/or alter the native ultrastructure of the sclera, to inhibit the excessive eye elongation underlying myopia. The sclera is a relatively accessible and safe target for therapeutic intervention. The significant accumulated evidence for the role of visual environmental factors in the development of human myopia (Morgan and Rose, 2005; Saw, 2003) supports the use of animal models relying on visual manipulations to induce myopia. The chick is the most commonly used animal model for myopia, although there are also tree shrew, guinea pig, and monkey models. For inducing myopia, there are two experimental paradigms, form-depriving diffusers and negative defocusing lenses (Norton, 1999; Wildsoet and Wallman, 1995). As in human myopia, the induced changes are largely confined to the posterior vitreous chamber of the eye, which is encased by the sclera (McBrien and Gentle, 2003; Rymer and Wildsoet, 2005).

Because the sclera represents the outer mechanical support layer of the eye and shows both ultrastructural and biomechanical changes in high myopia, it is arguably a prime target for therapeutic manipulation of myopia progression. The mammalian sclera is made up of fibrous connective tissue, with fibroblasts comprising the main cellular component of the mammalian sclera. These cells are enmeshed in extracellular matrix material that includes collagen and proteoglycans (Ihanamaki et al., 2004; McBrien and Gentle, 2003). In high myopia, the usual collagen fiber diameter gradient (smallest fibers innermost) is lost (Curtin et al., 1979; McBrien et al., 2001a), and there is also a significant decrease in amounts of glycosaminoglycans and proteoglycans in mammals (Avetisov et al., 1983; Norton and Rada, 1995). These changes likely reflect the increased scleral remodeling reported in both high human myopia and animal models of the same (Nickla et al., 1999a; Rada et al., 2000), rendering such eyes more vulnerable to the stretching influence of intraocular pressure (Friedman, 1966; Phillips and McBrien, 2004).

The sclera of the chick, which was used in the current study, shares some features with mammalian and primate scleras, but there are also important differences. In addition to a fibrous layer, as in mammals, there is an inner cartilaginous layer with chondrocytes and chondroblasts. The chondroblasts are transitional cells that lie between fibroblasts and chondrocytes morphologically, and are located at the boundary of the cartilaginous and fibrous layers of the sclera (Kusakari et al., 1997; Marzani and Wallman, 1997). These chondroblasts contribute to the appositional growth of the cartilage layer, as a result of mitosis and deposition of new matrix near the boundary. From within the cartilage, mitosis of chondrocytes and deposition of new matrix contributes to interstitial growth of the same cartilage layer (Hayes et al., 2001; Tortora and Grabowski, 1992). This layer is composed mainly of collagen type II, while the fibrous outer layer is composed mainly of collagen types I, III and V (McBrien and Gentle, 2003).

With myopia-inducing stimuli, the fibrous layer of the chick sclera thins (Gottlieb et al., 1990), similar to other fibrous only scleras, and there are increased numbers of smaller diameter collagen fibril in the posterior regions (Kusakari et al., 2001). The fibrous and cartilaginous layers appear to respond reciprocally to visual manipulations (Marzani and Wallman, 1997; Schippert et al., 2006). Thus, instead of thinning, the posterior cartilaginous sclera thickens (Gottlieb et al., 1990), correlating with observed increases in the number of proliferating chondrocytes and extracellular matrix deposition (Marzani and Wallman, 1997; Rada et al., 1994). These findings relate to form-deprived myopic eyes. Despite myopic scleras having a thicker than normal cartilage layer, they were found to be weaker than normal in an independent study of scleral creep (Phillips et al., 2000), lending support for our choice of the chick model for our initial exploration of scleral strengthening strategies. Equivalent histological data are not available for the defocus (negative lenses)-induced myopia in the chick, although increased accumulation of ECM in the cartilaginous layer of eyes exposed to negative lenses has been reported (Rada et al., 1998). Nonetheless, the rate of ocular elongation is reported to be slightly lower in negative lens-wearing eyes than that of form deprived eyes (Kee et al., 2001). While the mechanism by which these and other changes, e.g. in gene expression of matrix metalloproteinases (MMPs) and tissue inhibitors of metalloproteinases (TIMPs) (Schippert et al., 2006), are translated into eye size changes is not well understood, nonetheless, they appear fundamental to myopia progression.

The study reported here evaluated the scleral responses to two different polymer formulations, poly(2-hydroxyethyl methacrylate) (pHEMA) and poly(vinyl-pyrrolidone) (PVP), implanted adjacent to the outer scleral surface of normal chick eyes, as well as form-deprived and lens-induced myopic chick eyes for the latter formulation. Both polymers were considered as potential candidates for synthetic scleral grafts for treating high myopia. Our goal was to strengthen the sclera in both cases, although the underlying mechanisms were expected to be different. The choice of pHEMA hydrogel was based on their proven ocular biocompatibility as contact lenses (Kidane et al., 1998; Yasuda, 2006). We anticipated fibrous encapsulation of the pHEMA implant, which was not expected to show any substantial degradation over time. We speculated that the encapsulated implant could provide mechanical support to the sclera. On the other hand, the PVP hydrogel was expected to dissolve over time and thus offer no direct mechanical support. However, the stimulation of connective tissue formation as reported with sub-Tenon's capsule injections of PVP in a Russian-based human myopia control study (Avetisov et al., 1997) may serve to strengthen the sclera directly and slow ocular elongation.

Although granulomatous inflammatory reaction was mentioned, the specific mechanism was not elucidated. By using the chick in the current study, we aimed to learn more about the anti-myopia effect of this polymer as well as the differences in the mechanisms underlying normal and myopia eye enlargement, and also differences between avian and mammalian eyes.

2. Materials & Methods

2.1 Animals & experiments

White Leghorn chicks (*Gallus gallus domesticus*) were obtained as hatchlings from a commercial hatchery (Privett Hatchery, Portales, NM) and reared in 12/12-hour light/dark cycle, with food and water available ad libitum. The room temperature was maintained between 83-89°F. A total of fifty-four birds were used for this study. Care and use of the animals were in compliance with an animal use protocol approved by the Animal Care and Use Committee of the University of California, Berkeley, and adhered to the ARVO Statement for the Use of Animals in Ophthalmic and Vision Research.

Table 2-1. Treatments and animal numbers detailed for each of the 4 experiments in the study. All treatments were monocular, with random but equal distribution of L and R eyes. Chicks were 14 days old at the time of surgery.

Experiment	Number of birds	Implant surgery	Optical treatment	Days monitored
1	6	pHEMA	none	29
2	12	PVP	none	22
	4	saline	none	22
3	12	PVP	diffuser	25
	4	saline	diffuser	25
4	12	PVP	-10 D	25
	4	saline	-10 D	25

The study comprised four experiments, the details of which are summarized in Table 2-1. In brief, chicks underwent one of two types of monocular scleral implant surgery involving either a solid pHEMA implant or an injectable PVP implant material designed for in situ polymerization. Both procedures were performed on otherwise untreated eyes. In addition, because we were interested in the efficacy of such implants for myopia control, PVP implants were combined with 2 myopia-inducing optical manipulations, white plastic diffusers and -10 D lenses, which were fitted over the implanted eyes immediately after the surgical procedure. As a control for the surgical procedure, all experiments included birds that underwent sham surgery. All chicks were 14 days old at the time of implantation. Greater number of chicks was used for treatment groups than sham groups since treatment group chicks were sacrificed weekly for histological analyses. The small differences in the durations of treatment periods between

polymer treatment groups are solely due to logistical planning, but were kept as close as possible. Left and right eyes were randomly selected for treatments.

2.2 Preparations of implant materials

2.2.1 pHEMA synthesis (Song et al., 2003; Song et al., 2005)

Implant materials were used as provided by the Lawrence Berkeley National Laboratory (Berkeley, CA). The synthesis is briefly described here. All chemicals were from Aldrich (St. Louis, MO) and used without further purification unless otherwise specified. All water used was ultra pure ASTM type I reagent grade (18.2 MΩ-cm, pyrogen free, endotoxin < 0.03 EU/m). pHEMA was fabricated from the hydrogel monomer, 2-hydroxyethyl methacrylate (HEMA), with ethylene glycol dimethacrylate (EGDMA) as a crosslinker. The hydrogel monomer was freshly distilled under reduced pressure to remove radical inhibitors prior to its use. The crosslinker was stored over 4-Å molecular sieve prior to use. In a typical procedure, HEMA and EGDMA were mixed with Milli-Q water (100 µL water / 500 mg HEMA), ethylene glycol (EG)(150 µL EG / 500 mg HEMA), and 2 radical initiators, sodium metabisulfite (150 mg/mL aqueous solution, 50 µL / 500 mg HEMA) and ammonium persulfate (400 mg/mL aqueous solution, 50 µL / 500 mg HEMA). The mixture was thoroughly mixed, transferred into a glass chamber (approx. 5 cm X 2 cm X 1 mm), and left to polymerize overnight. The crosslinked hydrogels were then washed in Milli-Q water for a day with frequent changes of water to remove both the radical initiators and residual unpolymerized monomers and crosslinkers. pHEMA hydrogels were then sterilized in 70% ethanol, after which they were stored in sterile saline at room temperature until implantation. Although four different hydrogels corresponding to 4 different crosslinker densities - 2, 5, 10 and 20 wt% (weight of crosslinker EGDMA divided by the weight of monomer HEMA) were synthesized, the 2 wt% hydrogel had insufficient handling strength, and the 10 and 20 wt% hydrogels were too stiff for surgical implantation. Thus, only the 5 wt% hydrogel was implanted.

2.2.2 PVP preparation (Avetisov et al., 1997)

The polymer reagents were provided by the Helmholtz Research Institute of Eye Diseases (Moscow, Russia), and stored at room temperature away from light until used. They comprised a mixture of PVP, acrylamide hydrazide, and ethylacrylate, which accounted for 75% of the total mass of the polymer, and a catalytic solution containing iron monoxide, copper citrate, boric acid, and hydrochloric acid, which accounted for the residual 25% of the total mass. To prepare the polymer for injection, one drop of 3% hydrogen peroxide (approximately 5 µL) was added as an initiator to 500 µL total volume of the above mixture, followed by vigorous stirring to ensure its uniform distribution. Because this polymer is designed for in situ polymerization, it was always freshly prepared, then drawn into a 1 cc syringe for delivery.

2.3 Implant surgical procedures

Chicks were anesthetized with 2% isoflurane in oxygen for surgery. In both surgeries, access to the orbit was gained through a small temporal incision. To maximally expose the posterior pole, a 7-0 silk anchoring suture was placed in the anterior sclera to rotate and fix the

eye. With the pHEMA hydrogel, individual strips (~10 X 3 X 0.5 mm) were positioned over the posterior pole, longest dimension horizontally oriented, and sandwiched between the sclera and the dorsal oblique extraocular muscle. With the PVP hydrogel, about 100 µL was injected over the posterior pole using a curved, blunt-end 19G needle (sub-Tenon's anesthesia cannula needle, BD Ophthalmic Systems; Franklin Lakes, NJ). After injection, a gauze pad was applied over the incision site as the needle was withdrawn to prevent backflow of the liquid polymer. The incision site was then slightly massaged with the gauze to ensure even distribution of the polymer over the scleral surface. As the final step of both procedures, the incision site was sutured close and an antibiotic ointment was prophylactically applied. The procedure followed in the sham surgery was identical to that followed for PVP hydrogel except that sterile phosphate buffered saline (PBS) was injected instead.

2.4 Measurement & analyses of ocular dimensions

Axial eye growth was monitored *in vivo* using a custom high frequency (30 MHz) A-scan ultrasonography set-up (Nickla et al., 1998; Schmid et al., 1996), which offers measurement precision down to 10 µm. The axial dimensions of the main ocular components - anterior chamber, crystalline lens, and vitreous chamber, as well as thicknesses of the retina, choroid, and sclera were obtained by averaging a minimum number of 12 measurements per eye per time point. Chicks were anaesthetized with 1.5% isoflurane in oxygen during all measurements. Data were collected on the day of but before the surgery (day 0; baseline), as well as at 2-4 day intervals out to 29 days post-surgery for the pHEMA-implanted chicks, and at 3-7 day intervals out to 22 or 25 days for PVP-implanted chicks. The chosen time frame for the experiment involving the defocusing lenses took into account the fact that the myopic eye growth compensates for the imposed defocus. As such strategies cannot guarantee consistency of myopic growth signals, we chose to terminate the study at a time when the chicks were likely to have nearly compensated for the imposed defocus.

Of greatest interest in this study were the effects of the implants on scleral growth. Apart from scleral thickness, scleral cup depth was calculated as the sum of vitreous chamber depth, retinal thickness, and choroidal thickness, as an index of scleral surface area. Scleral thickness was not included in this parameter to allow for the possibility that it changed independently of sclera surface area. It was also not included in the derived axial length, which was calculated as the sum of anterior chamber depth, lens thickness, and scleral cup depth. Axial length is used as an index of ocular elongation.

Data from treated and fellow control eyes were compared statistically on the animals surviving the experimental duration (n = 6 chicks for each pHEMA or PVP treatment group analyzed; n = 4 chicks for each sham group), using two-way repeated measures ANOVAs, post-hoc tests, and paired t-tests (Statview, Version 4.0; SAS Institute, Cary, NC). ANOVAs used normalized data for both treated and fellow eyes; in each case, the baseline means for each group matched the overall baseline mean for all groups. A p-value of less than 0.05 was taken as an indicator of statistical significance. Data were reported as means with standard errors in tables, and normalized means with standard errors in graphs.

2.5 Histological analyses

To investigate the effects of the implants on scleral histology, three randomly selected chicks from the polymer-implanted groups were sacrificed by CO_2 asphyxiation at weekly intervals post-implantation, with the remainder six being sacrificed at the end of each experiment. All chicks undergoing sham surgery were sacrificed at the end of the experiments. Eyes were carefully enucleated immediately after sacrifice, leaving the implants and any associated connective tissue in place. The enucleated eyes and implants were visually inspected under a surgical microscope. The anterior segments of the eyes were then removed and the posterior scleral cups fixed overnight at 4 °C in 4% paraformaldehyde in 0.1 M Sorensen's buffer with 3% sucrose. The fixed scleral cups were then rinsed three times in 0.1 M Sorensen's buffer for 10 min each, before being cryoprotected overnight with 30% sucrose in 0.1 M Sorensen's buffer at 4 °C. Afterwards, samples were embedded in Tissue-Tek Optimal Cutting Temperature compound at -25 °C using a dry ice-chilled alcohol slurry. Posterior eyecups were embedded with clearly marked directions on the frozen sample block to allow localization of the posterior pole in subsequent sectioning. Ten µm horizontal (temporal-nasal direction) cryostat sections were cut, air-dried, and stained with 1% toluidine blue in benzoate buffer (pH 4.4, room temperature) for pHEMA treatment sections, and with Masson's Trichrome for PVP treatment sections.

Because changes in chondrocyte numbers are an expected feature of scleral growth changes, four sections representing each time interval for each treatment group were randomly selected for cell counting. Sections were spaced at least 0.5 mm apart (range: 0.5 to 1 mm). A 0.1 mm^2 area, randomly selected from the posterior pole region of each section was analyzed using ImageJ (Abramoff et al., 2004) with a Cell Counter plug-in installed (Kurt De Vos, University of Sheffield, UK). Only chondrocytes with distinct nuclei were counted. Data from each treatment group, expressed as mean counts per unit area (0.1 mm^2; ± standard error), were analyzed statistically and compared to their fellow groups across each time interval, using paired *t*-tests, with a value of $p < 0.05$ as the cut-off for statistical significance. These mean data were shown graphically with standard errors as error bars.

3. Results

The implantation procedures targeted the sclera, the intention being to promote scleral thickening at the posterior pole and slow ocular elongation. There were significant differences in responses induced by the two polymers. Additional fibrous tissue was observed, encapsulating the pHEMA implant. On the other hand, the PVP polymer induced significant scleral thickening although not under all conditions. The scleral implants did not affect the overall rate of elongation of eyes under any of the test conditions. These results are described in more detail below.

3.1 Ocular components

3.1.1 Effects of pHEMA hydrogel implants

Normal eyes: In terms of the axial growth of the principal ocular components, the pHEMA implants applied to otherwise untreated eyes had no significant effect, except on scleral thickness, which increased in response to the implant towards the end of the monitoring period. The mean axial dimensions of the principal ocular components collected at the last time point for implanted and fellow eyes are summarized in Table 2-2, and the changes across the monitoring period in scleral thickness, scleral cup depth, and axial length for implanted and fellow eyes are plotted in Figure 2-1. Interocular differences in scleral thickness reached statistical significance on days 22, 25, and 29 ($p < 0.05$, ANOVA post-hoc tests). By the end of the monitoring period (day 29), treated eyes recorded a mean scleral thickness of 170 ± 6 µm compared to 154 ± 6 µm for the fellow eyes, an increase of approximately 10%.

Table 2-2. Mean axial ocular dimensions (± standard error) of pHEMA group measured 29 days after implantation, normalized to pretreatment baseline (* $p < 0.05$, paired *t*-test).

Ocular Component	Eye	Mean ± SE (mm)
Anterior chamber	Treated	1.845 ± 0.020
	Fellow	1.877 ± 0.0015
Crystalline lens	Treated	2.826 ± 0.035
	Fellow	2.777 ± 0.035
Vitreous chamber	Treated	6.561 ± 0.101
	Fellow	6.587 ± 0.087
Retina	Treated	0.241 ± 0.004
	Fellow	0.245 ± 0.005
Choroid	Treated	0.189 ± 0.0015
	Fellow	0.217 ± 0.021
Sclera	Treated	0.170 ± 0.006*
	Fellow	0.154 ± 0.006
Scleral cup	Treated	6.991 ± 0.108
	Fellow	7.049 ± 0.080
Axial length	Treated	11.661 ± 0.114
	Fellow	11.703 ± 0.096

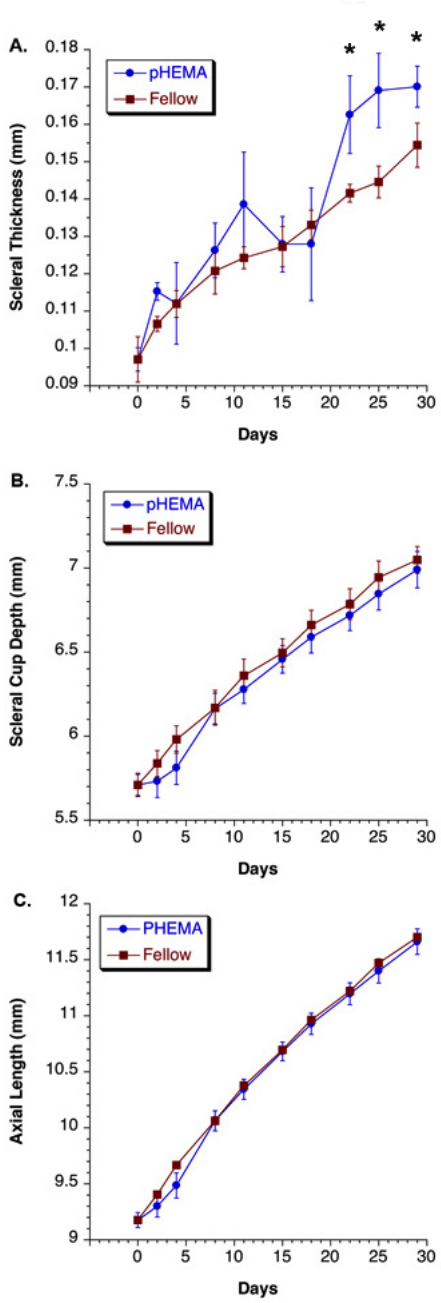

Figure 2-1. Mean scleral thickness (A), scleral cup depth (B) and axial length (C), plotted as a function of time for pHEMA-implanted eyes and their fellows. Asterisks indicate significant interocular differences ($p < 0.05$, ANOVA post-hoc tests; $n = 6$). Error bars = SEM.

3.1.2 Effects of PVP hydrogel implants

Normal eyes: As with the pHEMA implants, the PVP implants did not significantly affect the growth of the principal ocular components of implanted eyes except for scleral thickness (Table 2-3). Implanted eyes showed significant increases in scleral thickness, with the changes being more dramatic with this polymer. Scleral thickness increase reached statistical significance beyond 8 days post-implantation ($p < 0.01$, repeated measures ANOVA; Fig. 2-2A: PVP/No Lens), and by day 22, the last day of the monitoring period, the scleras of treated eyes were approximately 51% thicker than the scleras of fellow eyes, i.e. 206 ± 30 µm compared to 136 ±7 µm ($p < 0.01$, paired *t*-test; Table 2-3). Interestingly, despite the implanted eyes having thicker than normal scleras, there were no statistically significant differences between the implanted eyes and their fellows with respect to either axial length or scleral cup depth, the latter dimension providing an index of scleral surface area (Fig. 2-2B, C: PVP/No Lens).

Table 2-3. Mean axial ocular dimensions (± standard error) measured 22 days after implantation, normalized to pretreatment baseline values (* $p < 0.01$, paired *t*-test).

Ocular Component	Eye	Mean ± SE (mm)	
		PVP implant	Saline control
Anterior chamber	Treated	1.793 ± 0.023	1.770 ± 0.037
	Fellow	1.798 ± 0.022	1.764 ± 0.049
Crystalline lens	Treated	2.700 ± 0.002	2.722 ± 0.032
	Fellow	2.716 ± 0.046	2.746 ± 0.038
Vitreous chamber	Treated	6.478 ± 0.152	6.293 ± 0.129
	Fellow	6.451 ± 0.136	6.274 ± 0.145
Retina	Treated	0.238 ± 0.002	0.247 ± 0.008
	Fellow	0.235 ± 0.003	0.251 ± 0.007
Choroid	Treated	0.215 ± 0.001	0.194 ± 0.001
	Fellow	0.237 ± 0.030	0.175 ± 0.009
Sclera	Treated	0.206 ± 0.030*	0.140 ± 0.008
	Fellow	0.136 ± 0.007	0.137 ± 0.004
Scleral cup	Treated	6.931 ± 0.111	6.734 ± 0.137
	Fellow	6.923 ± 0.109	6.700 ± 0.149
Axial length	Treated	11.423 ± 0.147	11.226 ± 0.174
	Fellow	11.436 ± 0.126	11.210 ± 0.185

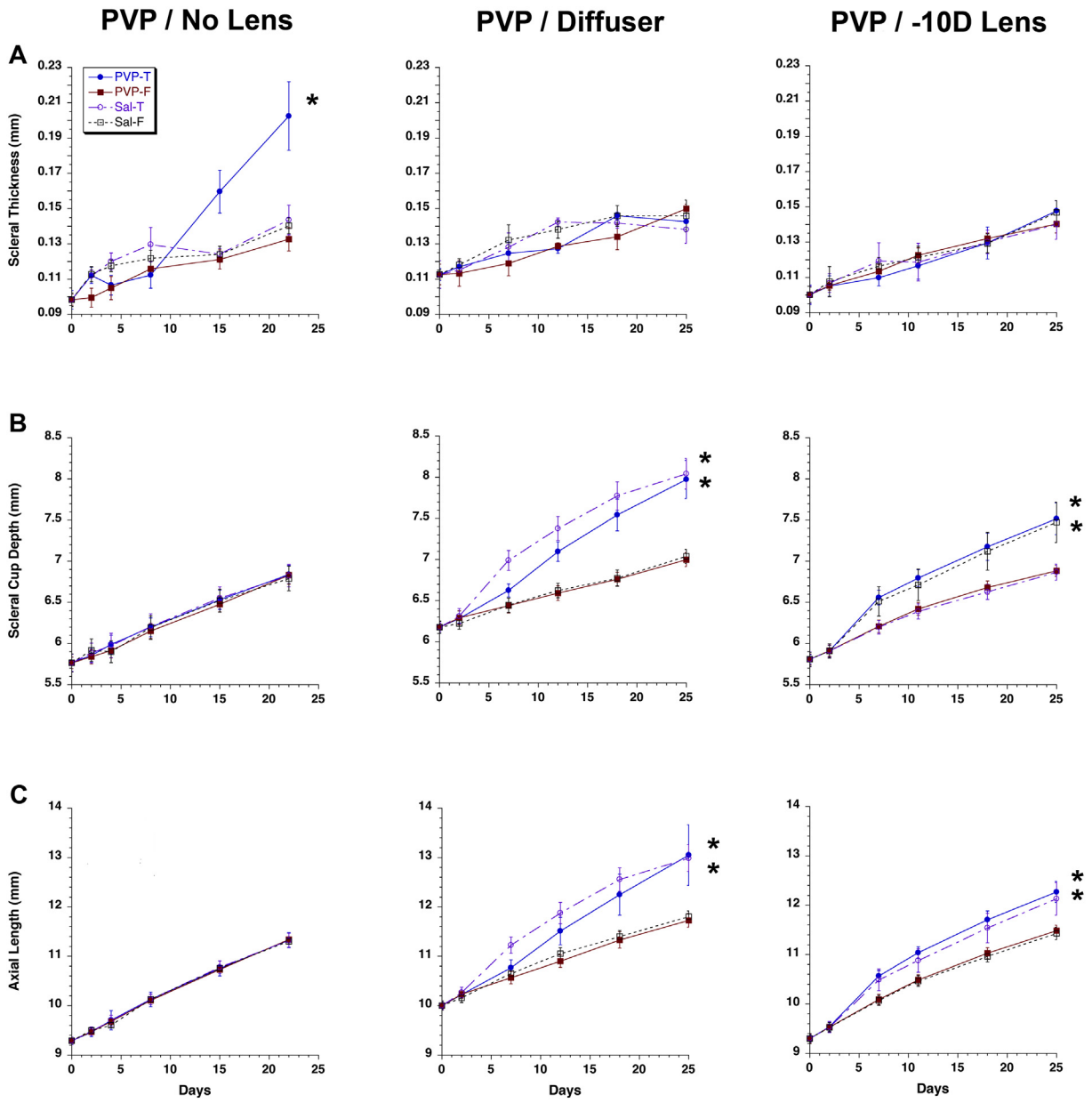

Figure 2-2. Mean scleral thickness (A), scleral cup depth (B), and axial length (C), plotted as a function of time for implanted treatment eyes (T) and their fellows (F) for *PVP/No Lens* group (left column), *PVP/Diffuser* group (middle column), and *PVP/-10D* Lens group (right column). Equivalent data for saline-injected (Sal) sham surgery groups are also shown. Asterisks indicate significant differences between treated and fellow eyes ($p < 0.01$, repeated measures ANOVA; $n = 6$). Error bars = SEM.

Form-deprived myopic eyes: As expected, the saline-injected, diffuser-treated eyes (sham-surgery group) showed significantly increased axial lengths, being approximately 10% longer than their fellow eyes by day 25 ($p < 0.01$, paired *t*-test; Table 2-4 & Fig. 2-2C: PVP/Diffuser). The PVP-injected, diffuser-treated eyes showed a similar growth profile to the sham-surgery group, increasing their axial lengths by 11% relative to their fellow eyes by day 25 ($p < 0.01$, paired *t*-test; Table 2-4 & Fig. 2-2C: PVP/Diffuser). Likewise, both PVP/diffuser

(13.8%) and saline/diffuser (14.4%) groups recorded significant increases in scleral cup depths of treated eyes compared to those of fellows by day 25 ($p < 0.01$, paired *t*-test; Table 2-4).

Table 2-4. Mean axial ocular dimensions (± standard error) measured 25 days after implantation, normalized to pretreatment baseline values (* $p < 0.05$, ** $p < 0.01$; paired *t*-test).

Ocular Component	Eye	Mean ± SE (mm)			
		PVP/Diffuser	Saline/Diffuser	PVP/-10 D	Saline/-10 D
Anterior chamber	Treated	2.309 ± 0.373	2.223 ± 0.075**	2.103 ± 0.071**	1.972 ± 0.099
	Fellow	1.876 ± 0.023	1.855 ± 0.002	1.812 ± 0.022	1.787 ± 0.024
Crystalline Lens	Treated	2.780 ± 0.034	2.711 ± 0.048	2.661 ± 0.029	2.670 ± 0.024
	Fellow	2.865 ± 0.033	2.896 ± 0.027	2.789 ± 0.036	2.773 ± 0.001
Vitreous chamber	Treated	7.670 ± 0.222*	7.597 ± 0.202*	7.118 ± 0.178**	7.048 ± 0.254*
	Fellow	6.619 ± 0.088	6.532 ± 0.083	6.431 ± 0.075	6.371 ± 0.085
Retina	Treated	0.224 ± 0.001*	0.191 ± 0.002	0.226 ± 0.008**	0.229 ± 0.005**
	Fellow	0.245 ± 0.003	0.244 ± 0.007	0.247 ± 0.005	0.250 ± 0.002
Choroid	Treated	0.131 ± 0.002	0.202 ± 0.035	0.182 ± 0.028	0.188 ± 0.001
	Fellow	0.188 ± 0.024	0.211 ± 0.002	0.222 ± 0.001	0.229 ± 0.002
Sclera	Treated	0.143 ± 0.003*	0.138 ± 0.001	0.148 ± 0.002	0.140 ± 0.001
	Fellow	0.151 ± 0.003	0.145 ± 0.009	0.142 ± 0.005	0.145 ± 0.009
Scleral cup	Treated	8.025 ± 0.232**	7.990 ± 0.185**	7.525 ± 0.193**	7.465 ± 0.246*
	Fellow	7.051 ± 0.084	6.987 ± 0.085	6.899 ± 0.067	6.850 ± 0.098
Axial length	Treated	13.113 ± 0.613**	12.924 ± 0.272**	12.289 ± 0.213**	12.108 ± 0.330**
	Fellow	11.792 ± 0.136	11.738 ± 0.115	11.500 ± 0.110	11.411 ± 0.125

In comparing the interocular differences between PVP and sham groups, statistical significance was obtained for scleral thickness at day 18 and for scleral cup depth at day 2 ($p < 0.05$, paired *t*-test; Table 2-5). Statistically significant increases in interocular differences were observed in both scleral cup depth and axial length from 2 to 25 days for both PVP and sham groups ($p < 0.01$, repeated-measures ANOVA; Table 2-5). The PVP-injected eyes did show a somewhat slower rate of growth in axial length and scleral cup depth initially relative to the sham group, perhaps indicating a subtle inhibitory effect of the PVP hydrogel implant on ocular elongation. However, this effect was both subtle and transient (Fig. 2-2B, C: PVP/Diffuser), and between-group differences in either scleral cup depth or axial length never reached statistical significance.

Statistically significant changes were also found in other components of the treated eyes, consistent with previously reported ocular effects of form deprivation in chicks (Kee et al., 2001;

Wildsoet and Wallman, 1995). The treated eyes of the saline/diffuser group exhibited significant increases in both anterior and vitreous chamber depths compared to their fellow eyes ($p < 0.01$ & $p < 0.05$, respectively, paired *t*-test; Table 2-4). Similarly, in the PVP/diffuser group, the vitreous chamber increase in treated compared to fellow eyes reached statistical significance ($p < 0.05$, paired *t*-test; Table 2-4). The treated eyes of both groups also recorded thinner retinas compared to their fellow eyes, although only the difference for the PVP/diffuser group reached statistical significance ($p < 0.05$, paired *t*-test; Table 2-4). Between-group interocular differences did not reach statistical significance for any of these ocular components.

Table 2-5. Mean interocular difference data (treated – fellow eyes; ± standard error) measured up to 25 days post implantation, normalized to pretreatment baseline values. (* $p < 0.05$, ** $p < 0.01$; between PVP and sham: unpaired *t*-test; within PVP or sham over 25 days: repeated-measures ANOVA)

Parameter (µm)	Lens	Treatment	Days				
			2	7	12	18	25
Scleral thickness	Diffuser	PVP	4±3	6±2	-1±3	12±6*	-8±2
		Sham	-3±3	-4±15	4±7	-4±7	-7±8
	-10 D	PVP	-2±5	-5±3	-8±7	-4±8	6±17
		Sham	1±5	5±5	-1±7	3±5	-5±5
Scleral cup depth	Diffuser	PVP**	-9±50*	186±46	504±30	779±111	974±151
		Sham**	89±28	543±132	753±178	1000±241	1004±228
	-10 D	PVP**	-10±32	344±46	368±67	488±101	626±140
		Sham**	6±39	322±123	330±132	503±183	615±181
Axial length	Diffuser	PVP**	-4±25	201±73	612±216	916±329	1322±519
		Sham**	109±16	574±167	822±253	1155±305	1187±312
	-10 D	PVP**	10±29	479±37	557±44	682±79	789±125
		Sham**	1±38	411±150	411±172	572±230	697±242

Lens-induced myopic eyes: Again as expected, saline-injected eyes fitted with -10 D defocusing lenses responded by significantly increasing their axial length, by approximately 6% compared to their fellow untreated eyes by day 25, their axial lengths being significantly different at this time point ($p < 0.01$, paired *t*-test; Table 2-4, Fig. 2-2C: PVP/-10D). Eyes implanted with PVP hydrogel and fitted with -10D lenses responded similarly, their axial lengths being significantly longer, by approximately 7% compared to their fellows by day 25 ($p < 0.01$, paired *t*-test; Table 2-4, Fig. 2-2C: PVP/-10D). There was no significant difference between the two groups in terms of the growth rates of fellow untreated eyes. The treated eyes of both groups also recorded similar and statistically significant increases in scleral cup depth, of approximately 9% by day 25 ($p < 0.05$ saline-injected, and $p < 0.01$ PVP-injected, paired *t*-test; Table 2-4, Fig. 2-2B: PVP/-10D). Interocular differences in scleral cup depth were significant for both PVP and sham groups over the 2 to 25 days period ($p < 0.01$, repeated measures ANOVA; Table 2-5), as were interocular differences for both PVP and sham groups in axial length ($p < 0.01$, repeated measures ANOVA, Table 2-5). However, with respect to scleral thickness there was no difference between treated eyes and their fellows for PVP/-10D lens group (e.g. 148 ± 1.6 vs. 142 ± 5 µm, day 25), or between the treated eyes of the PVP- and saline/-10D lens groups (e.g.

148 ± 1.6 vs. 140 ± 1.2 µm, day 25; Table 2-4, Fig. 2-2A: PVP/-10D). Interocular differences in scleral thickness were also not significantly different between the two groups (Table 2-5).

As with the form-deprived groups, the anterior chambers as well as the vitreous chambers of both the PVP- and saline-injected lens-treated groups were enlarged, although this effect on the anterior chamber reached statistical significance for only the PVP/-10D lens group ($p < 0.01$ anterior chamber, $p < 0.01$ and $p < 0.05$, respectively, vitreous chamber; paired *t*-test; Table 2-4). Here also, treated eyes showed significant retinal thinning, with interocular differences on day 25 reaching statistical significance for both groups ($p < 0.01$ PVP/-10D lens, $p < 0.01$ saline/-10D lens, paired *t*-test; Table 2-4).

3.2 Histological study

3.2.1 Effects of pHEMA hydrogel implants

Normal eyes: Inspection of implanted eyes after their enucleation confirmed that all pHEMA implants were still in place over the posterior pole, between the outer scleral surface and the extraocular muscles. Subsequent histological analyses revealed clearly defined fibrous capsules by 3 weeks post implantation; the capsules were about 50-75 µm thick and surrounded the implants, isolating them from the host tissue (Fig. 2-3A, B, C). The capsules were apparently continuous on their global side with the fibrous layer of the sclera. The pHEMA implants showed minimal change in either transparency or color, suggesting minimal chemical degradation. However, while most of the implants were still physically intact at the end of the monitoring period, some had fragmented, with the resulting smaller pieces of implant material becoming separately encapsulated (Fig. 2-3C). It is plausible that grip marks left by the forceps during positioning of the implants created vulnerable sites for cellular infiltration and subsequent fragmentation. Capsular contraction may also have contributed to fragmentation of the pHEMA implants.

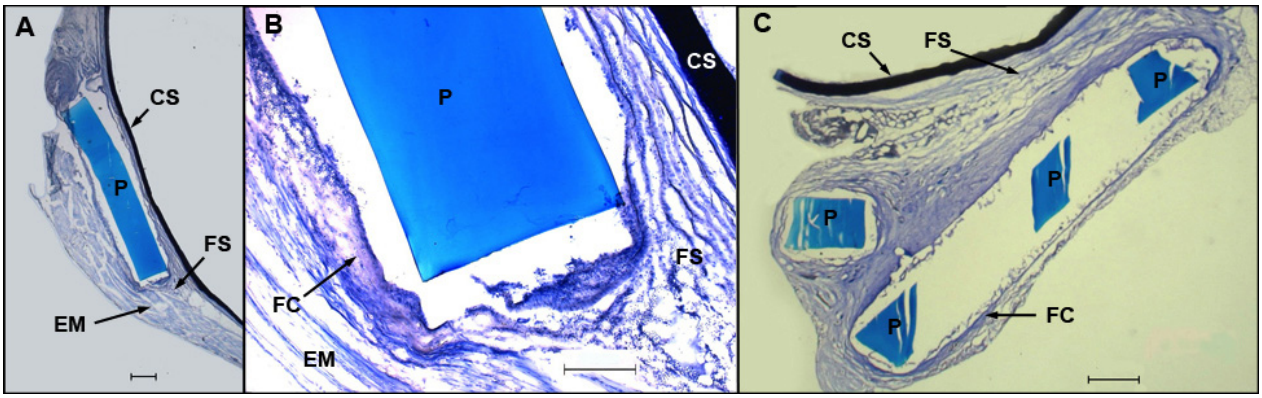

Figure 2-3. Toluidine blue-stained sections from posterior pole region of pHEMA-implanted eyes post implantation, showing (**A**) pHEMA implant (*P*), sandwiched between the fibrous sclera (*FS*) and extraocular muscles (*EM*) and (**B**) fibrous capsule (*FC*) surrounding implant, with cellular infiltration in capsule at 3 weeks; (**C**) encapsulated fragments of implant at 4 weeks. *CS* = cartilage sclera. Scale bars: 500, 200, and 500 µm, respectively.

3.2.2 Effects of PVP hydrogel implants

Normal eyes: The origin of the scleral thickness increase recorded with A-scan ultrasonography was a marked increase in the thickness of the cartilage component of the sclera, as revealed in histological analyses (Fig. 2-4IA, B, C). There was no clear visible sign of the PVP polymer when the eyes were inspected post-enucleation, and there was no evidence of the implanted polymer in any of the histology sections. The scleral thickness increase reflected greatly increased chondrocyte numbers. While there was no difference in the scleral cartilage layers of treated and fellow eyes on day 8 post-implantation, by day 15, the numbers of chondrocytes had significantly increased, by 204% in the scleras of treated eyes compared to those of their fellows (Fig. 2-5A, $p < 0.01$, paired *t*-test). Chondrocyte numbers were still significantly elevated in the scleras of implanted eyes on day 22, by 63% compared to the numbers for fellow eyes ($p < 0.01$, paired *t*-test). These differences imply an increased rate of chondrocyte mitosis in response to the implant.

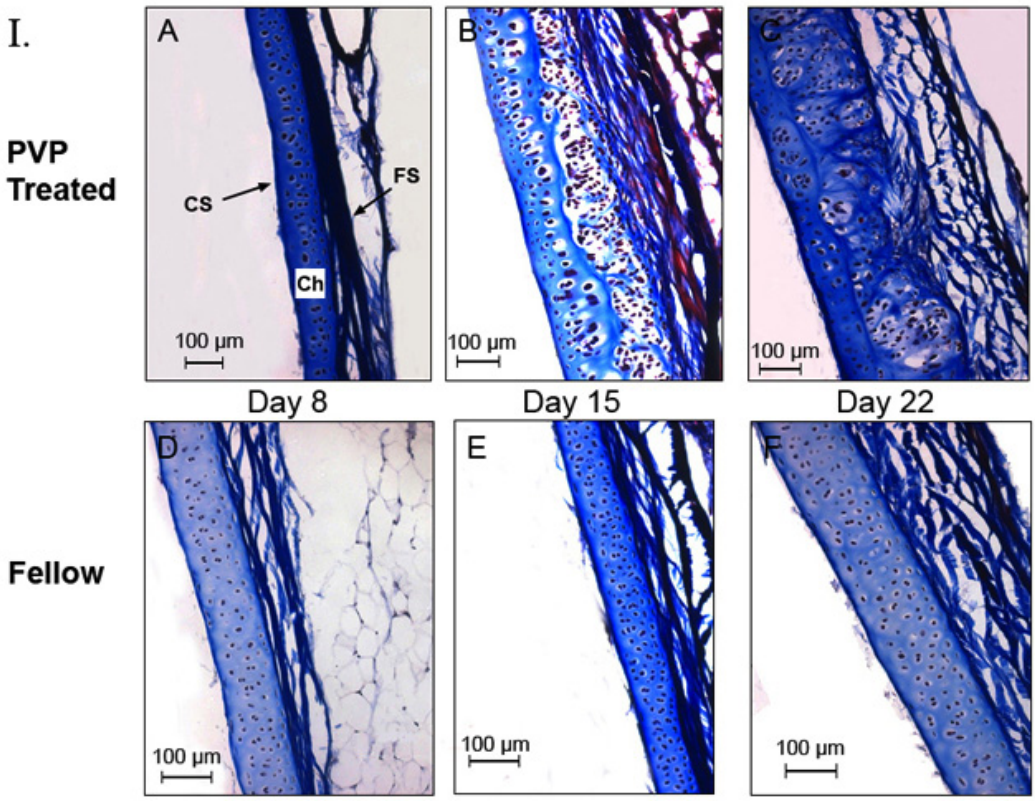

Figure 2-4I. Masson's trichrome-stained scleral sections from the posterior poles of otherwise untreated PVP-injected eyes and their fellows at 8 (A, D), 15 (B, E) and 22 (C, F) days after implantation. FS = fibrous sclera, CS = cartilaginous sclera, Ch = chondrocyte.

While the increase in mitotic activity did not appear to be localized, the outermost (orbital) region contained nests of chondrocytes, which were enclosed in large lacunae, cartilage spaces occupied by numerous proliferating chondrocytes. This gave the tissue a "Swiss cheese" appearance. The proliferating chondrocytes contributed to the increase in thickness of the

cartilage layer (Fig. 2-4IB) and this swiss cheese appearance had largely disappeared by day 22, suggesting that new extracellular matrix material had been added to fill the lacunae (Fig. 2-4IC). No comparable changes in either scleral chondrocyte numbers or histological appearance were evident in fellow eyes over the monitoring period (Figs. 2-5A; 2-4ID, E, F). Specifically, the chondrocytes remained relatively quiescent, although their density increased significantly over the monitoring period (from days 8 to 22; $p < 0.01$, paired *t*-test), likely representing the contribution of chondrocyte proliferation to normal scleral growth. The scleras of saline-injected (sham surgery) eyes were histologically similar to those of fellow eyes, and likewise, their chondrocyte density was significantly less compared to those of the PVP-injected eyes on day 22 (18,600 ± 1,000 vs. 29,400 ± 900 cells/mm^2, respectively, $p < 0.01$, paired *t*-test; Fig. 2-5A).

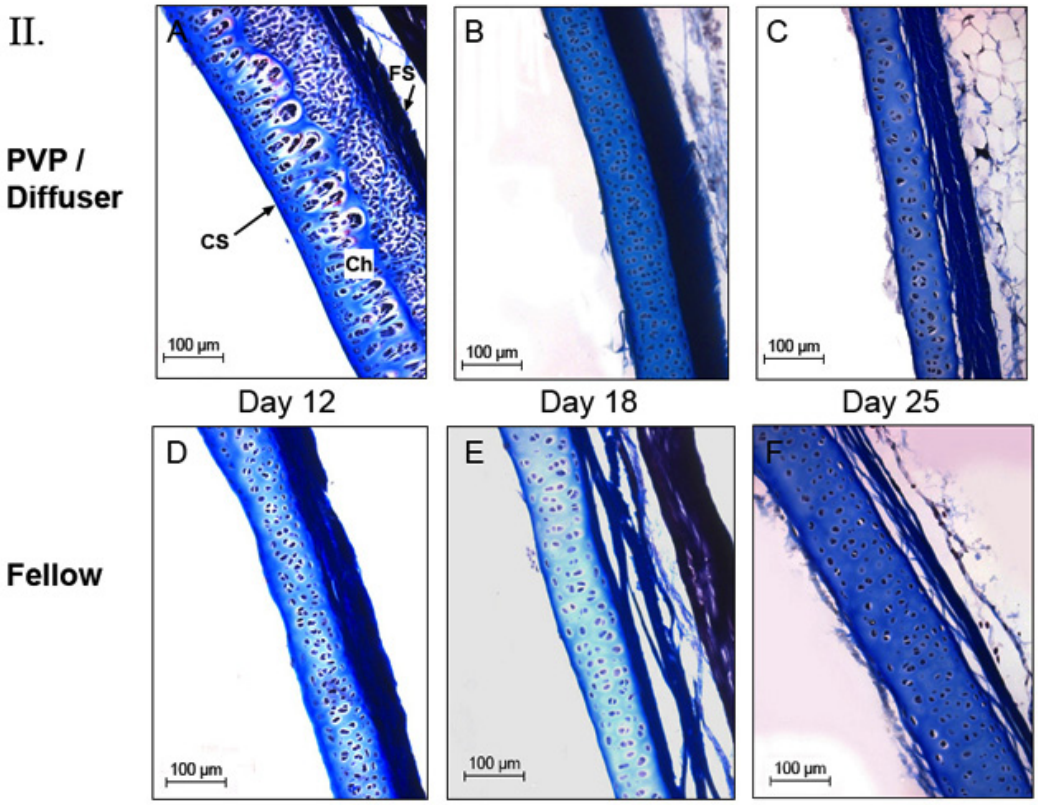

Figure 2-4II. Masson's trichrome-stained scleral sections from the posterior poles of PVP-injected and form-deprived eyes and their fellows at 12 (A, D), 18 (B, E) and 25 (C, F) days after implantation. FS = fibrous sclera, CS = cartilaginous sclera, Ch = chondrocyte.

Form-deprived myopic eyes: Histological analyses of the scleral tissue from form-deprived, PVP-injected eyes revealed both similarities and differences from the results described above for the non-deprived, PVP-injected eyes. Up to 12 days post implantation, treated eyes again showed significantly increased chondrocyte numbers compared to fellow eyes (64,150 ± 1,438 and 16,950 ± 507 cells/mm^2, respectively; $p < 0.01$, paired *t*-test; Fig. 2-5B) with numerous large lacunae in the scleras of implanted eyes (Fig. 2-4IIA). However, in the form-deprived eyes, the proliferative response to injected PVP was more transient than in non-deprived eyes. Thus, although chondrocyte density was still significantly elevated in treated

compared to fellow eyes on both days 18 and 25 ($p < 0.01$, paired *t*-test; Figs. 2-4IIB, C; 2-5B), the scleras of implanted eyes showed a significant decrease in chondrocyte density from day 12 to day 25 ($p < 0.01$, ANOVA post-hoc test). Qualitatively, the scleras of implanted eyes appeared near normal by day 18 (Fig. 2-4IIB). Fellow eyes did not show as much change in either chondrocyte density or histological appearance over the monitoring period (Figs. 2-4IID, E, F; 2-5B), although overall chondrocyte density did show a statistically significant decrease from day 12 to day 25 ($p < 0.01$, ANOVA post-hoc test). This occurred in parallel with the decrease from peak density in treated eyes. The transient nature of the scleral changes in the PVP-implanted eyes is also reflected in the similar chondrocyte densities recorded for the treated eyes of the two diffuser groups at day 25 (PVP 14,400 ± 1,200 vs. saline 16,000 ± 1,200 cells/mm^2; Fig. 2-5B); the treated scleras of these groups also appeared histologically similar. *In vivo* monitoring did not reveal any signs of either interocular or orbital inflammation in implanted eyes over the course of this experiment.

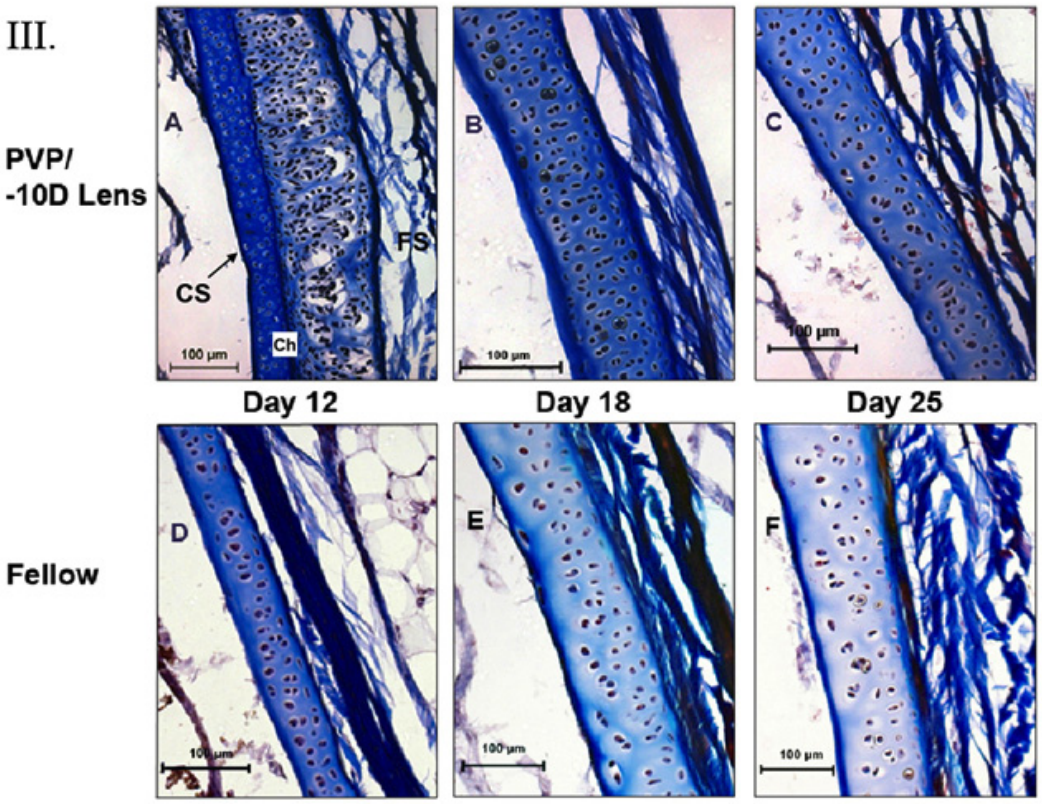

Figure 2-4III. Masson's trichrome-stained scleral sections from the posterior poles of PVP-injected/-10 D lens-wearing eyes and their fellows at 12 (A, D), 18 (B, E) and 25 (C, F) days after implantation. FS = fibrous sclera, CS = cartilaginous sclera, Ch = chondrocyte.

Lens-induced myopic eyes: Histological analyses revealed transient changes in the scleral cartilage of PVP-injected, lens wearing eyes, as described above for PVP-injected form-deprived eyes, with the only difference being that the changes were largely confined to the outer (orbital) scleral region for lens-wearing eyes.

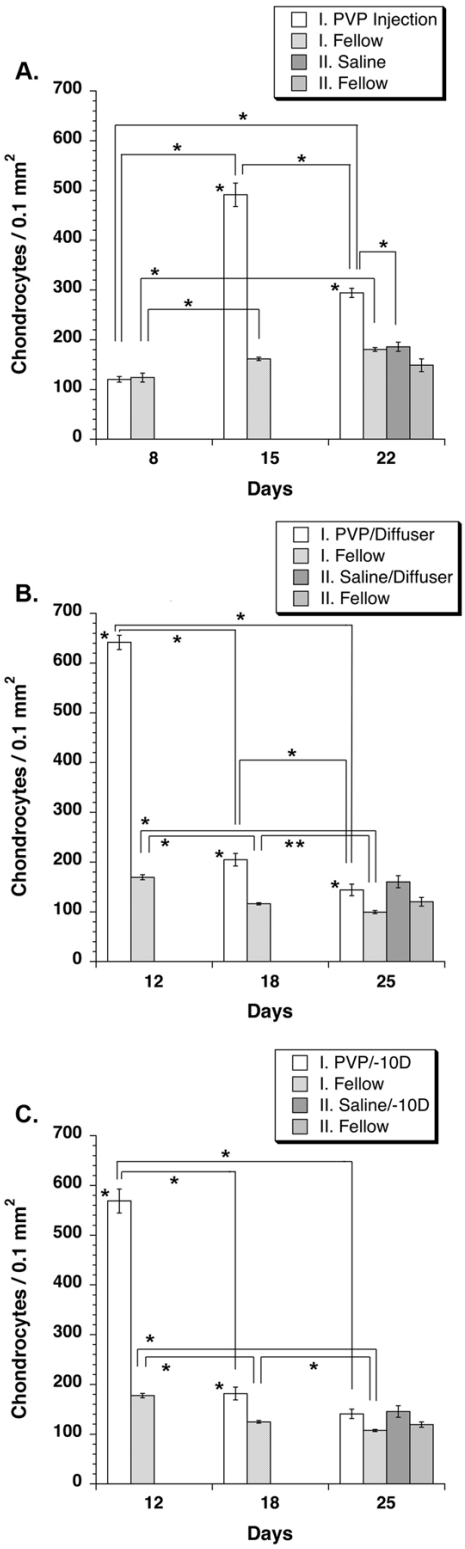

Figure 2-5. Mean scleral chondrocyte densities at posterior pole, averaged over 4 randomly selected sections, 0.5-1.0 mm apart, for PVP-injected eyes, their fellows and saline-injected eyes from (**A**) no visual manipulation, (**B**) form-deprivation, and (**C**) -10 D lens-wearing groups. Sampling time points as in Figure 3-4. (* $p < 0.01$, ** $p < 0.05$, paired *t*-test). Error bars = SEM.

Chondrocyte numbers were significantly increased by post implantation day 12 (Fig. 2-5C), and there were many large lacunae adjacent to the proliferating cells (Fig. 2-4IIIA). Beyond day 18, the scleras of implanted eyes appeared near normal histologically (Fig. 2-4IIIB, C), and by day 25, the last day of the experiment, there were no significant differences in either appearance or chondrocyte numbers between PVP-injected and either their fellow eyes (Figs. 2-4IIIC; 2-5C), or the treated eyes of the saline/-10D group (Fig. 2-5C). Fellow eyes showed a statistically significant decrease in chondrocyte density over the monitoring period ($p < 0.01$, paired *t*-test, Fig. 2-5B), similar to the fellow eyes of PVP-injected form-deprived eyes, and appeared histologically normal (Figs. 2-4IIID, E, F). No signs of either interocular or orbital inflammation were observed in implanted eyes *in vivo* over the monitoring period.

4. Discussion

We investigated the ocular effects of two different hydrogel polymers, pHEMA and PVP hydrogel, delivered as solid and liquid in situ polymerizing implants respectively. Each was applied to the outer posterior scleral surface with the goal of slowing ocular elongation, as required for myopia control. Increased scleral thickening produced by pHEMA or PVP did not inhibit normal growth of the eye. Neither pHEMA implantation nor PVP injection inhibited form-deprived or lens-induced axial elongation. Curiously, the scleral thickening associated with PVP injection in normal eyes was not present in form-deprived and lens-reared animals. Also noteworthy, there were fundamental differences in scleral responses to the two polymers at the histological level. These individual response patterns are discussed in more detail below, along with their significance for myopia control.

While the implanted pHEMA strips quickly became encapsulated, there were no signs of chronic inflammation with the pHEMA implants, which is consistent with the reported biocompatibility of this family of polymers (Yasuda, 2006). This result also attests to the quality of the fabrication process, specifically, the successful removal of toxic chemical contaminants such as the radical initiators. The pHEMA implants also appeared resistant to biodegradation, remaining clear throughout the experiment. Both features are attractive for the current application, in the first case, minimizing the risk to ocular health, and in the second case, ensuring the longevity of the implant, although fragmentation was observed in isolated cases. However, by adjusting the polymer composition (i.e. by increasing or decreasing the crosslinking ratio) and utilizing different tools (e.g. blunt and flat tipped forceps) to handle the implants in the surgery, it should be possible to reduce or eliminate the latter problem.

The encapsulation of the implanted pHEMA strips appears to be a typical tissue response to this type of polymer. For example, in one study, fibrous encapsulation of disks of pHEMA implanted into the flank of rats has been observed (Kermis et al., 2003). In this study, a 30-40 μm thick capsular layer was observed 3 weeks after implantation, on the same scale as the capsules enclosing our implants (50-75 μm). Encapsulation has also been reported with closely related polymer materials such as nonabsorbable scleral buckles, e.g. hydrogel copoly(methylacrylate-2-hydroxyethylacrylate), which are used after vitrectomy in retinal detachment surgery (D'Hermies et al., 1998). The latter study also reported hydrogel fragmentation, as observed in the current study. Similar encapsulating responses have been

observed with other nonabsorbable implant materials, including poly-dimethyl siloxane (Vacanti, 2004), polytetrafluoroethylene, polycarbonate urethane, polyethylene terephthalate, and polyacrylate (Jacob et al., 1996), suggesting that it is not a pHEMA specific response. However, compared to poly-dimethyl siloxane, pHEMA is reported to be more resistant to capsule formation (Vacanti, 2004). This may not be a desirable property, assuming that the fibrous capsule contributes to the mechanical strength of the sclera, a point taken up in later discussion. In addition, the capsule served to bind the implant in place, over the posterior pole.

The increased scleral thickness from fibrous encapsulation of pHEMA implant was not found to slow ocular elongation in the chick. A possible reason for this lack of effect on the rate of ocular elongation relates to the bilayered structure of the chick sclera. It is plausible that the stiffer cartilage component of the chick sclera determines the rate of elongation. In mammalian and primate eyes that have monolayer fibrous scleras, the addition of the fibrous capsule is likely to have a greater impact on scleral biomechanical properties and could plausibly slow ocular elongation. Furthermore, previous studies have found that the posterior sclera of myopic tree shrew eyes to be both thinner and show greater creep rates (Phillips et al., 2000; Siegwart and Norton, 1999). For these eyes, the addition of a fibrous capsule may normalize scleral thickness; it should also increase creep resistance and slow ocular elongation. Note that pHEMA implants have other merits. Specifically, they can be used for local drug delivery (Merrett et al., 2001; Pijls et al., 2007), which for the problem at hand could involve the delivery of peptides or growth factors to enhance the scleral response. However, such experiments were outside the scope of the study described here, and should be preceded by follow-up studies to investigate whether encapsulated pHEMA implants are able to slow elongation in mammalian eyes with fibrous only sclera. Because the pHEMA implants had minimal effect of the thickness of the cartilage layer in our chick eyes, we confined our studies of myopic chick eye to the PVP hydrogel, which induced a clearly distinguishable cartilaginous response in otherwise untreated eyes and for which there was already some evidence of its efficacy for myopia control (Avetisov et al., 1997; Tarutta et al., 1992).

Because the PVP hydrogel is delivered as a liquid mixture that polymerizes in situ, to form a thin transparent film over the posterior sclera in the current application, the possibility that the implant provides direct mechanical support to the sclera can be ruled out. Previously, Avetisov et al. (1997) found that the polymer was still visible after 1 month. However, in our study we found no visible sign of the PVP polymer when the eyes were inspected post-enucleation, possibly due to our lower injection volume, close adherence to the scleral surface after polymerization (thin film nature), and use of posterior outer scleral surface injection for the chick eye rather than sub-Tenon's injection as performed in the mammalian sclera. There also was no evidence in any of the histology sections of the implanted polymer, although it could have been lost during processing. Nonetheless, this polymer was observed to trigger a dramatic scleral response in the form of cartilage layer growth that could plausibly slow ocular elongation, yet we found little evidence of slowed ocular elongation under any condition, even after extending our investigations of this polymer to myopic eyes. These results provide important insights into the implant-tissue interactions for this polymer, and also offer a novel perspective on the mechanisms underlying eye elongation in the chick. Specifically, scleral thickening need not slow eye elongation in the chick.

In contrast to the pHEMA hydrogel implant, the PVP hydrogel had no effect on the fibrous layer of the sclera, but induced significant changes in the cartilaginous layer. Specifically, there was increased chondrocyte proliferation, mostly localized to the outermost, orbital region, under all three experimental conditions with differences in the temporal profile of the changes according to whether eyes were also subjected to optical manipulation. The same region acquired a "Swiss cheese" appearance created by large lacunae in the extracellular matrix (ECM). We interpret the lacunae as evidence of increased ECM remodeling; their transient nature is likely due to increased ECM synthesis. Likewise the decrease in chondrocyte density late in the monitoring period is also likely to be an effect of increased ECM synthesis. Note here that the increased chondrocyte proliferation occurred mostly in the outer region next to the fibrous sclera, indicating that the PVP hydrogel treatment activated appositional growth of the cartilage sclera. It is of interest that in response to form deprivation alone, Kusakari et al. (1997) reported a regional bias in ECM synthesis, being greatest in the inner zone, where the cell density was reduced. If a reduced capacity of the outer zone to synthesize ECM can be inferred from these data, then the lacunae may simply reflect a failure of ECM synthesis to keep pace with chondrocyte proliferation. The gradual return to normal of the sclera cartilage morphology of implanted eyes is presumably an indicator of the residence time of the polymer, although we were unable to detect its presence in histology preparations at any time point.

Similar to the changes in the scleral cartilage of otherwise untreated PVP-injected eyes, the responses of PVP-treated eyes that were fitted with either diffusers or negative lenses were also localized to the outer cartilage region, although more transient. Interactions between the signals underlying the increased elongation in these eyes and the growth modulatory signals induced by the polymer may be responsible for the truncation of the cartilage response to the polymer. As the origin of the signals in the first case is the retina (Wildsoet, 2003), the inner region of the sclera would come under their influence first, while the signals generated by the polymer implant will first affect the outer region. For the same reasons, there are likely to be associated concentration gradients, with the direction of the gradients being opposite. The retina-derived signals also likely outlived the polymer-derived signals, if our conclusion about its limited residence time is valid. Furthermore, it is likely that the retinal signal generated with the diffusers outlived that generated by the –10D lenses, due to the respective open- and closed-loop nature of the conditions imposed. As an aside, it is noteworthy that the scleral changes induced by the combination of the polymer with diffusers and -10 D lenses were very similar, suggesting that the same signal pathways are involved at the level of the sclera. While there is accumulating evidence that different mechanisms underlie form deprivation- and lens-induced myopia (Choh et al., 2006; Kee et al., 2001; Yew, 2004), it is plausible that different retinal signals could converge on a common downstream pathway.

Comparison of our data from sham (saline-injected) eyes with those of Kusakari et al. (1997) revealed qualitative similarities but quantitative differences for form deprived eyes. For example, they reported a chondrocyte density for form deprived eyes of approximately 10,000 cells/mm^2 at the posterior pole (combination of inner and outer zones of the cartilage sclera) compared to 5,000 cells/mm^2 for fellow eyes, representing a 2-fold increase of chondrocyte density due to the form deprivation treatment. Chicks were deprived as day-old chicks for 14 days in the latter study. In the current study, chicks were deprived for 25 days, starting at 14 days of age, resulting in a somewhat smaller, i.e. 1.32-fold, increase in chondrocyte density. However,

equivalent cell densities were consistently higher across all groups compared to those reported by Kusakari et al. For example, for the form-deprived saline-injected group, the values were 16,025 ± 1,211 cells/mm^2 (form-deprived, 60% greater) and 12,125 ± 882 cells/mm^2 (fellow, 142.5% greater). The older age of our experimental animals compared to their study is the most plausible explanation for the observed differences between the two studies. The contrasting results of Gottlieb et al. (1990) of reduced instead of increased chondrocyte density in the deprived nasal region compared to the corresponding region of fellow control eyes after 6 weeks of form deprivation of the temporal visual field adds another dimension to this picture, implying that the equatorial region of the chick sclera behaves differently from the posterior pole region.

The goal of the polymer treatments in the current study was to both reinforce the sclera and slow eye elongation. Why did the polymer injections fail to inhibit both normal eye elongation and the excessive axial elongation induced by the –10 D lenses, and only have a small effect on the excessive axial elongation induced by the diffusers? In the earlier study of form-deprived eyes by Kusakari et al. (1997), increased chondrocyte proliferation coupled to thickening of the cartilage layer at the posterior pole of the eye was associated with increased elongation. Although the magnitude of the proliferative response to the PVP polymer was much greater than that reported in the latter study (a 2-fold increase of chondrocyte density due to form deprivation treatment), these data sets provide convincing evidence that increases in cell density and/or increases in scleral thickness do not alone guarantee slowed eye growth in the chick eye, consistent with suggestions by others that changes in the phase relationships between various ocular rhythms are critical to such eye enlargement (Nickla et al., 1998).

Curiously, repeated PVP injections in children are reported to slow myopia progression (Avetisov et al., 1997; Tarutta et al., 1992). This result is at odds with our observation. Nonetheless, there are differences in the morphology of the mammalian and chick scleras, and likely there are additional differences in the hydraulic and growth modulatory influences on these two types of sclera. Although the chick model provides a readily accessible model for biocompatibility testing of polymer implant material, the implied difference in responses between primate (human) and chick eyes to the PVP polymer argues for the use of a mammalian or primate model for efficacy testing of implants intended to slow eye elongation. Nonetheless, the relatively short-lived nature of the observed effect of the PVP polymer in the current study is consistent with the protocol of repeated injections used in the clinical study referred to above. A longer duration of effect would be clinically desirable, both from a practical perspective and in the interest of minimizing the risk of surgical complications. It is also noteworthy that in the chick eye, the fibrous layer of the sclera appeared to be minimally affected by the PVP polymer. This apparent difference between the responses of primate and chick fibrous scleral tissue may reflect feedback interactions between the fibrous and cartilaginous layers of the chick sclera (Marzani and Wallman, 1997), lending further support for follow-up studies with a mammalian model.

5. Conclusion

In summary, the results represent proof of principle that scleral growth can be manipulated using polymeric implants at the outer sclera. Both the physical properties of the

polymer and their chemical composition influenced the pattern of response in the chick eye. The solid pHEMA implant induced fibrous capsule formation adjacent to the sclera, while the liquid PVP hydrogel induced a local growth response in the scleral cartilage. Neither affected the rate of ocular elongation. Because of differences in the morphology of the avian and mammalian scleras, follow-up testing of promising polymers in mammalian eyes will be a necessary prerequisite for establishing their suitability for myopia control in humans. Finally, it will be important to develop methods of extending the duration of action of such polymer treatments to minimize the need for repeated surgical intervention.

Chapter III

Defocus Duration and Power Dependence of Chick Scleral MMP-2, MMP-13, TGF-β2, and TIMP-2 mRNA Expression

Abstract

The purpose of this project was to investigate the effects of manipulating treatment duration and power magnitudes for myopic and hyperopic defocus on scleral mRNA expression levels for gelatinase-A (MMP-2), collagenase-3 (MMP-13), tissue inhibitor of metalloproteinase-2 (TIMP-2), and transforming growth factor-beta 2 (TGF-β2). We looked at response patterns for these gene products that have been implicated in scleral remodeling and have the potential to be used to tailor novel biomaterials to treat high myopia. Monocular myopic or hyperopic defocus was imposed on 3-wks old White Leghorn chicks (*Gallus gallus domesticus*) by fitting them with either -10, -5, plano, +5 or +10 D lens for 4 or 48 hours. Fellow eyes were left untreated as controls. The harvest and separation of the two scleral layers was performed in the afternoon, and relative mRNA levels of MMP-2, MMP-13, TIMP-2 and TGF-β2 were measured by real-time quantitative PCR. Statistical significance was computed by paired student's *t*-test and two-way ANOVA. Statistically significant changes in mRNA expression were observed for all 4 proteins, albeit not at each time point. Typically, the results for fibrous and cartilaginous layers showed opposite trends, as did responses to positive and negative lenses. Expression levels in the fellow eyes of the plus and minus lens groups were not significantly different, i.e. there was no interocular yoking. TGF-β2 expression showed an early increase with positive lenses in both scleral layers, similar to an independent finding in the retinal pigment epithelium after 48h lens wear, and consistent with a role as an inhibitory growth modulator. However, the transient nature of its up-regulation in sclera suggests additional growth modulatory influences on the latter. The cartilage expression patterns for MMP-2 and MMP-13 are consistent with the opposite directions of growth induced by positive and negative lenses. TIMP-2 expression showed robust expression changes, mostly in the fibrous sclera. Their suitability as targets for treatment of high myopia depends on there being equivalent changes with long-term myopia.

1. Introduction

During emmetropization, the posterior scleral extracellular matrix is actively remodeled in an iterative process of synthesis and degradation to match the axial length to the optical power of the eye. In the chick eye, this dynamic remodeling process is finely tuned to allow emmetropization to occur during imposed lens defocus, independent of the central nervous system (Troilo et al., 1987; Wildsoet and Pettigrew, 1988). Specifically, ocular elongation rate increases with negative lens wearing (imposed hyperopia) and the choroid thins. With positive lens wearing (imposed myopia), the ocular elongation rate decreases and the choroid thickens (Wildsoet and Wallman, 1995). Both cases lead to changes in scleral growth rates in the avian eye, and these findings have analogies in mammalian eyes; specifically, similar visually-driven scleral growth responses have also been described in guinea pigs (McFadden et al., 2004), tree shrews (Siegwart and Norton, 2005), marmosets (Graham and Judge, 1999), and rhesus monkeys (Smith et al., 1999). Eyes wearing negative lenses exhibit myopia when the lens is removed. The exact molecular mechanism underlying scleral changes during myopia development is not well understood, but researchers have made some headway in understanding the biological processes by investigating how the eye senses and translates defocus signals to alter scleral growth rate.

Although the actual activation signal producing myopic sclera is not known, specific changes in the matrix composition of sclera is better understood. Scleral thinning and distension of the posterior pole are characteristic changes in high myopia. In highly myopic human eyes, scleral tissue thinning is associated with thinning of the collagen fiber bundles as well as a reduction in the diameters of individual collagen fibrils, averaging below 60-70 nm. These changes are also accompanied by increase in unusual star-shaped fibrils with irregular, serrated borders when observed at cross-sections (Curtin et al., 1979). It is important to note, however, that at least some of the changes in myopic sclera are likely a consequence rather than a cause of myopia. In support of this notion are observations that normal collagen fibril diameters and spacing are present in the sclera of myopic tree shrew eyes after 12 days of treatment, despite significant posterior scleral thinning and a reduction in posterior scleral dry weight (McBrien et al., 2001a). This implies that either rapid tissue loss is attributable to general scleral collagen fibril degradation without bias toward specific collagen fibril diameter populations, or that the fibrous sclera experiences initial degradation only at the proteoglycan level, reducing the amount of the filler extracellular matrix (ECM) to produce the initial scleral thinning observed. The scleral thinning would allow normal intraocular pressure to exert greater stresses directly on the scleral wall, which could further activate the scleral fibroblasts or myofibroblasts, leading to production of new and thus smaller diameter fibrils and subsequent biomechanical changes (McBrien et al., 2009a).

Activated proteases are normally responsible for the degradation of the ECM in the body when the native ECM requires renewal or regeneration due to aging, disease, or injury. Matrix metalloproteinases (MMPs) and their specific regulators, tissue inhibitors of metalloproteinases (TIMPs), regulate the process of ECM renewal or regeneration through the proteolytic cleavage of the core protein structure in collagens and proteoglycans. Members of the MMP and the TIMP families have been found to have an active role in eye growth regulation, with observations in becoming myopia eyes of up-regulation of MMP-2 (gelatinase-A), MMP-14 (membrane type-1 matrix metalloproteinase, MT1-MMP), and down-regulation of TIMP-2 and TIMP-3 (Jones et

al., 1996; Rada and Brenza, 1995; Schippert et al., 2006; Siegwart and Norton, 2005). Several other MMP family members are also known to be present in the mouse eye, including MMP-1 (collagenase-1), MMP-3 (stromelysin-1), MMP-9 (gelatinase-B), and MMP-13 (collagenase-3), but their specific roles, if any, in eye growth regulation are unclear (Ihanamaki et al., 2004). The elevation of MMP activity associated with scleral fibroblasts during myopia progression has been proposed as a potential mechanism for scleral matrix degradation and subsequent axial elongation (Shelton and Rada, 2007; Siegwart and Norton, 2005). The activities of MMP-2, fibroblast proliferation, and proteoglycan synthesis are affected by transforming growth factor-beta (TGF-β), consistent with a role for TGF-β in the control of scleral remodeling during myopic eye growth (Jobling et al., 2004; Overall et al., 1989). Specifically, TGF-β2 expression level was found to be regulated according to the sign of defocus in chick cartilaginous sclera; expression decreased under negative lens treatment, and increased during positive lens treatment (Schippert et al., 2006). However, in the chick fibrous sclera, there was no change in gene expression. Additional clarification with respect to the involvement of the MMPs and TIMPs in scleral remodeling and the role of TGF-β2 as their regulator would not only contribute to understanding scleral remodeling during myopia progression, but also allow potential incorporation of this knowledge into the design of scleral treatments for high axial myopia.

Building on previous findings of visually-induced transcriptional regulation of various proteins in the chick sclera, this study further investigated the effects of treatment duration and lens power for hyperopic and myopic defocus on the mRNA expression for gelatinase-A (MMP-2), collagenase-3 (MMP-13), transforming growth factor beta-2 (TGF-β2), and tissue inhibitor of matrix metalloproteinase-2 (TIMP-2) in the chick outer fibrous and inner cartilaginous scleral layers. The study also sought to confirm whether there were yoked gene expression effects at the transcriptional level for contralateral untreated eyes. To control for possible gene expression changes due to covering the eye with a lens, a group of chicks wearing monocular plano lenses was included in the study. Furthermore, the expression of aggrecan mRNA was measured to verify satisfactory separation of the two chick scleral layers, since aggrecan mRNA is known to be expressed mainly in the cartilaginous chick sclera (Rada et al., 1994). By using different treatment durations and magnitudes of hyperopic and myopic defocus, we aimed to determine whether the scleral response to eye growth modulatory signals involved graded changes in expression or an all-or-none response, independent of the magnitude of defocus and treatment duration.

2. Materials & Methods

2.1 Animals & experiments

White Leghorn chicks (*Gallus gallus domesticus*) were obtained as hatchlings from a commercial hatchery (Privett Hatchery, Portales, NM) and reared in 12/12-hour light/dark cycle, with food and water available ad libitum. Coarse food was provided to prevent clouding of the lens surface during wear. The room temperature was maintained between 83 and 89 ºF. A total of 60 chicks were used for this study. Care and use of the animals were in compliance with an animal use protocol approved by the Animal Care and Use Committee of the University of

California, Berkeley, and adhered to the ARVO Statement for the Use of Animals in Ophthalmic and Vision Research.

The study comprised 10 groups of chicks, the details of which are summarized in Table 3-1. All chicks were 3 weeks old at the start of experiments. In brief, chicks underwent +10, +5, plano, -5, or -10 D monocular (right or left) lens treatment for a duration of either 4 or 48 hours. Lens fitting proceeded in a staggered fashion with a 15 min interval between animals. The positive lenses inhibit eye growth (induce hyperopia), while the negative lenses enhance eye growth (induce myopia). Plano lens group served as controls. Lenses were fitted over the chick eyes using Velcro rings, which were glued to the skin and feathers around the eyes at the start of the experiment. The contralateral eyes were left untreated, but were included to study yoking effects.

Table 3-1. Experimental groups describing lens treatments and treatment durations. All treatments were monocular, with random but equal distribution across right and left eyes. Chicks were 3 weeks old at the start of the experiment.

Number of birds	Lens Treatment (D)	Time (h)
6	+10	4
6	+10	48
6	+5	4
6	+5	48
6	Plano	4
6	Plano	48
6	-5	4
6	-5	48
6	-10	4
6	-10	48

2.2 Measurement & analyses of ocular dimensions

Ocular dimensions were monitored *in vivo* using a custom high frequency 30 MHz A-scan ultrasonography set-up (Nickla et al., 1998). Thickness data for all axial components (anterior chamber, lens, vitreous chamber, retina, choroid, and sclera) were obtained by averaging a minimum of 12 measurements per eye per time point. Chicks were anesthetized with 1.5% isoflurane in oxygen during all measurements, which were taken immediately before lens wearing (baseline), as well as at either 4 or 48 h after. Choroidal thicknesses were reported and used as an index of defocus effects. Axial lengths, which represent the sum of all ocular components except the sclera, were also reported and used as an index of ocular elongation. Data were reported as normalized means with standard errors as error bars in graphs.

2.3 Scleral tissue harvesting and processing

All work surfaces and surgical instruments that could potentially come into contact with tissue samples were cleaned thoroughly with RNase*Zap*® (Ambion, Foster City, CA), followed

by rinsing with DNase/RNase-free distilled water (Invitrogen, Carlsbad, CA) prior to use. Microcentrifuge tubes used in the study were certified DNase/RNase-Free. Chicks were sacrificed at the end of respective treatment period, i.e. after 4 or 48h, by guillotine. To minimize possible circadian rhythm effects on gene expression, animals were always sacrificed in the early afternoon starting at 1 p.m. and continuing at 15 min intervals between animals. Eyes were carefully enucleated immediately after sacrifice. Any attached extraocular muscle, connective tissue, and orbital fat were carefully removed from the sclera. The enucleated eyes were visually inspected under a surgical microscope, and then the anterior segments of the eyes were removed with a pair of surgical scissors cut through around the circumferential edge. The vitreous body was discarded and the pecten was excised from the posterior segment with a minimal V-shape cut. The resulting posterior scleral cup was then placed in cold Ringer's buffer, and retina, retinal pigment epithelium, and choroid were carefully scraped off the sclera. Using very fine sharp surgical forceps, the outer fibrous scleral layer was then separated from the inner cartilaginous layer under a dissecting microscope. The cartilaginous layer was further finely sliced with a scalpel. Harvested scleral tissue samples were immediately placed in individual 1.5 ml microcentrifuge tubes chilled on ice with 500 µl of RNA*later*® RNA Stabilization Reagent (Qiagen, Valencia, CA), incubated overnight at 4 ºC, then stored in the reagent at -20 ºC.

2.4 Scleral RNA isolation

A custom tissue disruption method was followed for both scleral fibrous and cartilage tissue samples. Scleral tissue was removed from the reagent and put into a new microcentrifuge tube. A custom-made 10 cm long stainless steel rod with 3 mm diameter was used as pestle for crushing and grinding the tissue within the microcentrifuge tube. The tissue sample and the pestle were first immersed and snapped frozen under liquid nitrogen in the microcentrifuge tube. The scleral tissue was then crushed and ground to fine powder. Tissue homogenization and total RNA isolation was carried out using an RNeasy Mini Kit (Qiagen, Valencia, CA) following the manufacturer's protocol. All samples were treated with DNase I (RNase-Free DNase Set, Qiagen) using the manufacturer's recommended on-column DNase digestion protocol. RNA yield was determined spectrophotometrically in 10 mM Tris-HCl buffer (pH 7.5) at 260 and 280 nm. Optical density ratios (OD_{260}/OD_{280}) were measured to determine the yield and quality of the isolated RNA. RNA integrity was confirmed using 1% w/v agarose gel electrophoresis in 1X Tris/Borate/EDTA buffer stained with ethidium bromide.

2.5 RNA reverse transcription

Reverse transcription of isolated RNA from both scleral fibrous and cartilage tissue samples was conducted using Sensiscript® RT Kit (Qiagen) following the manufacturer's protocol. A mastermix was created with 0.5 µM oligo-dT primer, 10 µM random hexamer primers (Invitrogen), 10X buffer RT, RNase inhibitor (10 U/µl), Sensiscript reverse transcriptase, dNTP mix (5 mM), and RNase-free water. All RNA samples were reverse transcribed to cDNA using the same mastermix to ensure stable conditions for all samples. The variability of the transcription reaction was estimated by transcribing the same RNA samples twice.

2.6 Real-time PCR

All sequences were obtained from the National Center for Biotechnology Information nucleotide database (NCBI, Bethesda, MD). Primer sequences were designed by using Primer3 v.0.4.0 web interface software (Rozen and Skaletsky, 2000). Primer amplification efficiencies (*E*) were calculated by taking the slope of the regression line of cDNA standard curves with the following equation:

$$E = 10^{\left(-1/slope\right)} \qquad \text{(Equation 2-1)},$$

where a value of 2.0 represents 100% efficiency. In general, efficiencies of 80% or higher are reasonable, while a lower value indicates poor primer binding and/or inhibition of the reaction (Rasmussen et al., 2001). The accession numbers, sequences of designed forward and reverse primer pairs, length of amplified sequences, and calculated amplification efficiencies are shown in Table 3-2. Prior to thermal cycling, each reaction plate was covered by optical adhesive covers to prevent evaporation, and briefly centrifuged for 2 min at 1000 rpm to free any air bubble present in the reaction wells. PCR products amplified by the primer pairs were verified by melt curve analysis and agarose gel electrophoresis.

Table 3-2. Accession numbers of genes investigated in this study, with primer pairs (5' to 3') for real-time PCR and length of amplified sequence with calculated amplification efficiencies.

Gene	Accession Number	Forward Primer	Reverse Primer	Length (bp)	*E*
β-actin	X00182	CTG AAC CCC AAA GCC AAC	CAC CAT CAC CAG AGT CCA TCA C	147	1.91
MMP-2	U07775	TGG TGT GCT TCT ACC AGC AG	GAG TGC TCT AAT CCC ATC GC	122	1.99
MMP-13	AF070478	GAC CCT GGA GCA CTG ATG TT	TGG GTT GGG ATC TCT GTC TC	123	1.95
TGF-β2	X58071	TGG CTC CAT CAC AGA GAC AG	TTG CTT CAG GCT CCT CAC TT	118	1.95
TIMP-2	AF004664	AGT GCC TCT GGA CAG ACT GG	GTC GAG AAA CTC CTC CTG CTT CG	137	1.95
Aggrecan	M88101	ACT GGG ATT TAT CGC TGT G	GCC TGC TTT GCC CTC TCG	140	1.90

Real-time PCR was performed using StepOnePlus™ Real-Time PCR System (Applied Biosystems, Foster City, CA) with StepOne Software v2.0. Primer concentration used was 0.5 μM for both the fibrous and cartilaginous scleras. For quantification of mRNA amounts, the Fast SYBR® Green Master Mix (Applied Biosystems) was used. The thermal cycling protocol comprised enzyme activation duration of 20 s at 95 ºC, denaturation cycle duration of 3 s at 95

ºC, and primer annealing and extension cycle duration of 30 s at 60 ºC. Fluorescence was measured with every cycle at 60 ºC for a total of 40 cycles. A total reaction volume of 20 µl/well included 10% excess volume and a cDNA template amount corresponding to 1 ng RNA per well. Each sample was analyzed in triplicate.

2.7 Real-time PCR data analyses

Analyses of real-time PCR data were based on the threshold cycle (CT) values of the PCR products, following previously described methods (Simon, 2003; Vandesompele et al., 2002). Mean normalized expressions were calculated from our real-time PCR data based on the threshold cycle means and standard errors for the references as well as for the targets. A standard curve was generated for each gene under study for quantitative analysis. The Sequence Detection System software (Applied Biosystems) was used to calculate the baseline and threshold for the amplification curves. The baseline was set to the initial cycles in which there is little change in fluorescence signal, and the threshold was set within the exponential growth phase of the amplification curve.

Mean normalized expressions (*MNE*) were calculated from the derived amplification efficiency for each of the reference and target genes using Equation 2-2 (Simon, 2003):

$$MNE = \frac{\left(E_{reference}\right)^{CT_{reference,\,mean}}}{\left(E_{target}\right)^{CT_{target,\,mean}}} \qquad \text{(Equation 2-2)},$$

The standard errors of the mean normalized expressions (SE_{MNE}) were also calculated by applying the differential equation of Gauss for error propagation, represented by Equation 2-3 (Simon, 2003):

$$SE_{MNE} = MNE \times \sqrt{\left[\left(\ln\left(E_{target}\right) \times SE_{CT_{target,\,mean}}\right)^2 + \left(\ln\left(E_{reference}\right) \times SE_{CT_{target,\,mean}}\right)^2\right]}$$

(Equation 2-3).

Calculated data were tabulated and reported as MNE ± SE_{MNE} and plotted over 4 and 48h for +10, +5, plano, -5 and -10 D monocular lens treatments.

2.8 Statistical analyses

Both ocular dimensions and mean normalized expressions from eyes treated with the same lens and their contralateral control eyes were compared statistically using paired *t*-test. Treatment groups were also compared using two-way ANOVA (Statview, Version 4.0; SAS Institute; Cary, NC). A *p*-value of less than 0.05 was used for statistical significance.

3. Results

3.1 Ocular dimensions

3.1.1 Choroidal thickness

Changes in choroidal thickness are a good measure of short term defocus effects, as choroidal thickening during hyperopic defocus and choroidal thinning during myopic defocus are well known and rapidly occurring responses (Wildsoet and Wallman, 1995). Choroidal thickness was found to significantly increase compared to fellow untreated eyes for chicks wearing +5 D lenses by 67% and 151% at 4 and 48h, respectively ($p < 0.01$). Similarly, a significant choroidal thickness increase was recorded for chicks wearing +10D lenses compared to fellow untreated eyes with increases of 26% and 156% at 4 and 48h, respectively ($p < 0.01$; Figure 3-1A). When the chicks wore negative lenses, the opposite choroidal thickness change was observed (Figure 3-1B). For chicks wearing -5 D lenses, choroidal thickness was significantly reduced by 19% and 20% at 4 and 48h, respectively ($p < 0.05$). However, chicks wearing -10 D lenses did not have significant thickness reduction at 4h, although the mean choroidal thickness was lower in the lens treated eye (0.171 mm vs 0.193 mm in the fellow eye). At 48h, chicks wearing -10 D lenses had significantly lower choroidal thickness by 29% compared to fellow untreated eyes ($p < 0.01$). Plano lens-wearing group was included to determine if there was any effect of simply wearing a lens without defocusing power. Chicks wearing plano lenses had significantly increased choroidal thickness in the lens treated eye compared to the fellow untreated eye by 20% and 18% at 4 and 48h, respectively ($p < 0.05$; Figure 3-1C).

3.1.2 Axial length

In this study, the axial length, a measurement along the optical axis of the eye including all ocular components except the sclera, was calculated to detect changes in overall ocular elongation during treatment. No statistically significant changes in axial length were found in the treated eyes of the positive, negative, or plano lens groups compared to their respective fellow eyes (Figure 3-1D, E, F). Overall, in almost all groups, both treated eyes and their fellows elongated, representing normal ocular growth over 48h.

3.2 Yield and quality of RNA

The average OD_{260}/OD_{280} ratio was 1.87 for fibrous sclera and 1.97 for cartilage sclera. RNA integrity was confirmed by agarose gel electrophoresis as the 28S and 18S ribosomal RNA bands are visible and no DNA band was observed (Figure 3-2A). The mean difference in the threshold cycle value was 0.28±0.22 in the cartilaginous sclera and 0.23±0.32 in the fibrous sclera ($n = 6$, each).

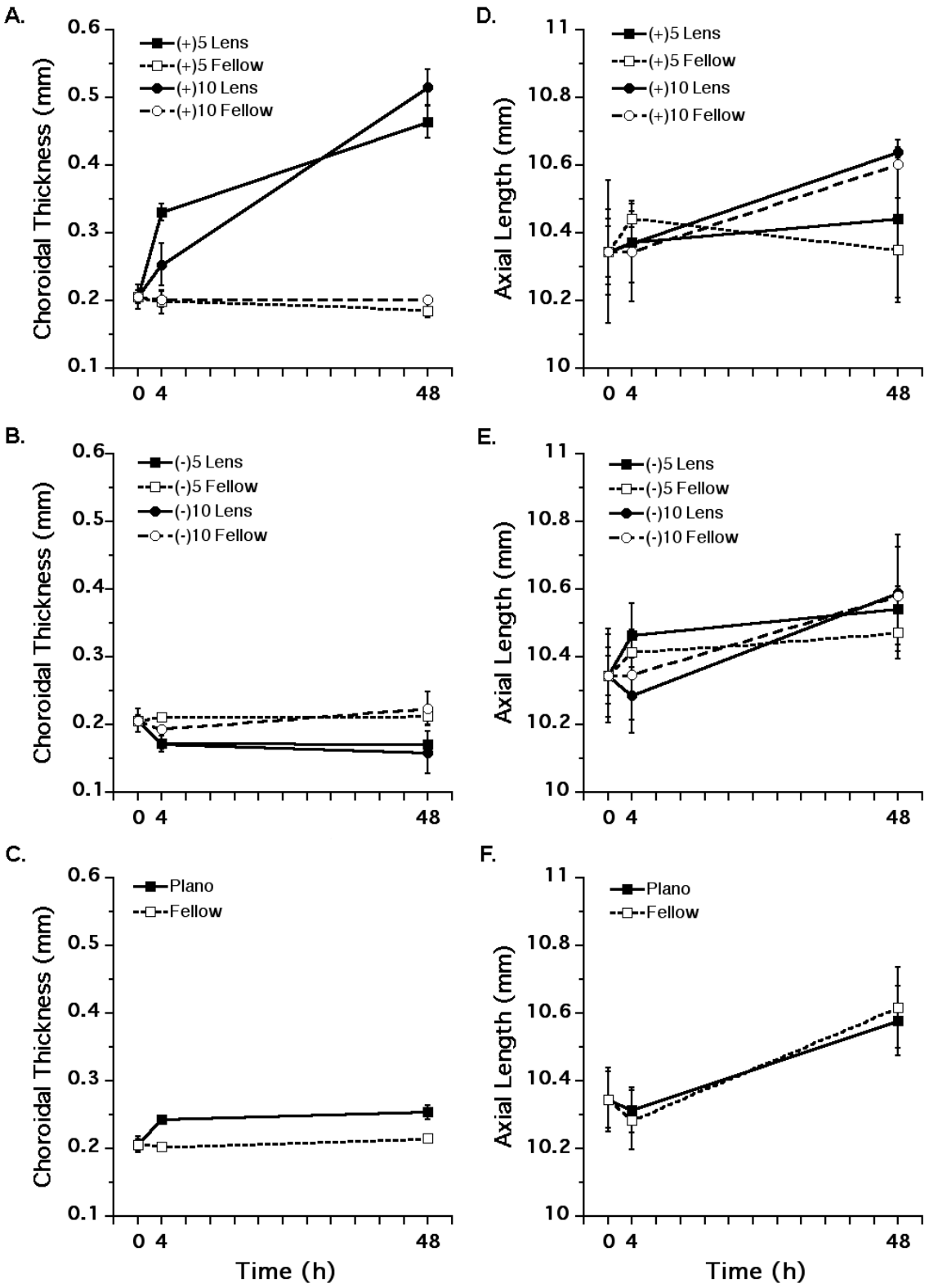

Figure 3-1. Choroidal thicknesses and axial lengths of positive (A, D), negative (B, E), and plano (C, F) lens-treated groups measured (*n* = 6 for each group) at 0, and either 4 or 48 h. Chicks were 3-wks old at start of experiments.

3.3 Real-time PCR product verification

Specificity of the real-time PCR assay was confirmed by both agarose gel electrophoresis and melt curve analyses. Agarose gel electrophoresis demonstrated single bands between 100-200 bp, further confirming reliability of the PCR runs (Figure 3-2B). Melt curve analyses showed individual peaks corresponding to a single DNA product for each gene, with melting points for β-actin at 85.5ºC, MMP-2 and MMP-13 at 74.5ºC, TGF-β2 at 72.5ºC, TIMP-2 at 78.5ºC, and aggrecan at 78.5 ºC (Figure 3-2C).

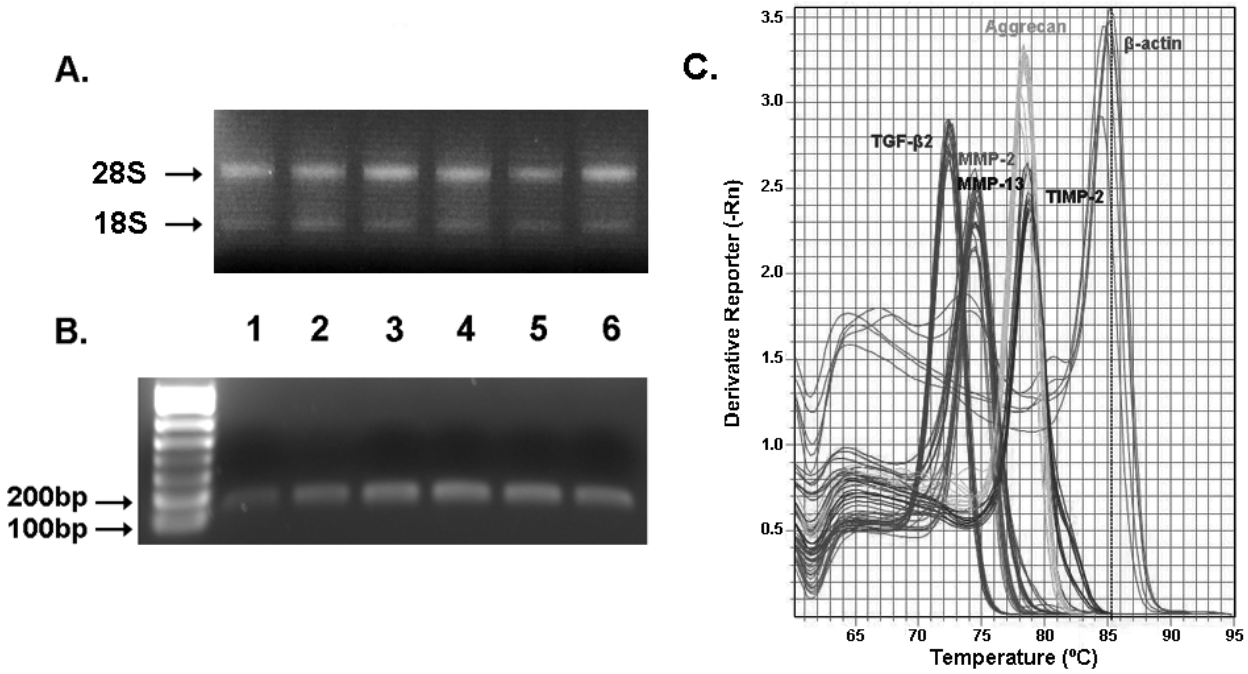

Figure 3-2. Diagrams showing (A) agarose gel electrophoresis, displaying distinct bands of 28S and 18S ribosomal RNA, verifying RNA integrity, (B) agarose gel electrophoresis, confirming single distinct bands for each PCR product, and (C) melt curve analyses showing distinct melting temperatures of each PCR product. Lanes 1 through 6 in (A) and (B) correspond to β-actin, MMP-2, MMP-13, TGF-β2, TIMP-2, and aggrecan, respectively.

3.4 Gene expression in cartilaginous sclera versus fibrous sclera

Gene expression levels in the chick cartilaginous and fibrous scleral layers were different, with all CT values higher (i.e. lower mRNA expression) in the fibrous sclera than in the cartilage sclera for all genes tested (Figure 3-3). In particular, aggrecan mRNA expression was found to be much lower in the fibrous sclera than in the cartilaginous sclera, by approximately 8.8 cycles. With the quantity of DNA doubling every cycle, this expression difference is equivalent to $2^{8.8}$ (about 450) times higher expression in the cartilaginous layer.

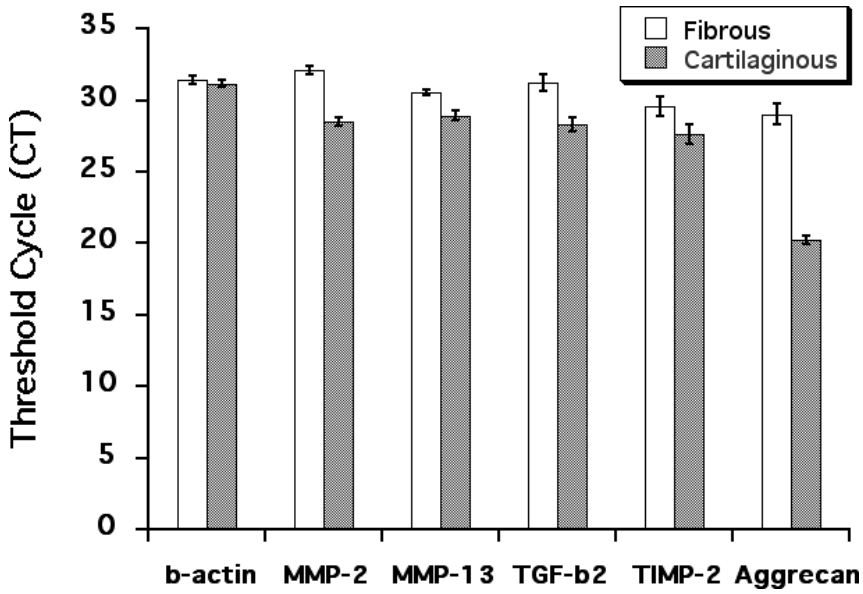

Figure 3-3. Threshold cycle (CT) values for all genes measured in the fibrous and cartilaginous scleras. Reported values are mean ± standard deviation. *N* = 60 for each of the fibrous and the cartilaginous sclera. Higher CT values correspond to lower mRNA expression levels.

3.5 Changes in mRNA expression levels in the fibrous sclera

3.5.1 Positive lens treatment

Eyes treated with +5 D lens showed a more than 3 fold decrease in MMP-2 expression compared to the fellow eye from 4 to 48h (ANOVA, $p = 0.0262$; Figure 3-4A), while plano lens-treated eyes showed significantly increased MMP-2 expression compared to fellow eye at 48h (paired t-test, $p < 0.01$; Figure 3-4A). MMP-13 expression for eyes treated with +10 D lens had significantly lower expression compared to fellow eye at 48h (paired t-test, $p < 0.01$; Figure 3-4B). Plano lens had significantly increased MMP-13 expression compared to fellow eye at 48h (paired *t*-test, $p < 0.01$; Figure 3-4B). Eyes with +5D lens treatments showed significantly higher TIMP-2 expression levels compared to plano lens group from 4 to 48h (ANOVA, $p < 0.05$; Figure 3-4C). No significant differences in TIMP-2 expression levels were found between positive lenses and their fellow eyes in any treatment group. TGF-β2 was expressed in significantly higher amounts for +10 D lens treatment compared to plano lens treatment (paired *t*-test, $p < 0.05$). At 4 h, TGF-β2 expression was significantly lower for both +5 and +10 D lens treatments compared to respectively fellow eyes (paired *t*-test, $p < 0.05$).

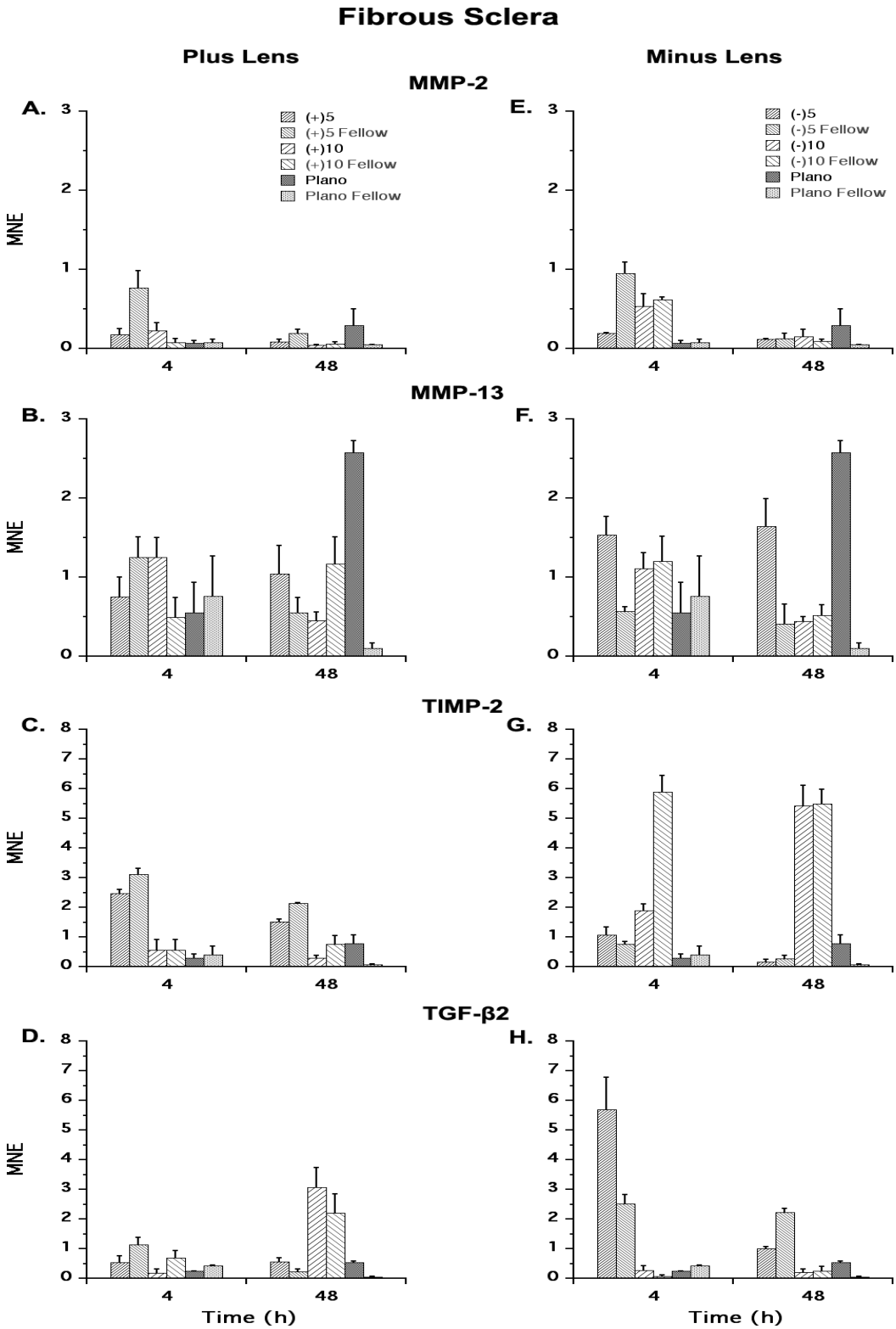

Figure 3-4. Mean normalized expressions in the fibrous sclera of MMP-2 (A, E), MMP-13 (B, F), TIMP-2 (C, G), and TGF-β2 (D, H) after monocular treatment with +10, +5, plano, -5, or -10 D lenses for 4 or 48h. *N* = 6 in each lens treatment group.

3.5.2 Negative lens treatment

Eyes treated with -5 D lens had significantly lower MMP-2 expression compared to the fellow eye at 4h (paired *t*-test, $p = 0.0189$; Figure 3-4E), but had significantly higher expression compared to the plano lens group at 4h (paired *t*-test, $p < 0.05$; Figure 3-4E). Eyes treated with -10 D lens had significantly higher expression of MMP-2 compared to plano lens group at 4 h (paired *t*-test, $p < 0.01$; Figure 3-4E). MMP-13 expression for eyes treated with -5 D lens had significantly higher expression compared to fellow eye at 4h (paired *t*-test, $p < 0.01$; Figure 3-4F) and 48 h (paired *t*-test, $p < 0.01$; Figure 3-4F). Both -5 and -10 D treatment groups had significantly higher expressions compared to the plano treatment group at 4h (paired *t*-test, $p < 0.05$; Figure 3-4F), but had significantly lower expressions compared to the plano treatment group at 48h (paired *t*-test, $p < 0.01$; Figure 3-4F). Chick eyes treated with -10 D lenses had significantly lower TIMP-2 expression compared to plano lens treatment and fellow eyes at 4h (paired *t*-test, $p < 0.01$; Figure 3-4G). Treatment with -10 D lenses significantly increased TIMP-2 expression compared to plano eyes from 4 to 48h (ANOVA, $p < 0.05$; Figure 3-4G). Treatment with -5 D lenses significantly increased TGF-β2 expression compared to fellow eye at 4h (paired *t*-test, $p < 0.01$; Figure 3-4H), but was significantly decreased at 48 h (paired *t*-test, $p < 0.01$; Figure 3-4H). On the other hand, TGF-β2 expression was significantly higher compared to plano lens treatment groups from 4 to 48h (ANOVA, $p < 0.05$; Figure 3-4H).

3.6 Changes in mRNA expression levels in the cartilaginous sclera

3.6.1 Positive lens treatment

Eyes treated with +10 D lenses showed significantly higher MMP-2 expression compared to fellow eyes at 4h (paired *t*-test, $p < 0.01$; Figure 3-5A), and also compared to plano lens treated eyes at 4 and 48h (paired *t*-test, $p < 0.01$; Figure 3-5A). Eyes treated with +5 D lens had significantly greater increase in MMP-2 expression from 4 to 48h (ANOVA, $p < 0.05$; Figure 3-5A). The plano lens treated eyes showed significantly decreased expression of MMP-13 compared to fellow eyes at both 4 and 48h (paired *t*-test, $p < 0.01$; Figure 3-5B). Eyes treated with +5 D lenses had significantly reduced MMP-13 expression compared to plano treated eyes from 4 to 48h (ANOVA, $p < 0.05$; Figure 3-5B). Eyes treated with +10 D lenses had significantly higher TIMP-2 expression at 4h compared to fellow eyes (paired *t*-test, $p < 0.01$; Figure 3-5C). TGF-β2 level was significantly increased in +10 D lens-treated eyes compared to fellow eyes at 4h (paired *t*-test, $p < 0.01$; Figure 3-5D). For +5 D lens-treated groups, TGF-β2 expression was significantly lower from 4 to 48h compared to plano lens treated eyes (ANOVA, $p < 0.05$; Figure 3-5D). At 48h, both +5 and +10 D lens-treated eyes had significantly decreased TGF-β2 compared to plano lens treated eyes (paired *t*-test, $p < 0.01$; Figure 3-5D).

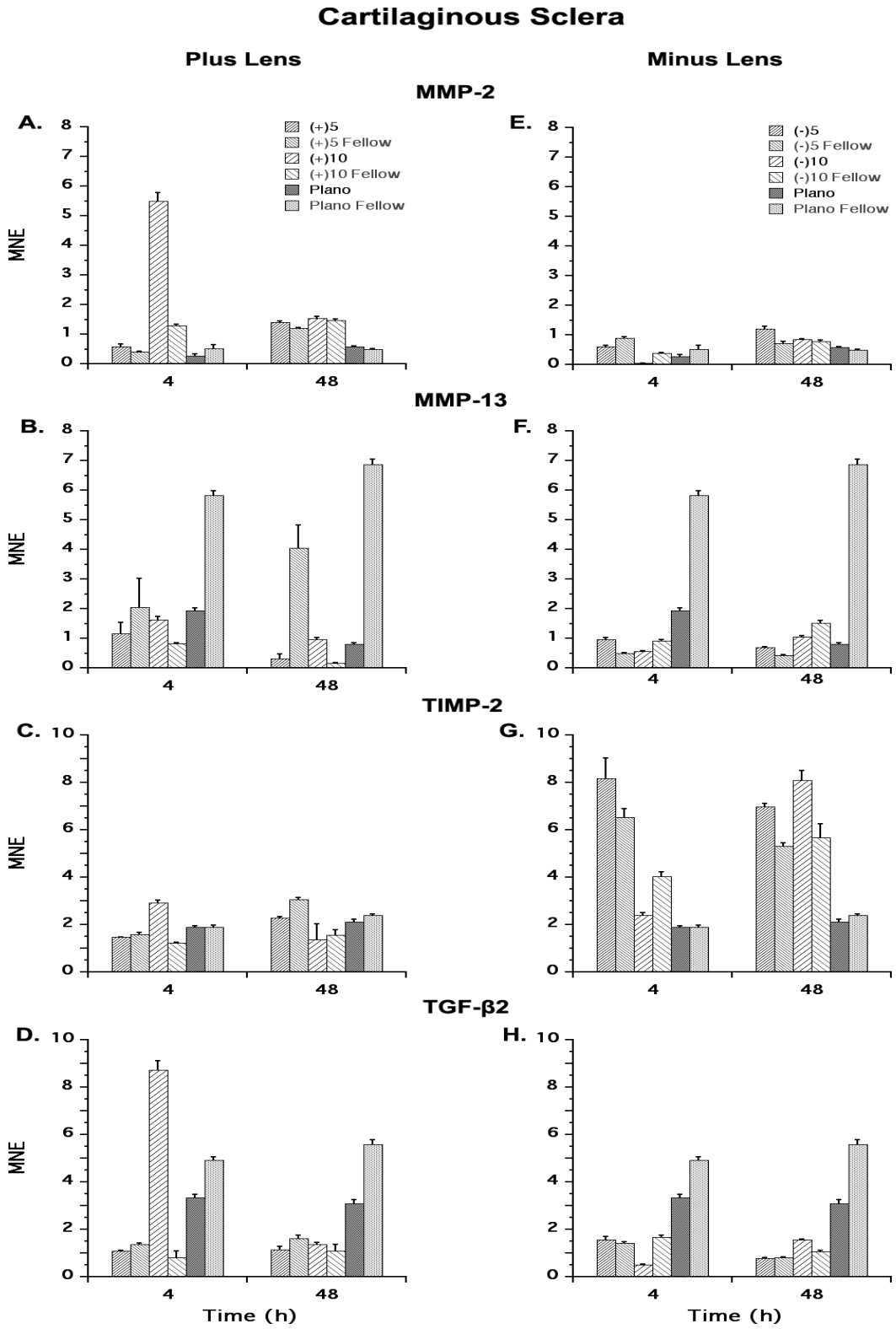

Figure 3-5. Mean normalized expressions in the cartilaginous sclera of MMP-2 (A, E), MMP-13 (B, F), TIMP-2 (C, G), and TGF-β2 (D, H) after monocular treatment with +10, +5, plano, -5, or -10 D lenses for 4 or 48h. *N* = 6 in each lens treatment group.

3.6.2 Negative lens treatment

Eyes treated with -5 D lenses had significantly increased MMP-2 expression compared to plano treated eyes from 4 to 48h (ANOVA, $p < 0.05$; Figure 3-5E). At 48h, -10 D lens treatment resulted in significantly greater MMP-2 expression compared to plano treated eyes (paired *t*-test, $p < 0.05$; Figure 3-5E). For MMP-13 expression, -5 and -10 D lens-treated eyes had significantly lower expression compared to plano treated eyes at 4h (paired *t*-test, $p < 0.01$; Figure 3-5F). Plano lens treated eyes had significantly reduced MMP-13 expression compared to fellow eyes (paired *t*-test, $p < 0.01$; Figure 3-5F). TIMP-2 expression was significantly increased for both -5 and -10 D lenses compared to plano treated eyes from 4 to 48h (ANOVA, $p < 0.01$; Figure 3-5G). Eyes treated with -5 and -10 D lenses at 4 and 48h all had significantly higher TIMP-2 expression compared to respective fellow eyes (paired *t*-test, $p < 0.05$; Figure 3-5G) except for -10 D lens treated eyes at 4h, which had significantly lower TIMP-2 expression compared to fellow eyes (paired *t*-test, $p < 0.05$; Figure 3-5G). TGF-β2 expression for both -5 and -10 D lenses were significantly lower compared to plano lens treated eyes from 4 to 48h (ANOVA, $p < 0.01$; Figure 3-5H). Plano and -10 D lens-treated eyes had significantly lower TGF-β2 expression compared to their respective fellow eyes (paired *t*-test, $p < 0.05$; Figure 3-5H).

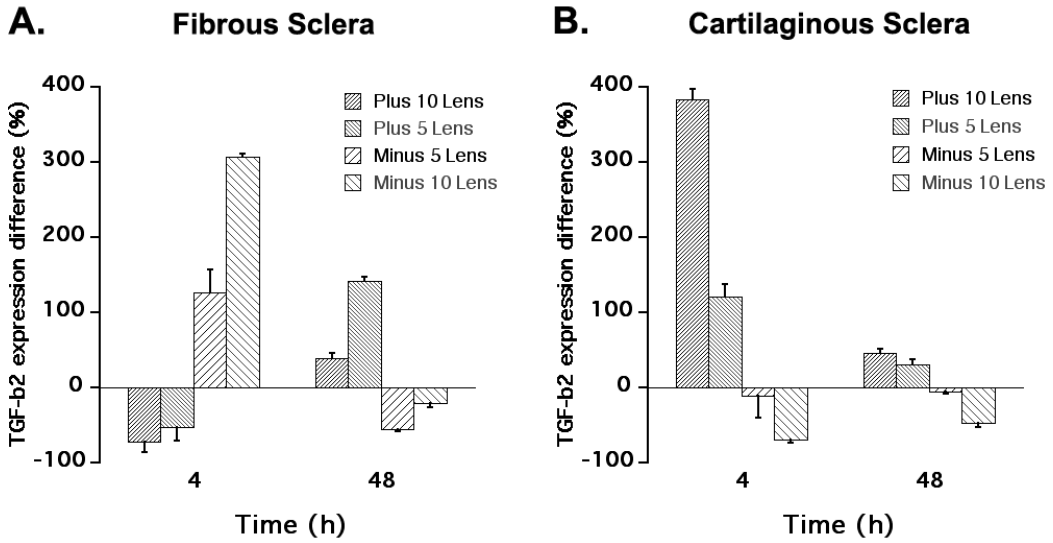

Figure 3-6. Percent differences of mean normalized expressions of TGF-β2 between lens-treated eyes and fellow eyes in both the (A) fibrous and (B) cartilaginous scleral layers at 4 and 48h treatment duration. *N* = 6 in each group.

3.7 Interocular differences in TGF-β2 expression

Analysis of interocular differences in TGF-β2 expression in +10, +5, -5, and -10 D lens-treated groups in the fibrous sclera revealed that mRNA levels at 4h were significantly decreased for positive lens wear, but increased for negative lens wear (paired *t*-test, $p < 0.01$; Figure 3-6A). This effect was reversed by 48h, with positive lens treatment inducing significantly higher TGF-β2 expression than the negative lens treatment (paired *t*-test, $p < 0.01$; Figure 3-6A). In contrast,

TGF-β2 expression in the cartilaginous sclera was significantly increased with the +5 and +10 D treatments compared to -5 and -10 D treatments at both 4 and 48h (paired *t*-test, $p < 0.01$; Figure 3-6B).

4. Discussion

Although gene expression changes in the two layers of the chick sclera during experimental myopia and hyperopia were previously studied (Schippert et al., 2006), we sought to investigate further the gene expression changes in response to changes in treatment duration and the magnitude of the imposed defocus, in addition to providing data on another matrix metalloproteinase, MMP-13, which might play a role in eye growth regulation and could be utilized in future biomaterials development for the inhibition of myopia progression (Su et al., 2009b).

The transcription of mRNA from a DNA strand occurs rapidly, at about 30 nucleotides per second at 37 ºC, and thus transcription takes about 2 minutes for a typical strand of primary RNA around 3000-4000 nucleotides. Thus, small proteins of 100-200 amino acids are typically made by the ribosome in a minute or less, and very large proteins of up to 30,000 amino acid residues, in 2 to 3 hours (Lodish et al., 2000). Considering that chick MMP-2 has 663 amino acids, MMP-13 has 378 amino acids, TGF-β2 has 412 amino acids, and TIMP-2 has 220 amino acids, each of these may be translated into proteins from the mRNA in less than 5 minutes in the body. In short, all of the genes under study can generate protein products in less than 10 minutes upon activation by defocus signals. Once these proteins begin to work on the extracellular matrix, the physical effects may be observable within a relatively short time. We have chosen 4 hours as the time period by which the imposed defocus effects would have been well in progress, and 48 hours as the time period by which other compensatory mechanisms might have intervened. It is important to keep in mind that due to signal relays, compensation to defocus will not have occurred by 48h. One can only expect decrease in imposed defocus effect only if feedback mechanisms and protein products are stable.

The changes in mRNA levels in response to lens treatment could occur either as a result of lens treatment itself (i.e. attaching a lens) or the imposed defocus. A mild (relative to imposed positive defocus) but significant increase in choroidal thickness was observed in plano lens-treated eyes in our study. This could be due to several reasons, including changes in temperature or optical aberrations. In a previous study (Schippert et al., 2006), chicks wearing binocular plano lenses for 3 days did not significantly influence any mRNA expression levels. However, in this study, the plano lens-treatment was monocular, thus leaving the contralateral eye untreated. The detected change with the plano lens treatment, if an artifact of lens wearing, could influence overall trends, attenuating the effects of negative lens treatments, since the choroid responded by increasing thickness in the same direction as the positive lens treatments. However, as for positive lens treatments, we would expect exaggeration of the response since the positive lens treatment elicited a choroidal thickness increase in the same direction, albeit a 4-fold higher increase in thickness compared to the plano lens treatment. Nonetheless, changes due to the positive lens treatments should have overshadowed the effects of the plano lens treatment in this study.

Treatment duration was an important determinant of mRNA levels for several of the genes studied here for both chick scleral layers. In the fibrous layer, MMP-2 expression was found to have significantly lower expression in positive lens-treated eyes compared to fellow eyes, and significantly higher expression in negative lens-treated eyes compared to plano lens-treated group. TIMP-2 expression was higher with the +5 lens treatment from 4 to 48h compared to plano lens-treated group. Other studies have also shown opposite results (Rada and Brenza, 1995; Rada et al., 1999), with increased MMP-2 and decreased TIMP-2 mRNA levels in the myopic fibrous chick sclera. Note that since our scleral harvesting method included the posterior scleral cup (cut at the equator of eye) except the area containing the pecten, this could have acted to either dampen or heighten the effects that may be confined to the posterior pole sclera immediately around the optic nerve head.

For the cartilaginous sclera, MMP-2 expression was significantly higher with +10 D lens wear compared to fellow eyes at 4h, and +5 D lens wear also induced significantly higher increase from 4 to 48h. Changes in the mRNA expressions of MMP-2 and TIMP-2 are also reported in tree shrews, with early MMP-2 expression increases, and some suppression of TIMP-2 expression in myopic eyes, and returns in expression to baseline levels after 11 days of treatment (Siegwart and Norton, 2005). Complicating the whole picture is the fact that a lack of observable changes in mRNA levels of these genes does not necessarily mean a lack of their involvement in eye growth regulation. Specifically, the activation of pro-MMP-2 occurs through cleavage by a cell surface complex including MT1-MMP and TIMP-2. Combined with the fact that upregulation of TIMP-2 is inhibitive to the active MMP-2, this interplay necessarily require that TIMP-2 has to be tightly regulated. Thus, it is likely that the rate of activation of MMP-2 from pro-MMP2 might be a better index of the regulatory role of MMP-2 rather than changes in its production during eye growth changes (Guggenheim and McBrien, 1996; Siegwart and Norton, 2005).

The role of TGF-β2 has been previously examined in other scleral studies (Jobling et al., 2004; Jobling et al., 2009; Schippert et al., 2006). In our study, we found that TGF-β2 mRNA expression levels changed in opposite directions, depending on the sign of defocus. Also, in the fibrous sclera, the direction of the responses at 4h was reversed by 48h for both positive and negative lens treatments. In contrast, in the cartilage sclera, response magnitudes at 4h were markedly higher than at 48h, but the directions of the responses were not reversed. Similar findings in the cartilaginous sclera has been reported previously (Schippert et al., 2006). Furthermore, responses appear to be graded, increasing with the magnitude of defocus, in that both +10 and -10 D lenses tend to elicit larger differential responses than +5 and -5 D lenses in both fibrous sclera (except 48h, Figure 2-6A) and cartilaginous sclera (Figure 2-6B), which has not been previously reported.

5. Conclusion

In summary, the results added further evidence to support roles for MMPs, TIMPs, and TGF-β2 in scleral growth regulation. The mRNA expression levels of TIMP-2 and TGF-β2 in the fibrous and cartilaginous layers showed opposite trends in response to positive and negative

lens defocus. Expression levels in the fellow eyes of the two lens groups were not significantly different, implying that there was no interocular yoking. TGF-β2 expression showed an early increase with positive lenses in both scleral layers, similar to the finding in the retinal pigment epithelium after 48h lens wear, and consistent with a role as an inhibitory growth modulator. However, the transient nature of its up-regulation in the chick sclera suggests additional growth modulatory influences on the latter. The cartilage expression patterns for MMP-2 and MMP-13 are consistent with the opposite directions of growth induced by positive and negative lenses, although the lack of changes in some cases suggests additional influences, perhaps reflecting the additional steps required for MMP activation. Lastly, with the observed changes and previously demonstrated ability to fabricate MMP degradable biomaterials, the potential for further development of biomaterials that can respond to MMP activity in myopia progression will largely depend on there being equivalent changes during myopia development.

Chapter IV

Scleral Reinforcement through Host Tissue Integration with Biomimetic Enzymatically-Degradable Semi-Interpenetrating Polymer Network

Abstract

Enzymatically-degradable semi-interpenetrating polymer networks (edsIPNs) were explored for their biocompatibility and ability to promote new scleral tissue growth, as a means of reinforcing the posterior wall of the eye. The edsIPNs comprised thermoresponsive poly(*N*-isopropylacrylamide-*co*-acrylic acid), customizable peptide crosslinkers cleavable by matrix metalloproteinases, and interpenetrating linear poly(acrylic acid)-*graft*-peptide chains to engage with cell-surface receptors. Rheological studies revealed an increase in stiffness at body temperature; the complex shear modulus $|G^*|$ was 14.13 ± 6.13 Pa at 22 ºC and 63.18 ± 12.24 Pa at 37 ºC, compatible with injection at room temperature. Primary chick scleral fibroblasts and chondrocytes cultured on edsIPN increased by 15.1 and 11.1 fold respectively over 11 days; both exhibited delayed onset of exponential growth compared to cells plated on tissue-culture polystyrene. The edsIPN was delivered by retrobulbar injection (100 µl) to 9 two-week old chicks to assess biocompatibility *in vivo*. Ocular axial dimensions were assessed using A-scan ultrasonography over 28 days, after which eyes were processed for histological analysis. While edsIPN injections did not affect the rate of ocular elongation, the outer fibrous sclera showed significant thickening. The demonstration that injectable biomimetic edsIPNs stimulate scleral fibrous tissue growth represents proof-of-principle for a novel approach for scleral reinforcement, and a potential therapy for high myopia.

Chapter IV was reproduced with modification from the following published paper:

Su J, Wall ST, Healy KE, Wildsoet CF, 2009. Scleral reinforcement through host tissue integration with biomimetic enzymatically-degradable semi-interpenetrating polymer network. *Tissue Engineering Part A*, ahead of print. doi:10.1089/ten.TEA.2009.0488.

1. Introduction

The sclera, being the outer wall of the eye, plays a fundamental role in axial ocular elongation, undergoing increased remodeling, thinning, and in some cases progressive biomechanical failure in the region of the posterior pole, leading to the development of staphylomas. In mammalian and primate eyes, the sclera represents the outer mechanical support layer of the eye, and is comprised of avascular fibrous connective tissue containing various collagens and proteoglycans (Ihanamaki et al., 2004; McBrien and Gentle, 2003). In mature sclera, the collagen fibers are layered anisotropically and show a gradient in fiber diameter, with the smallest fibers found innermost towards the retina. This gradient is lost in high myopia (Curtin et al., 1979; McBrien et al., 2001a), and the myopic sclera shows additional ultrastructural and biomechanical changes. For example, there are significant decreases in the amounts of glycosaminoglycans and proteoglycans in myopic eyes (Avetisov et al., 1983; Norton and Rada, 1995; Phillips et al., 2000). These changes likely all contribute to the scleral thinning reported in high myopia in humans and animal models of the same (Marzani and Wallman, 1997; Nickla et al., 1999a; Norton and Rada, 1995; Rada et al., 1994; Rada et al., 2000), contributing to observed increases in scleral creep rates and rendering such eyes more vulnerable to the stretching influence of intraocular pressure (Friedman, 1966; Phillips and McBrien, 2004; Wildsoet and Wallman, 1995). The fibrous sclera of the avian eye (Figure 4-1A) shares many of the same features of the mammalian sclera, as well as changes with myopia, but the avian sclera also includes an additional inner cartilaginous layer, making it much more rigid.

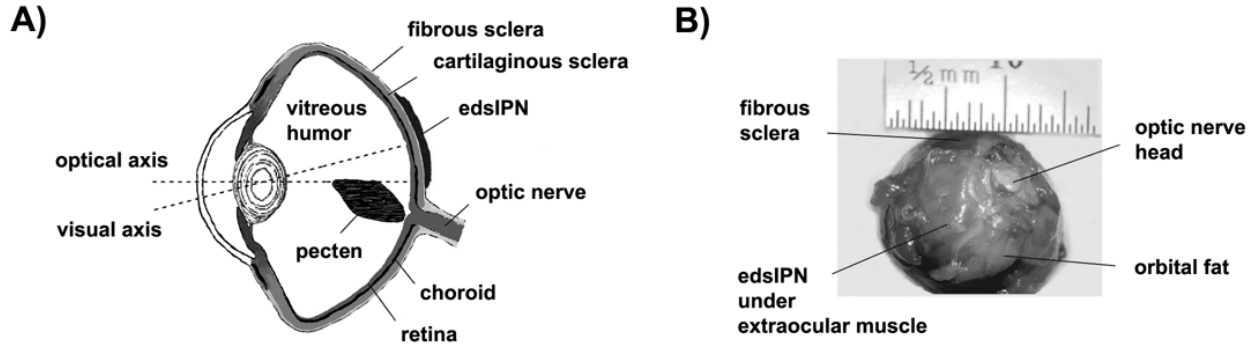

Figure 4-1. (A) Transverse cross-sectional diagram of a chick eye showing the location of the injected edsIPN on the outer surface of fibrous sclera with respect to the visual and optical axes, and (B) posterior view of an enucleated chick eye showing injection site.

Various interventions have been explored to strengthen the myopic sclera, including chemical- and irradiation-induced scleral collagen crosslinking (Wollensak and Spoerl, 2004), systemic delivery of methylxanthines to increase scleral collagen concentration and fiber diameters (Trier et al., 1999), and scleroplasty involving the attachment over the posterior sclera of allografts or synthetic materials to provide direct mechanical support (Avetisov et al., 1997; Gerinec and Slezakova, 2001; Tarutta et al., 1999), A sub-Tenon's injection of a polymeric gel formulation comprised mainly of polyvinylpyrrolidone has been used to control myopia progression, but testing has been limited to a Moscow-based small human study and a mechanistic animal study (Avetisov et al., 1997; Su et al., 2009a), These options have yet to gain

wide clinical acceptance because of high toxicity (glutaraldehyde, etc.), lack of complete understanding of the mechanism of action (methylxanthines), limited access to clinical trial data (polyvinylpyrrolidone injections), and for scleroplasty, limited supply of allograft material, its invasive nature, and limited data supporting its long-term efficacy (Ward et al., 2009).

As an alternative, we proposed a minimally invasive scleral reinforcement strategy that takes advantage of the biochemical properties of the host sclera. We have begun testing injectable and highly tunable biomimetic hydrogels based on poly(*N*-isopropylacrylamide) [p(NIPAAm)]. The merits of these synthetic hydrogels include environmental responsiveness and independent tunability with respect to mechanical properties, customizable biological ligands that promote cell and tissue adhesion, and controllable protease degradation of the hydrogel to mediate cellular infiltration (Stile et al., 1999). In particular, hydrogels based on p(NIPAAm) are known to be injectable at room temperature, while forming viscoelastic solids *in situ* at higher physiological (body) temperatures (Stile et al., 1999). In the study reported here, we used enzymatically degradable semi-interpenetrating polymer networks (edsIPN) composed of poly(*N*-isopropylacrylamide-*co*-acrylic acid) [p(NIPAAm-*co*-AAc)] with proteolytically degradable peptide crosslinkers, and physically entangled peptide-functionalized linear poly(acrylic acid) [p(AAc)] chains that interpenetrate the synthetic hydrogel matrix (Chung et al., 2006; Kim et al., 2005). Enzymatically-degradable hydrogels, used as biomimetic extracellular matrix (ECM), have been reported to support human embryonic stem cell self-renewal (Li et al., 2006), act as vehicles for cell transplantation by sustaining early cellular remodeling and growth (Kutty et al., 2007), aid myocardium regeneration (Wall, 2008), and promote mesenchymal stem cell proliferation and bone formation *in vivo* (Chung et al., 2006).

Based on the known biochemistry of the fibrous sclera and characterization of various edsIPNs, one formulation was selected for evaluation. Rheological testing was initially performed to establish the injectability of the edsIPN material and its likely stabilization after injection *in vivo*. *In vitro* cellular proliferation studies, using chick scleral fibroblasts and chondrocytes, were conducted to establish the cytocompatibility of the edsIPN. *In vivo* biocompatibility testing assessed the effects on ocular growth and scleral histology of a one-time retrobulbar injection of edsIPN, applied against the external scleral surface at the posterior pole of normal chick eyes. We found that the injected hydrogels preserved the phenotypes of chick scleral cells, allowed proliferation of both cell types *in vitro*, and stimulated the addition of fibrous tissue to the native fibrous sclera when injected *in vivo*.

2. Materials & Methods

2.1 Synthesis & chemical composition of edsIPNs

All chemicals were purchased from Aldrich (St. Louis, MO) and used without further purification unless otherwise specified. All water used was ultra pure ASTM type I reagent grade (18.2 MΩ•cm, pyrogen free, endotoxin <0.03 EU/mL). The edsIPN was synthesized (Figure 4-2A) by redox radical addition polymerization at room temperature with molar ratios of 95:5:0.3 (NIPAAm: acrylic acid: crosslinker) in 1X Dulbecco's phosphate buffered saline (PBS; Invitrogen; Carlsbad, CA) without calcium and magnesium as previously described (Chung et

al., 2006; Kim and Healy, 2003; Kim et al., 2005). The peptide crosslinker, Gln-Pro-Gln-Gly-Leu-Ala-Lys-NH_2 (QPQGLAK-NH_2; American Peptide Co.; Sunnyvale, CA), was cleavable by matrix metalloproteinase-13 (MMP-13) and other collagenases (Kim and Healy, 2003), and included a glutamine residue to promote solubility, and a lysine residue to provide amine functional groups for modification. Reacting the peptide with acryloyl chloride in presence of triethylamine generated amide linkages between the peptide and acrylic group, thereby introducing bifunctional acryl groups amenable to addition polymerization.

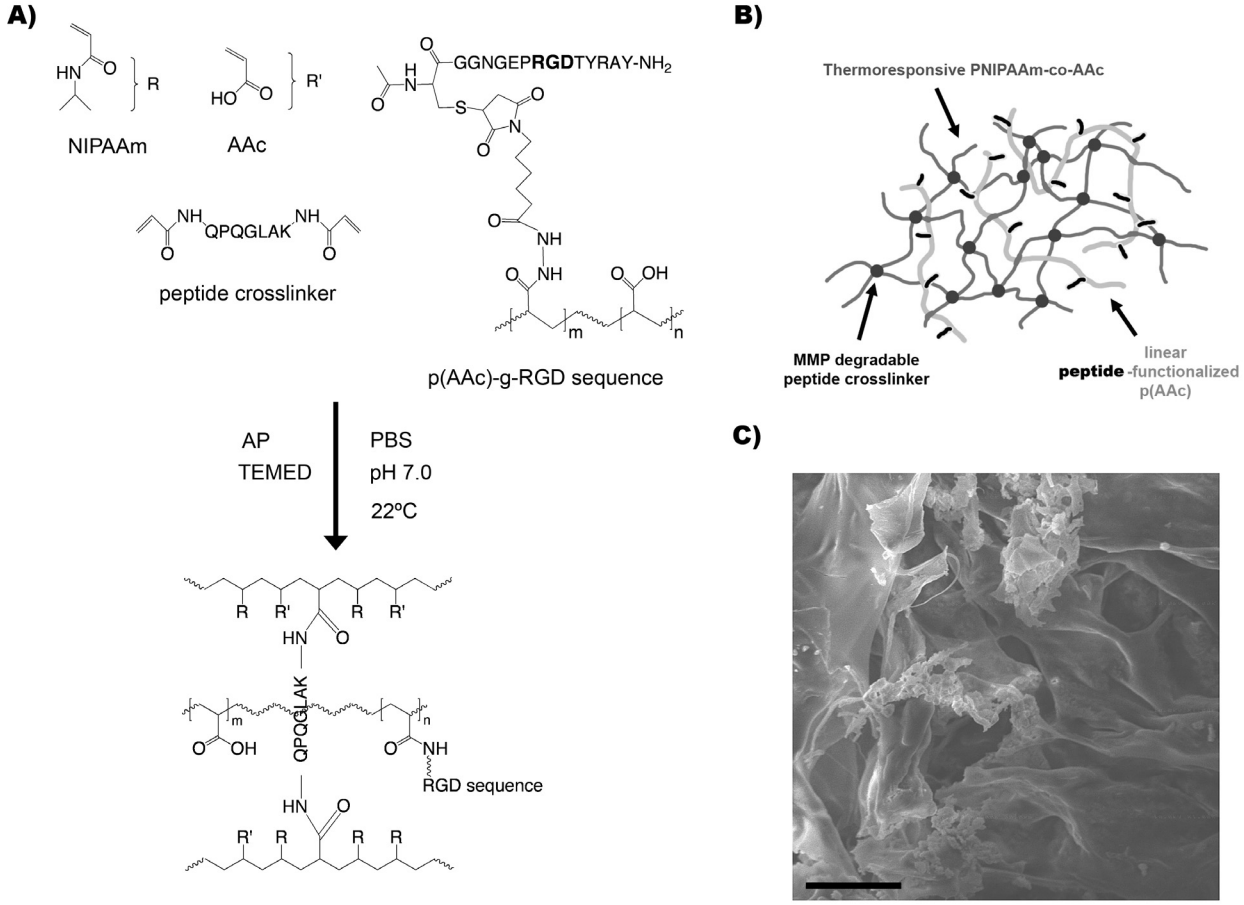

Figure 4-2. (A) Schematic diagram illustrating the reaction steps involved in the synthesis of edsIPNs. (B) The thermoresponsive edsIPN acts as a synthetic extracellular matrix containing proteolytically degradable peptide crosslinkers and peptide-functionalized cell adhesion signals. (C) Scanning electron microscopy image, showing the 3-dimensional structure of the edsIPN. 1000X magnification, scale bar = 20 μm.

The inclusion of MMP degradable peptide crosslinkers offers potential control over the rate of polymer degradation and thus allows control over cellular infiltration, given that MMPs are known to be involved in scleral remodeling (Schippert et al., 2006; Siegwart and Norton, 2005). The p(NIPAAm-*co*-AAc) polymer network was interpenetrated by polyacrylic acid-graft-Ac-CGGNGEP**RGD**TYRAY-NH_2 [p(AAc)-*g*-RGD] linear polymer chains to promote cell adhesion (Kim et al., 2005). Linear p(AAc) chains (MW 450,000; Polysciences; Warrington,

PA) were first grafted with maleimide side groups, then the synthetic peptide, Ac-CGGNGEP**RGD**TYRAY-NH_2 derived from bone sialoprotein (bsp-RGD(15), American Peptide Co.), was grafted to the maleimide side groups to produce p(AAc)-*g*-RGD linear chains. The selection of the bsp-RGD(15) motif was based on its known binding activity to several integrin receptors, including α_2, $\alpha_V\beta_3$, β_1, and $\alpha_2\beta_1$ and known angiogenic activity (Bellahcene et al., 2000; Harbers and Healy, 2005; Rezania and Healy, 1999). Furthermore, bsp-RGD(15) has been shown to enhance attachment of fibroblasts (Somerman et al., 1988), and associated integrin receptors have been implicated in the growth of both normal and myopic mammalian sclera (Metlapally et al., 2006).

The synthesis of the edsIPNs was achieved by first bubbling nitrogen gas through a solution of NIPAAm, acrylic acid (AAc), acrylated peptide crosslinker, and p(AAc)-*g*-RGD in calcium and magnesium-free PBS for 30 minutes to remove dissolved oxygen. Following nitrogen purging, 0.8 wt % of ammonium persulfate (AP; Polysciences) and 4% v/v of *N,N,N',N'*-tetramethylenediamine (TEMED; Polysciences) were added as initiator and accelerator, respectively. The mixture was stirred vigorously for 10 s and allowed to polymerize for 24 h. After polymerization, edsIPNs were washed 3 times in excess water to remove unreacted reagents, sterilized with 70% ethanol, and again washed 3 times in water to remove the ethanol. This technique was previously shown to be effective in sterilizing peptide-modified hydrogels without peptide degradation (Huebsch et al., 2005). The resulting edsIPN structure is depicted in Figure 4-2B. All edsIPNs were stored in sterile PBS at room temperature prior to use.

2.2 Determination of concentration of grafted RGD

The degree of substitution of bsp-RGD(15) on the p(AAc) chains was assessed using previously developed methods (Barber et al., 2005; Harbers and Healy, 2005). Briefly, fluorescein isothiocyanate (FITC) labeled bsp-RGD(15) peptide (Ac-CGGNGEP**RGD**TYRAYK(FITC)GG-NH_2, American Peptide Co.) was grafted to the p(AAc) chains as described above and fluorescence was measured in a SpectraMax Gemini XS fluorometer (Molecular Devices; Sunnyvale, CA) (excitation: 485nm, emission: 438 nm, cut-off: 530 nm). A digestion buffer containing 100 µL of 10 mM Tris-HCl (pH = 8.0, 100 mM $CaCl_2$) and 1,546 units/mL bovine chymotrypsin was added to each well. Control solution standards (100 µL/well) containing 0.001-10 µM of peptide were digested in parallel. The fluorescence of the wells was monitored *in situ* at 10 min intervals over 2 h period at 25ºC. The concentration of the grafted RGD was then determined and normalized to the weight of the linear p(AAc) chains. In this study, 300 µM bsp-RGD(15) was chosen to present a significant number of RGD motifs to the scleral cells. Previous studies indicated that this concentration was sufficient for adhesion, migration, and proliferation of osteoblasts and cardiac myofibroblasts (Chung et al., 2006; Kim et al., 2005; Wall, 2008). The grafted bsp-RGD(15) peptide chains have a statistical bulk distribution within the edsIPN, since the linear p(AAc) chains interpenetrate the synthetic network (Kim et al., 2005; Stile et al., 2004).

2.3 Electron microscopy imaging of edsIPN

The general surface features of the edsIPN were studied by scanning electron microscopy. Samples were lyophilized to constant weight. Small thin samples were then broken

off the lyophilized edsIPN with forceps, placed on adhesive carbon conductive tape, and sputter-coated with 1-2 nm of gold. Samples were visualized by cold field emission electron microscopy (Hitachi S-5000) using an accelerating voltage of 10 kV.

2.4 Rheological characterization of edsIPN

To characterize the viscoelastic properties of the edsIPN, dynamic oscillatory shear measurements were undertaken using a parallel plate rheometer (Paar Physica MCR 300, Anton Paar; Ashland, VA) with sanded 50 mm parallel plates at a gap height of 1.0 mm. A humidity chamber was placed around samples during testing to prevent dehydration. The lower plate temperature was regulated with a Peltier heating element connected to a recirculating water bath. The complex shear modulus $|G^*|$ was determined by measuring the storage modulus $|G'|$ and loss modulus $|G''|$ over a temperature range of 22 – 40 ºC and a frequency range of 0.001 – 14 Hz at 5% strain, which is within the linear elastic region for the set gels. Samples were heated at a rate of 1 ºC/min. The lower critical solution temperature (LCST) phase transition was determined using a UV-Vis spectrophotometer to monitor transmittance at λ = 500 nm, as a function of temperature. All rheological measurements were repeated five times for each of five samples of the synthesized edsIPN.

2.5 *In vitro* cytocompatibility testing of edsIPNs using chick scleral cells

The presence in the chick sclera of an outer fibrous layer similar in structure to the mammalian sclera, combined with the fast eye growth and the practical advantages of working with chicks, provided the rationale for using the chick model in this study. White Leghorn chicks (*Gallus gallus domesticus*) were obtained as hatchlings from a commercial hatchery (Privett Hatchery, New Mexico) and reared in 12/12-hour light/dark cycle, with food and water available *ad libitum*. Care and use of the animals were in compliance with the animal use protocol approved by the Animal Care and Use Committee of the University of California, Berkeley.

Primary chick scleral fibroblasts and chondrocytes were isolated from the eyes of a 1-week old chick. Immediately after sacrifice, both eyes were enucleated and their outer scleral surface cleared of extraocular muscles and other adherent orbital tissue. Circumferential incisions at the equator were performed to remove the anterior ocular segments, and subsequently the vitreous, retina, and choroid were removed from the remaining scleral cups. The scleral cups were then put into Ringer's buffer, and the outer fibrous sclera separated from the inner cartilaginous sclera using sharp (fine pointed) forceps. The separated tissues were cut into small, 1 mm x 1 mm pieces, and digested by incubation with 0.3% w/v dispase (*Bacillus polymyxa*; Calbiochem; La Jolla, CA) and 0.2% w/v collagenase (*Clostridium histolyticum*; Calbiochem) in Dulbecco's modified Eagle medium (DMEM) and Ham's F-12 media (1:1) with 10% fetal bovine serum (FBS; Invitrogen) supplemented with 1% penicillin-streptomycin antibiotic (Invitrogen) at 37ºC. In each case, the media was removed by centrifugation (1200 *g* for 1 min) after a 48 h enzymatic digestion period, and the softened tissue was gently pipetted 3 times in additional 1:1 DMEM/F-12 media to physically dissociate the cells. The cell-containing media was then filtered through a 40-µm sieve (Falcon cell strainer nylon; Becton Dickinson; Franklin Lakes, NJ) to remove undissociated cell and tissue aggregates. The filtered media with

dissociated cells was centrifuged and then replaced with fresh media prior to cell counting with a hemacytometer.

Primary chick fibroblasts and chondrocytes were seeded at a cell density of 2.0 x 10^3 cells/cm^2 onto 48-well tissue culture-treated polystyrene (TCPS) plates, either directly onto TCPS or on top of the edsIPN, which uniformly covered the bottom of the wells. Cells were subsequently cultured in 1:1 DMEM/F-12 media with 1% penicillin-streptomycin and 10% FBS, and placed in 5% CO_2 incubator at 37ºC. Phase contrast microscope images of the cell cultures were taken at 1, 6, and 11 days post-seeding. A CyQUANT® cell proliferation assay kit (Molecular Probes) was used, following the manufacturer's instructions, to quantify cell proliferation on a daily basis over an 11 day period. A hemacytometer was also used to independently confirm the cell numbers. Five samples were used for each time period and measured in triplicate.

2.6 *In vivo* ocular biocompatibility assessment of edsIPNs

To assess the effect of the designed edsIPN on the ocular sclera, an *in vivo* experiment using 2-week old White Leghorn chicks (*G. gallus domesticus*; n = 9) was undertaken. The chicks received a retrobulbar injection of 100 µL edsIPN. All polymer injections were monocular, assigned randomly to the left or the right eye; the untreated fellow eye served as controls. Prior to implantation, chicks were first anesthetized with 2% isoflurane in oxygen. Access to the orbit was gained through a small temporal incision. A 7-0 silk anchoring suture was placed in the anterior sclera to rotate and fixate the eye to allow easier access to the posterior pole. The polymer was delivered over the posterior pole, between the sclera and the dorsal oblique extraocular muscle using a curved, blunt-end 19-gauge needle (sub-Tenon's anesthesia cannula needle, BD Ophthalmic Systems; Franklin Lakes, NJ) with the aid of a surgical microscope, which also allowed unwanted anterior diffusion of the injected edsIPN to be ruled out. An antibiotic ointment was applied prophylactically, after suturing closed the incision site. The anatomical position of the injected edsIPN is shown with respect to the visual axis (Figure 4-1A) and for an enucleated eye (Figure 4-1B).

2.7 Measurement and analyses of ocular dimensions & refractions

Axial eye growth was monitored *in vivo* using a custom high frequency 30 MHz A-scan ultrasonography set-up that offers measurement precision down to 10 µm (Nickla et al., 1998). The thickness of the sclera and all other axial ocular components (anterior chamber depth, lens thickness, vitreous chamber depth, retina, and choroid) were obtained by averaging data from a minimum of 12 measurements per eye per time point. Chicks were anesthetized with 1.5% isoflurane in oxygen for all measurements. Data were collected for all chicks on the day of but before the injection (day 0; baseline), as well as at weekly intervals out to 28 days. Only data from the 6 birds that completed the 4-week monitoring period were included in ultrasonography data analyses. Data for treated and fellow eyes were normalized so that their baseline means matched the overall baseline mean for all eyes. Scleral cup depth data were obtained by adding together the vitreous chamber depth, retinal thickness, and choroidal thickness, as an index of scleral surface area. Scleral thickness was not included in this parameter to allow for the possibility that it changed independently of scleral surface area. It was also not included in the

derived axial length parameter, which was calculated as the sum of anterior chamber depth, lens thickness, and scleral cup depth. Neither anterior chamber depth or lens thickness was reported separately as they were not affected by the treatment. Axial length was used as an index of ocular elongation. In addition to ultrasonography, endpoint refractions were measured by streak retinoscopy on the eyes of the same birds at end of the monitoring period. Treatment-induced changes in refraction can be expected from effects on either or both the curvature of the optical components of the eye, and ocular growth. Normalized data from treated and fellow control eyes were compared statistically using two-way repeated-measures ANOVA and paired *t*-test (Statview, Version 4.0; SAS Institute; Cary, NC). A *p*-value of less than 0.05 was used for statistical significance.

2.8 Histological analyses of *in vivo* effects of injected edsIPN

To further investigate the scleral effects of the edsIPN implants, one chick was randomly picked for sacrifice at weekly intervals post-injection for histological analysis. Eyes were carefully enucleated immediately after sacrifice, leaving the implants and any associated connective tissue in place, and visually inspected under a surgical microscope. The anterior segments of the eyes were then removed and the posterior eyecups fixed overnight at 4°C in 4% paraformaldehyde in 0.1M Sorensen's buffer with 3% sucrose. The fixed eyecups were then rinsed three times in 0.1M Sorensen's buffer for 10 min each, before being cryoprotected overnight with 30% sucrose in 0.1M Sorensen's buffer at 4°C. Afterwards, eyecups were embedded in Tissue-Tek O.C.T. compound at -25°C using a dry ice-chilled alcohol slurry. The frozen blocks were clearly marked to allow localization of the posterior pole of the eyecups in subsequent sectioning. Cryostat sections, 10 µm in thickness, were cut in a temporal to nasal direction, air-dried and stained by hematoxylin and eosin (H&E) and Masson's trichrome (American MasterTech Scientific; Lodi, CA). Histological findings are qualitatively described for all time points, and thickness data for the band of new fibrous tissue generated by cellular infiltration of the implants, i.e. the scleral integration layer, are also described for the 4-week time point.

3. Results

3.1 Characterization of the edsIPNs

At room temperature, the synthesized edsIPNs were optically clear and easily deformable. Scanning electron microscopy images revealed the edsIPN to have an overall porous structure with interconnected pores and rough surface (Figure 4-2C). The concentration of the grafted bsp-RGD(15) was 36.5 µmol/g of p(AAc), established using a FITC-conjugated bsp-RGD(15) peptide.

The viscoelastic properties of edsIPN, shown as plots of the complex shear modulus $|G^*|$ as functions of frequency and temperature (Figures 4-3A, B), were similar to previously reported data (Kim and Healy, 2003; Kim et al., 2005). The edsIPN had a lower $|G^*|$ at 22 ºC than at 37 ºC (Figure 4-3A). The temperature-dependent viscoelastic behavior was also consistent with the measured onset of the phase transition, starting at 35ºC (Figure 4-3B). The phase angle varied

from 5º to 10º during the experiments. The mean |*G**| was 14.13 ± 6.13 Pa at 22 ºC and 1 Hz, and was 63.18 ± 12.24 Pa at 37 ºC at the same frequency, representing a 4.5 fold increase in |*G**| due to the LCST transition. These properties were compatible with our requirement of a polymer that can be easily injected through a 19G needle at room temperature, and yet will set and so remain localized to the site of injection at body temperature.

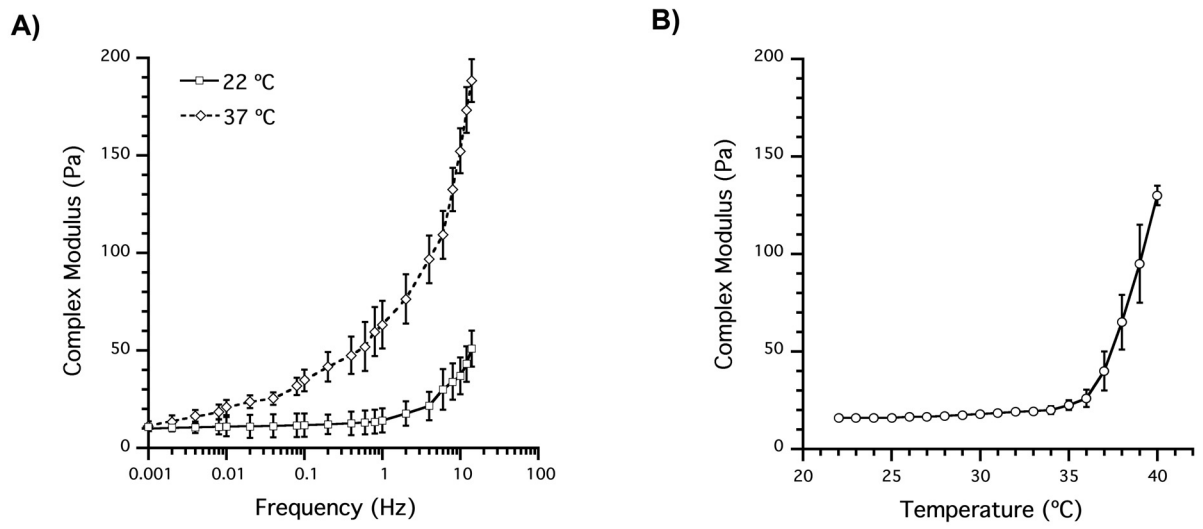

Figure 4-3. Results of rheological measurements of 95:5:0.3 (NIPAAm: AAc: crosslinker) edsIPN with 300 μM bsp-RGD(15). The complex modulus plotted against frequency at 22 and 37 ºC (A), and plotted against temperature at frequency setting of 1 Hz (B).

3.2 *In vitro* cytocompatibility assay using chick scleral cells

The chick scleral fibroblasts and chondrocytes exhibited different morphology, depending on whether they were cultured on the edsIPNs or TCPS (Figure 4-4A). On TCPS, the fibroblasts spread and possessed a spindle shaped morphology throughout the growth period (ScF TCPS, Figure 4-4A), while in contrast, scleral fibroblasts cultured on edsIPN had a rounded morphology from the outset, and maintained this morphology throughout the 11-day culture period (ScF edsIPN, Figure 4-4A). On edsIPN, the scleral chondrocytes also exhibited at 1 day after seeding, a phenotypic rounded morphology, which was maintained throughout the growth period (ScC edsIPN, Figure 4-4A). Although the chondrocytes cultured on TCPS initially also exhibited a rounded morphology, they started to lose this morphology by day 6, exhibiting a fibroblast-like morphology by day 11, suggesting dedifferentiation into fibroblasts (ScC TCPS, Figure 4-4A).

In addition to the above morphological differences observed with the two different culture surfaces, the scleral cells also exhibited related differences in their rates of proliferation. Scleral fibroblasts proliferated more rapidly over the 11-day period when cultured on TCPS compared to edsIPN (Figure 4-4B). On TCPS, the exponential growth phase for scleral fibroblasts began around day 3 and ended around day 7, after which the cells continued to proliferate at a slower pace, reaching confluence at 7.98 ± 0.48 x 10^4 cells/cm^2 (filled circles, Figure 4-4B), a 38.9 fold increase over seeding density.

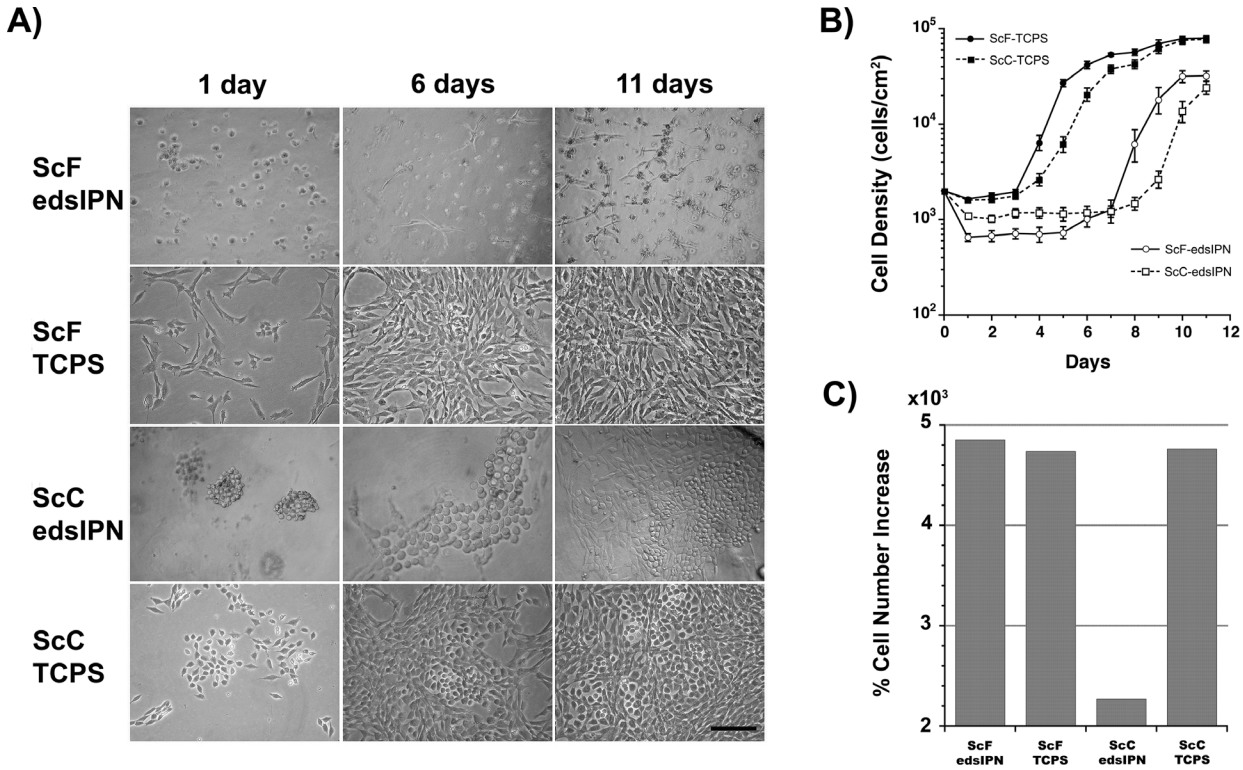

Figure 4-4. Phase contrast images of scleral fibroblasts (ScF) and scleral chondrocytes (ScC) cultured on edsIPN and tissue culture polystyrene (TCPS) at 1, 6, and 11 days post-seeding (A) (10X magnification. Scale bar = 100 μm); cells retained normal phenotypic appearance longer on edsIPN but grew more slowly. Cell density plotted against days in culture for ScF and ScC on either edsIPN or TCPS over 11 days (B); both cell types proliferated slower on edsIPN than on TCPS. Bar chart shows percent increase of cells over initial attached number of cells (C); lower growth rate recorded for ScC on edsIPN compared to all other groups.

On the other hand, the exponential growth phase for scleral fibroblasts cultured on edsIPN was delayed until day 7, and lasted until around day 10, with a cell count at that time of $3.22 \pm 0.39 \times 10^4$ cells/cm^2 (open circles, Figure 4-4B), a 15.1 fold increase over their initial seeding density. Similarly, scleral chondrocytes exhibited delayed growth profiles on the edsIPN. For these cells, the exponential growth phase started on day 7 when cultured on edsIPN, compared to day 3 for TCPS. On TCPS, scleral chondrocyte density reached confluence at $7.78 \pm 0.64 \times 10^4$ cells/cm^2, a 37.9 fold increase over seeding density, similar to the density achieved by scleral fibroblasts on TCPS (filled squares, Figure 4-4B). On edsIPN, scleral chondrocytes grew exponentially from day 7 to 11, when the cell density reached $2.42 \pm 0.37 \times 10^4$ cells/cm^2 (open squares, Figure 4-4B), an 11.1 fold increase over seeding density. In addition to the delayed growth responses seen with edsIPN, both cell types showed significant early losses over the first day in culture. On the edsIPN, fibroblast density decreased by 67.5% from their seeding density to 650 cells/cm^2, with comparable figures for chondrocytes of 46.5% and 1,070 cells/cm^2. Early losses were much smaller for the TCPS, a decrease of 17.5% to 1,650 cells/cm^2, for scleral fibroblasts, and of 20.0% to 1,600 cells/cm^2 for scleral chondrocytes.

Cell density data were further analyzed with Verhulst's logistic growth model (Harbers and Healy, 2005; Thieme, 2003), which assumes exponential growth with contact inhibition, and

contains the following parameters: effective growth rate (r), time in days (t), maximal substrate carrying capacity (K), and initial cell number (N_0).

$$N(t) = \frac{K}{1 + \left(\frac{K}{N_0} - 1\right)\exp(-rt)} \quad \text{(Eqn. 4-1)}$$

For each culture surface and cell type, both the initial cell numbers and carrying capacity were determined experimentally, by counting cells 2 h after seeding as well as after reaching confluence or near confluence, respectively. For scleral chondrocytes and fibroblasts cultured on edsIPN, effective growth rates (r) were 0.19 and 0.27 day^{-1}, corresponding to cell population-doubling times ($1/r$) of 5.3 and 3.7 days, respectively. The effective growth rates of scleral chondrocytes and fibroblasts cultured on TCPS were both higher than those recorded for edsIPN, i.e. 0.51 and 0.60 day^{-1}, corresponding to cell population-doubling times of 2.0 and 1.7 days, respectively. The calculated carrying capacity was 8.0 x 10^4 cells/cm^2 for TCPS; approximately double the capacity of the edsIPN of 3.9 x 10^4 cells/cm^2. In order to normalize the effect of initial cell adhesion on cell proliferation, the percent cell number increase was calculated using the following equation,

$$\%\ \text{cell increase} = \frac{N_f - N_i}{N_i} \times 100 \quad \text{(Eqn. 4-2)}$$

where N_f is the maximum cell density at day 11, and N_i is the initial attached cell density after day 1. The ScF edsIPN, ScF TCPS, and ScC TCPS groups all recorded similar percent increases, i.e., 4853.8%, 4736.4%, and 4762.5%, respectively. However, ScC edsIPN group increased just 2272.5%, slightly less than half of the values recorded by the other groups (Figure 4-4C).

3.3 Effect of edsIPN on *in vivo* axial ocular dimensions & refractions

A sample ultrasonography trace obtained from an eye 28 days after the edsIPN injection is shown in Figure 4-5A. The injected edsIPN had no negative effects on either ocular growth or refractions. Only parameters likely to be affected by the treatment are described here.

Comparison of the normalized axial length data for edsIPN treated eyes and their fellows revealed no significant difference between them (Figure 4-5C). Over the 28-day monitoring period, the axial lengths of edsIPN-injected eyes grew by 1.450 mm to 12.464 ± 0.052 mm, compared to 1.444 mm to 12.458 ± 0.051 mm for fellow eyes.

Scleral cup depths, which served as an index of scleral surface area, also did not show any significant differences between treatment and fellow eyes (Figure 4-5C). Over the 28-day monitoring period, the scleral cup depth of edsIPN-injected eyes grew by 0.705 mm to 7.403 ± 0.042 mm, compared to 0.703 mm to 7.401 ± 0.038 mm for fellow eyes.

Normalized scleral thickness increased for edsIPN-injected eyes from 124 ± 3 μm at baseline to 142 ± 6 μm by day 28, compared to 148 ± 4 μm for fellow eyes (Figure 4-5B).

Additional peaks were observed in some of the ultrasonography traces behind the peak corresponding to the external sclera, perhaps originating from the injected edsIPN and/or added fibrous tissue, but such peaks were not consistently observed and thus were not analyzed in this study.

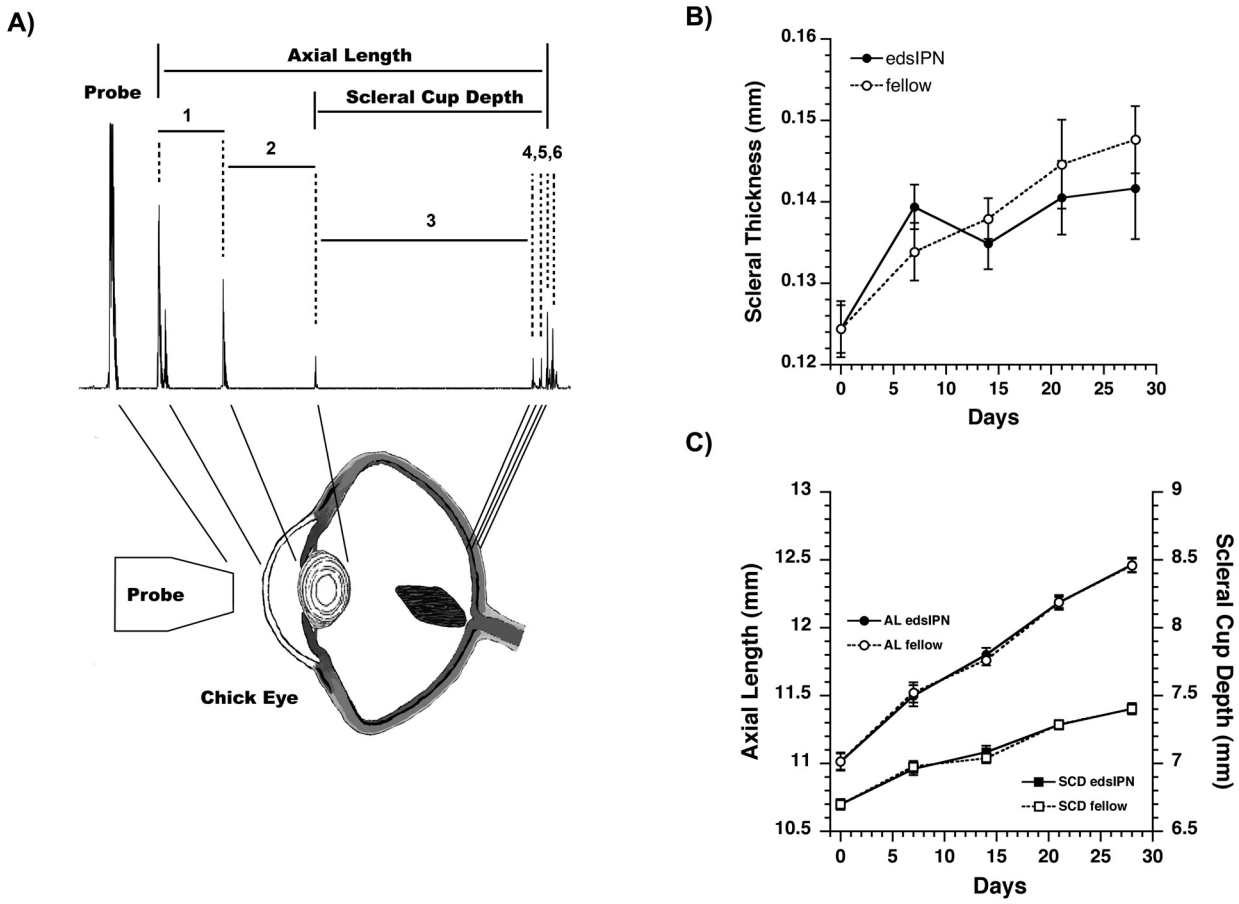

Figure 4-5. Sample trace recorded using high frequency A-scan ultrasonography (A), showing ocular components of interest: 1) anterior chamber, 2) lens, 3) vitreous chamber, 4) retina, 5) choroid, and 6) sclera. Scleral thickness (B) as well as scleral cup depth and axial length (C) plotted against time for edsIPN-injected or fellow chick eyes, which show similar growth patterns, confirming the biocompatibility of the edsIPN.

Endpoint refractions (measured in diopters, *D*) and number of eyes measured at 28 days are summarized in Table 4-1. The refractions of the edsIPN injected and fellow control eyes were near zero (emmetropic) and not statistically different from each other.

Table 4-1. Mean endpoint refraction ± standard error (in diopters, *D*) of chick eyes at 28 days post-injection.

Eye	Refraction (D)	Number of Eyes
Control (fellow)	0.3 ± 1.1	6
edsIPN injected	0.2 ± 1.9	6

3.4 Scleral histology

With careful enucleation and subsequent removal of adhering fatty tissues from enucleated eyes, it proved possible to visualize the injected edsIPNs at their expected location, attached to the sclera at the posterior pole of eyes (Figure 4-1B). However, their location was more readily visualized in the frozen sections, which were prepared from edsIPN treated and untreated control eyes, collected at weekly intervals over 4-week treatment period (Figure 4-6). One week after its injection, the edsIPN was seen positioned between the posterior outer scleral surface and the inner surface of extraocular muscle (week 1, Figure 4-6), bringing the edsIPN in close proximity to blood vessels in the latter case (red arrow, week 1, Figure 4-6). The numerous small clear vesicles within the edsIPN-injected space were most likely fractured gels due to injection and/or histological processing.

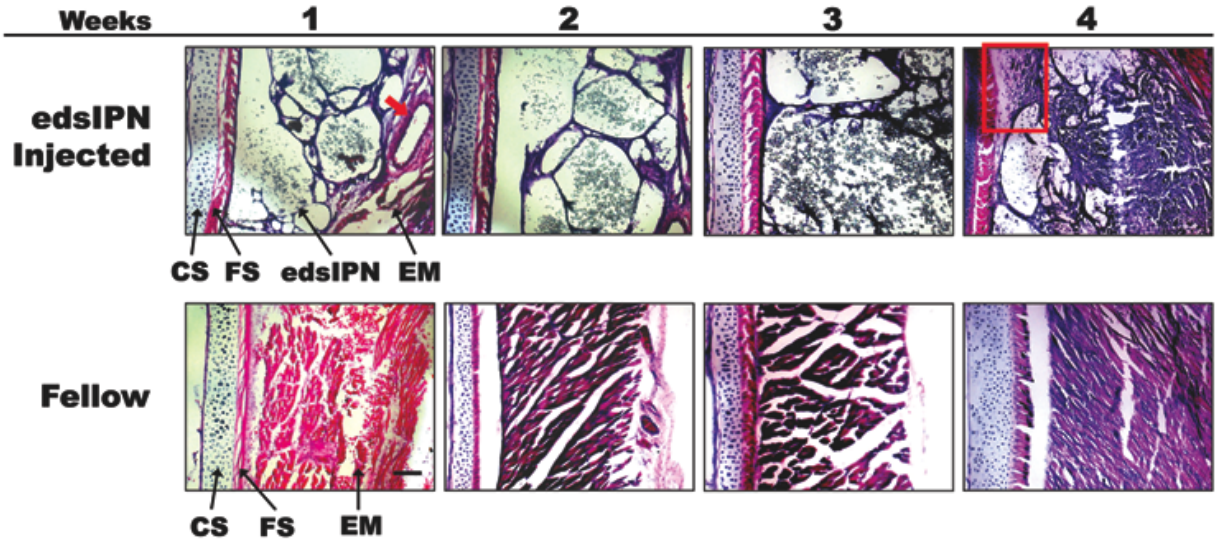

Figure 4-6. Representative H&E-stained histological sections of scleras from eyes treated with edsIPN compared to fellow untreated eyes, collected at weekly intervals from 1 to 4 weeks (10X magnification; scale bar = 100 μm; CS = cartilage sclera; FS = fibrous sclera; EM = extraocular muscle). Red arrow points to blood vessel in 1 wk post edsIPN-injected section. Red box indicates region where substantial fibrous tissue integration with edsIPN has occurred in 4 wks edsIPN-injected section.

Over the remainder of the treatment period, progressively more collagen was deposited and cell infiltration increased (weeks 2, 3 & 4, Figure 4-6). By week 4, the edsIPN was largely

replaced by dense fibrous connective tissue (red box, week 4, Figure 4-6), and there was clear indication of cell migration from the fibrous sclera into the edsIPN matrix (Figure 4-7A thru C), demonstrating integration of the edsIPN with the host fibrous layer. The thickness of the scleral integration layer adjacent to the host fibrous layer ranged approximately between 20-180 µm at 4 weeks. The cells observed in the edsIPN matrix are likely to be fibroblasts originating from the host sclera, monocytes originating from blood vessels in extraocular muscles, or both, although no specific markers were used to identify the cells in this study. In addition, at 4 weeks, there was evidence of deposition of collagen-like fibers within the edsIPN matrix (Figure 4-7D and E); the orientation of these fibers was more disorderly than in those of the native fibrous sclera. None of the chick eyes showed any evidence of inflammation, i.e. redness or swelling, over the course of the treatment period.

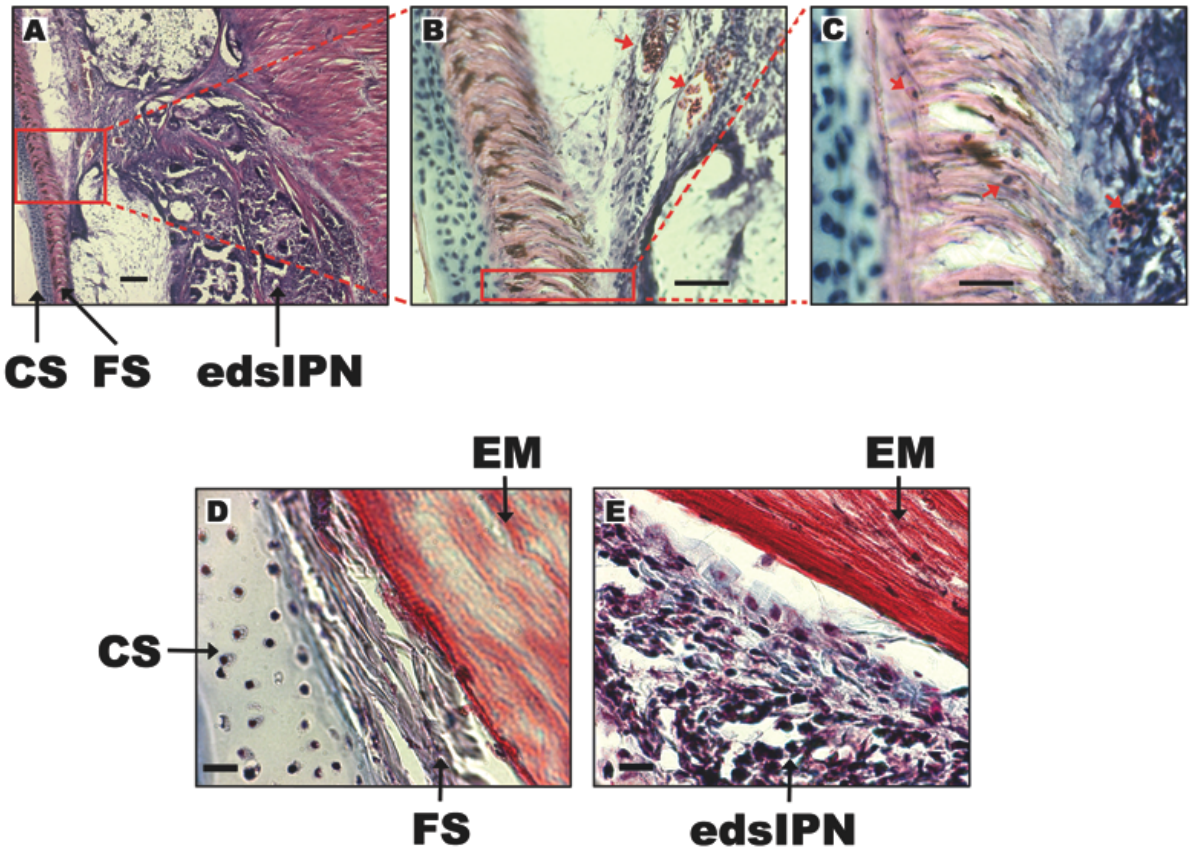

Figure 4-7. Histology section of posterior pole region of sclera from eye injected with edsIPN, sampled at 4 weeks, stained with H&E (A-C) or Masson's trichrome (D-E), and photographed at increasing magnification. CS = cartilage sclera, FS = fibrous sclera, EM = extraocular muscle. EdsIPN partly integrated with fibrous sclera (A, 10X magnification, scale bar = 100 µm); red arrows in B points to nests of cells within the edsIPN matrix (40X magnification, bar = 50 µm); red arrows in C indicate presumed fibroblasts in fibrous sclera and fibrotic edsIPN matrix (100X magnification, bar = 20 µm); light-blue stained collagen fibers within edsIPN (E, 63X magnification, bar = 50 µm); section from posterior sclera from fellow untreated eye shown at same magnification for comparison (D) .

4. Discussion

This study aimed to establish the *in vitro* cytocompatibility of a biomimetic edsIPN with ocular scleral cells and to investigate its ocular effects *in vivo* when applied to the outer scleral surface at the posterior pole of the eye. Although edsIPN of a specific composition and modulus was used in this study, as a class of materials, edsIPNs are mechanically and biologically tunable, and degrade when exposed to matrix metalloproteinases (Chung et al., 2006; Kim and Healy, 2003; Kim et al., 2005). The edsIPN preserved the phenotypes of the scleral cells *in vitro*, and the injected edsIPN increased the thickness of the outer wall of the eye by promoting cellular infiltration and subsequent deposition of collagen into the edsIPN. In addition, eye growth rate was not affected by the injected edsIPN. These findings suggest that a novel approach to the treatment of high myopia using injectable biomimetic hydrogels, e.g., edsIPNs, is possible.

For our application, we required the edsIPN to be sufficiently fluid as to be injectible but to stiffen in the body, to facilitate its retention at the injection site, where its primary role was to support attachment, migration, and proliferation of scleral cells. *In vitro* measurements of the edsIPN and experience from *in vivo* studies confirmed the suitability of the tested hydrogel. Its phase transition was compatible with easy passage through the 19-gauge needle used for retrobulbar injections, and the stiffening of the edsIPN on exposure to body temperature stabilized the edsIPN on the posterior sclera. *In vitro* measurements indicated an approximately 4.5 fold increase in the complex shear modulus with an increase from room to body temperature. Its modulus never reached that of the native stiffness of the sclera. The shear modulus for chick sclera is around 5.2 MPa, approximated by using 15.38 MPa as the elastic modulus and 0.48 as the Poisson ratio, (Battaglioli and Kamm, 1984; Phillips et al., 2000), and for human sclera is on the order of 0.6 – 1 MPa, approximated by using 1.8 – 2.9 MPa as the elastic modulus and 0.48 as the Poisson ratio (Battaglioli and Kamm, 1984; Friberg and Lace, 1988). Thus, this edsIPN would not have provided significant mechanical support to the sclera. The low substrate stiffness of our edsIPN likely also explains why treated eyes showed normal, rather than slowed rates of scleral cup and overall axial elongation.

The influence of ECM mechanical properties on cell growth is well established, with relevant observations reported for several cell types including fibroblasts and chondrocytes (Eckes et al., 2000; Nakagawa et al., 1989; Shieh and Athanasiou, 2003). Specifically, soft substrates tend to inhibit cell spreading and slow migration compared to their stiffer counterparts (Irwin et al., 2008; Saha et al., 2008); they also induce differentiation of mesenchymal stem cells to specific phenotypes (Engler et al., 2006). In the current study, a mechanical influence could explain both the delayed proliferation and slower overall rates of proliferation for cells cultured on edsIPN compared to TCPS. After initial attachment, both scleral cell types began proliferating on TCPS on day 3, while their proliferation was delayed on edsIPN to day 7. From our calculated percent increase in cell numbers, it is clear that proliferation was slowest for scleral chondrocytes cultured on edsIPN. Specifically, scleral chondrocytes cultured on edsIPN did not proliferate as much as the other groups, independent of their low initial cell attachment. It is likely that their lack of initial attachment was primarily due to the low complex modulus of the edsIPN, given that scleral chondrocytes naturally reside within a more rigid environment. Furthermore, it was shown previously that adult human dermal fibroblasts did not proliferate much, if at all, over 3 days when cultured on gels of similar stiffness (95 Pa in that study

compared to 63 Pa for our edsIPN at body temperature), but do proliferate significantly when cultured on higher stiffness gels (Ghosh et al., 2007). Thus, our results for chick scleral fibroblasts and chondrocytes were consistent with published findings. In follow-up studies we will optimize the mechanical properties of edsIPN for our intended therapeutic application for human myopia, and also employ a mammalian *in vitro* scleral cell culture model, which do not have a chondrocyte population.

The inclusion of MMP degradable peptide crosslinkers allows controlled cellular migration for in-growth into the synthetic ECM (Kim et al., 2005). Without the MMP degradable peptide crosslinkers, the synthetic ECM would not be degradable and would lose the control mechanism for cellular infiltration based on cell-mediated degradation. The testing of a material containing biodegradable peptide crosslinkers is in line with our long-term goal to develop a hydrogel for use in myopia control, since MMP-2 and MMP-13 are known to be upregulated during myopia progression (Schippert et al., 2006; Siegwart and Norton, 2005). Support for cell attachment was provided in the design of our edsIPN by grafting of the bsp-RGD(15) peptide sequences onto the linear interpenetrating p(AAc) chains (Harbers and Healy, 2005). The 300 μM bsp-RGD(15) concentration for the edsIPN was chosen to provide adequate support for scleral cell adhesion, and this was confirmed in our cell culture study. The statistical bulk distribution of the grafted bsp-RGD(15) was expected to aid the *in vivo* performance of the material by allowing cells to continually attach, proliferate, and infiltrate the synthetic ECM as an extension of the sclera. However, we observed significantly more early cell loss for scleral cells cultured on the edsIPN compared to the TCPS. It is possible that our choice of the peptide ligand was suboptimal or the modulus was too low for *in vitro* scleral cell culture. It is also known that ligand presentation and density can affect the phenotypic expression of differentiated cells (Hsiong et al., 2008; Rezania and Healy, 2000). The effect of substituting alternative peptide ligands and varying ligand density on initial attachment and growth rates of cells cultured on the edsIPN will be explored in follow-up studies.

Having established the *in vitro* cytocompatibility of the edsIPN for chick scleral cells, we undertook *in vivo* biocompatibility testing of the same edsIPN. Based on ultrasonography data, ocular axial dimensions, including scleral cup depth and axial length, were unaffected by the presence of the edsIPN on its outer surface, suggesting good biocompatibility with scleral tissue. Note that for both treated and fellow eyes, increases in scleral cup depth over the monitoring period was slower than that of axial length increase, reflecting the contribution to axial lengths of the anterior chamber segments, which grew faster than the posterior segment (Figure 4-5C). However, treated and fellow eyes showed no difference in endpoint refractions, consistent with the lack of treatment effects on the axial dimensions of the anterior chamber and lens, and ruling out even subtle effects on the curvature of the cornea and lens, and confirming the safety of the edsIPN injections.

Over the 4-week experimental period, there was progressive cellular invasion of the edsIPN with subsequent collagen deposition, as evidenced in histology sections, which revealed collagen-like fibers highlighted with Masson's trichrome stain. Remnants of non-degraded edsIPN were likely present at the 4-week time point since there were small clear regions within the newly formed fibrous tissue. This interpretation is also consistent with the relatively slow degradation rate for the degradable peptide crosslinker used in our study, quantified in a separate

in vitro study (Wall et al., 2009). Compared to native untreated fibrous sclera, the collagen fibers within the edsIPN appeared to be less organized in orientation. Although the cellular infiltration of the implants resulted in an apparent thickening of the outer fibrous layer of the sclera, this increase in thickness was not detected by high frequency ultrasonography, suggesting either that this scleral integration layer had altered impedance compared to the native sclera, or that the combined attenuating effect of all the preceding intervening ocular surfaces rendered our device insufficiently sensitive to detect the boundaries of this most posterior layer. While an extra fibrous layer was added to the posterior native sclera, the rate of elongation of treated eyes was not retarded compared to that of untreated fellow eyes. This lack of effect on ocular elongation is similar to that reported by our group for previously tested HEMA and PVP implants in chick (Su et al., 2009a), and points to complex interactions between scleral tissue growth and intraocular pressure as determinants of eye enlargement in the avian eye. It is likely that the same edsIPN-induced changes will have different effects on the elongation of mammalian eyes, which lack a rigid inner cartilaginous layer, and also on myopic mammalian eyes whose scleras show increased remodeling and subsequent thinning (Norton and Rada, 1995).

5. Conclusion

In summary, exploiting the unique properties of the edsIPN has enabled us to design and synthesize a biomimetic ECM that supports the growth of chick scleral fibroblast and chondrocyte *in vitro*, that is compatible with its delivery by retrobulbar injection, and that is able to support fibrous connective tissue in growth *in vivo*. Future research will emphasize design strategies for scleral strengthening in a mammalian model for myopia through the application of edsIPNs, used on their own or as a vehicle for controlled delivery of myopia retarding agents.

Chapter V

Polymeric Drug Delivery Vehicles for the Delivery of Atropine at Posterior Sclera for the Inhibition of Myopia Progression

Abstract

Atropine, a potent muscarinic antagonist, had been investigated in several clinical studies for its ability to inhibit myopia progression in recent decades. Most reported data were promising, showing some degree of efficacy over a period of years, but the exact mechanism of action for this inhibitory effect on myopia progression is still largely unknown. The aim of this project was to synthesize and test the suitability of a synthetic extracellular matrix (ECM) hydrogel as an atropine delivery vehicle that allows localized targeting of the posterior sclera for the control of myopia progression. A synthetic ECM hydrogel composed of a thermo-responsive enzymatically-degradable semi-interpenetrating polymer network (edsIPN) was synthesized by redox radical addition polymerization. The edsIPN was lyophilized and allowed to soak overnight in 1% w/v atropine sulfate solution. *In vitro* release kinetics was assessed using UV-Vis spectroscopy measured at 230 nm and 37 °C. For in vivo testing, forty-eight 12 day-old chicks (4 groups of 12) wore monocular -10 D lenses for 1 wk to induce myopia, then the lens power was increased to -15 D and the treated eyes subjected for 2 weeks to either: 1) daily topical atropine ointment (4 µl, 10 mg/ml); 2) retrobulbar hydrogel-saline (sham) injection (100 µl); 3) retrobulbar hydrogel-atropine injection (100 µl, 10 mg/ml); or 4) no additional treatment. Ocular dimensions were measured by high frequency A-scan ultrasonography and refractions by retinoscopy at 0, 1, 2, and 3 wks. Initial burst release *in vitro* showed that approximately 47% of atropine was released within the first 30 min, while 90% of atropine was released by 8h. Wile all treated eyes were significantly longer than their fellows ($p < 0.05$), interocular axial length differences were significantly smaller by 21 days for hydrogel-atropine treatment compared to lens only treatment ($p < 0.01$). However, endpoint refractions (mean spherical equivalent) of treated eyes were not statistically different between the treatment groups, although there is a general trend towards lower refractive errors in the atropine treatment groups. Overall, this study demonstrated the feasibility of using a synthetic ECM hydrogel to deliver atropine to the posterior sclera for myopia control.

1. Introduction

The use of semi-interpenetrating polymer networks (sIPNs) have been widely explored as potential vehicles for sustained delivery of a number of other drugs, e.g. insulin (Park, 1999; Vernon et al., 1999), indomethacin (Okano et al., 1990) and diclofenac (Geever et al., 2008). More widely classified as hydrogels, the benefits of using sIPNs as drug delivery vehicles include their good overall biocompatibility and ease of solute transport control (Peppas et al., 2000; Qiu and Park, 2001). Chemical composition, water content, cross linking density, and crystallinity are some of the major parameters that can be varied to control the release rate of drug molecules from sIPNs, with the optimal design depending on the delivery route and physiological conditions encountered *in vivo*. In this study, we proposed to design and characterize an injectable sIPN-based sustained drug delivery system for atropine for application in the treatment of myopia.

Polymeric systems such as enzymatically-degradable sIPNs (edsIPNs) not only open up the possibility of creating novel tissue scaffolds for controlling scleral remodeling as previously reported (Su et al., 2009b), but also could potentially be utilized to deliver drugs for the control of eye growth. The specific properties of sIPNs that could be beneficial for atropine delivery at the posterior sclera include: (1) being easily handled at room temperature and slightly above, and able to be delivered through a syringe needle, (2) undergoing a phase transition *in situ,* allowing transformation from a soft viscous fluid to stiff elastic solid, to become more similar to the native extracellular matrix (ECM) environment, and more conducive to cell migration into the gel, (3) having a high water content, which allows for the transport of O_2 and macromolecules, (4) a degradation rate, which is sensitive to the enzymatic activities of matrix metalloproteinases (MMPs), released by and so regulated by native scleral cells, and (5) allows for the modulation of the release rate of atropine through variations in the crosslinking density and the degradation rate of the synthetic polymer matrix.

With respect to pharmacological treatments, atropine, applied topically as eye drops to the cornea, is the only drug currently in clinical use off-label for the treatment of myopia. First tested in a clinical trial in 1985 (Bedrossian, 1985), its use remains largely limited to Asian countries with very high prevalences of myopia because of the many ocular side effects of topical atropine (Chua et al., 2006; Fan et al., 2007; Lee et al., 2006). These side effects reflect both the wide distribution of muscarinic cholinergic receptors in the eye and nonselective binding of atropine to this family of receptors (Hardman et al., 2001). Paralysis of accommodation resulting in blurred near vision, pupil dilation eliciting glare symptoms, and inhibitory effects on tear secretion resulting in dry eyes, all contribute to noncompliance problems associated with chronic use of topical atropine for myopia control.

In addition to its demonstrated efficacy for the control of myopia and the likely reduction in ocular side-effects with the delivery of atropine directly to the sclera, the possibility that the anti-myopia action of atropine is effected through a scleral site is an additional reason underlying our choice of atropine to examine the efficacy of edsIPNs as a slow release delivery device in the treatment of myopia. With respect to the anti-myopia effect of atropine, the sclera is one of two sites of action under consideration. The plausibility of a scleral site of action for atropine is supported by reports of (1) muscarinic receptors on human scleral cells (Qu et al., 2006), (2) up-

regulation of M1 and M4 subtypes on scleral cells from myopic (form deprived) guinea pig eyes (Liu et al., 2007), and (3) changes in chick sclera of DNA and glycosaminoglycan synthesis *in vitro* induced by muscarinic antagonists, including atropine (Lind et al., 1998). Evidence for alternative retinal site of action for atropine comes from studies in chick: (1) when atropine is administered immediately before form deprivation, a myopia-inducing visual manipulation, it decreases retinal expression of ZENK, a marker of altered eye growth (Ashby et al., 2007), (2) atropine alters the effect of dopaminergic drugs such as apomorphine, which have a presumed retinal site of action for their anti-myopia action (Schmid and Wildsoet, 2004; Schwahn et al., 2000). Nonetheless, the latter drug interactions were not additive and so a nonretinal site for atropine could not be ruled out. Also, eliminating the source of retinal acetylcholine by obliterating cholinergic amacrine cells does not prevent either form deprivation myopia (Fischer et al., 1998b), or lens-induced myopia (Yew, 2004). While a scleral site of action for atropine is optimal for the proposed scleral site of application, there is also evidence that drugs applied at the posterior sclera can reach retinal sites (Barocas and Balachandran, 2008). Therefore, the lack of resolution on the site for atropine's anti-myopia action, i.e. retina versus sclera, does not argue against our approach.

The study reported here investigated ocular growth changes in response to intraorbital injection of atropine-loaded edsIPNs at the posterior pole of chick eyes wearing negative lenses to induce myopic growth. The edsIPNs was considered in this study as a platform to deliver atropine for treating high myopia, not only because this approach will target the posterior sclera location and thus minimizing ocular complications, but also because the same biomaterial was previously demonstrated to integrate with and thus potentially strengthen the fibrous sclera. Our goal was to achieve immediate inhibition of myopia progression through the pharmacological action of atropine, and provide long-term scleral stability through the thickening of the fibrous sclera. We anticipated that the atropine would be released within a relatively short time frame from the edsIPN due to the loose structure of the synthetic polymer matrix. However, we also predicted some inhibition of myopia progression due to early action of atropine. By using the chick in the current study, we aimed to learn more about the anti-myopia effect of this drug-polymer combination as well as provide additional insight into the atropine site of action for the inhibition of myopia progression, although we also acknowledged the limitation of the chick model related to its bilayered sclera.

2. Materials & Methods

2.1 Preparation of edsIPNs

The synthesis of edsIPNs followed that described in Materials & Methods section of Chapter IV. All edsIPNs were synthesized separately in 5 ml volumes. Immediately after the final rinsing step, the edsIPNs were freeze-dried until constant weight is reached for each sample. The lyophilized edsIPNs were rehydrated by soaking in 1% w/v atropine sulfate (Aldrich, St. Luis, MO) solution in phosphate buffered saline at room temperature for 24h. Since the edsIPNs have the same material characteristics of a hydrogel, the names "edsIPNs" and "hydrogel" are used interchangeably in describing this study.

2.2 *In vitro* release kinetics

Each individual rehydrated edsIPN was sealed separately in tubes of 500 MWCO dialysis membranes (Spectrum Laboratories, Rancho Dominguez, CA). Approximately 1" of air space was left to promote floatation of the dialysis tube. Each tube was placed in 200 ml of phosphate buffered saline (PBS) in sink condition at 37 °C with stirring. The release of atropine into the surrounding buffer was monitored by UV-Vis spectroscopy at wavelength of 230 nm (Ceyhan et al., 2001). A standard curve was established using serial dilutions of atropine in PBS, and used to determine atropine concentrations in test samples. Data were initially collected every 10 min for the first hour, then hourly until no further changes were observed in the atropine concentration. Data were plotted as mean concentration ± standard deviation.

2.3 Animals & experiments

White Leghorn chicks (*Gallus gallus domesticus*) were obtained as hatchlings from a commercial hatchery (Privett Hatchery, Portales, NM) and reared in 12/12-hour light/dark cycle, with food and water available ad libitum. The room temperature was maintained between 83-89°F. A total of 48 birds at 12 days old were used for this study. The presence in the chick sclera of an outer fibrous layer similar in structure to the mammalian sclera, combined with the fast growth of the chick eye and the practical advantages of working with chicks, provided the rationale for using the chick model in this study. Care and use of the animals were in compliance with an animal use protocol approved by the Animal Care and Use Committee of the University of California, Berkeley, and adhered to the ARVO Statement for the Use of Animals in Ophthalmic and Vision Research.

All chicks (4 groups of 12 each) wore monocular -10 D lenses for 1 wk to induce myopia, then the lens power was increased to -15 D when treated eyes were also subjected for 2 weeks to either: 1) daily topical atropine ointment (4 µl, 10 mg/ml); 2) one retrobulbar hydrogel-saline (sham) injection (100 µl); or 3) one retrobulbar hydrogel-atropine injection (100 µl, 10 mg/ml). A fourth group wore lenses but had no drug treatment (see Table 5-1). The initial -10 D lens treatment served to initiate the myopic growth in treated eyes, and the switch to -15 D lens at week 1 served to sustain this myopic growth pattern over the remainder of the study period. All treatments were monocular and randomly assigned to either the left or right eye. The contralateral eyes were left untreated. Prior to injections, chicks were first anesthetized with 2% isoflurane in oxygen. Access to the orbit was gained through a small temporal incision. A 7-0 silk anchoring suture was placed in the anterior sclera to rotate and fix the eye, to allow easier access to the posterior pole. The polymer was delivered over the posterior pole, between the sclera and the dorsal oblique extraocular muscle using a curved, blunt-end 19-gauge needle (sub-Tenon's anesthesia cannula needle, BD Ophthalmic Systems; Franklin Lakes, NJ) with the aid of a surgical microscope, which also allowed unwanted anterior diffusion of the injected edsIPN to be ruled out. An antibiotic ointment was applied prophylactically, after suturing closed the incision site.

Table 5-1. Treatment groups for *in vivo* assessment of edsIPN-atropine delivery at posterior pole sclera. All chicks were 12 days old at start of experiment.

Drug Treatment	Abbr.	Lens Power (D)	*N* (chicks)	Atropine conc. (mg/ml)	Volume (µl)	Dosing Frequency
atropine ointment	A-O	-10 then -15 @ 1 wk	12	10	4	daily
hydrogel-saline	H-S	-10 then -15 @ 1 wk	12	0	100	once
hydrogel-atropine	H-A	-10 then -15 @ 1 wk	12	10	100	once
none	Lens Only	-10 then -15 @ 1 wk	12	0	0	0

2.4 Measurement and analyses of ocular dimensions & refractions

Axial eye growth was monitored *in vivo* using a custom high frequency 30 MHz A-scan ultrasonography set-up that offers measurement precision down to 10 µm (Nickla et al., 1998). The thickness of the sclera and all other axial ocular components (anterior chamber depth, lens thickness, vitreous chamber depth, retina, and choroid) were obtained by averaging data from a minimum of 12 measurements per eye per time point. Chicks were anesthetized with 1.5% isoflurane in oxygen for all measurements. Data were collected for all chicks on the day of but before the injection (day 0; baseline), as well as at 1, 2, and 3 weeks after injection.

Data for treated and fellow eyes were normalized so that their baseline means matched the overall baseline mean for all eyes. Scleral cup depth data were obtained by adding together the vitreous chamber depth, retinal thickness, and choroidal thickness, as an index of scleral surface area. Scleral thickness was not included in this parameter to allow for the possibility that it changed independently of scleral surface area. It was also not included in the derived axial length parameter, which was calculated as the sum of anterior chamber depth, lens thickness, and scleral cup depth. Axial length was used as an index of ocular elongation.

In addition to ultrasonography, endpoint refractions were measured by streak retinoscopy on the eyes of the same birds at end of the monitoring period. Birds were anaesthetized with 1.5% isoflurane during measurements. Treatment-induced changes in refraction can be expected from effects on either or both the curvature of the optical components of the eye, and ocular growth. Normalized data from treated and fellow control eyes were compared statistically using two-way repeated-measures ANOVA, Tukey/Kramer post-hoc test, and paired *t*-test (Statview, Version 4.0; SAS Institute; Cary, NC). A *p*-value of less than 0.05 was used for statistical significance.

3. Results

3.1 *In vitro* atropine release

The atropine release from the edsIPN itself was rapid (Figure 5-1), with initial burst release occurring within the first 30 minutes of testing in PBS. During this initial period, approximately 47% of the drug content was released into the surrounding PBS solution. After this time, approximately 90% of the drug was released by 8h. As minimal additional release was observed up to 12h, it is likely that the rest of the atropine remained in the gel due to equilibration with the surrounding media and entrapment within the edsIPN matrix. The calculated release rate of atropine was approximately 5.6 µg/ml/h.

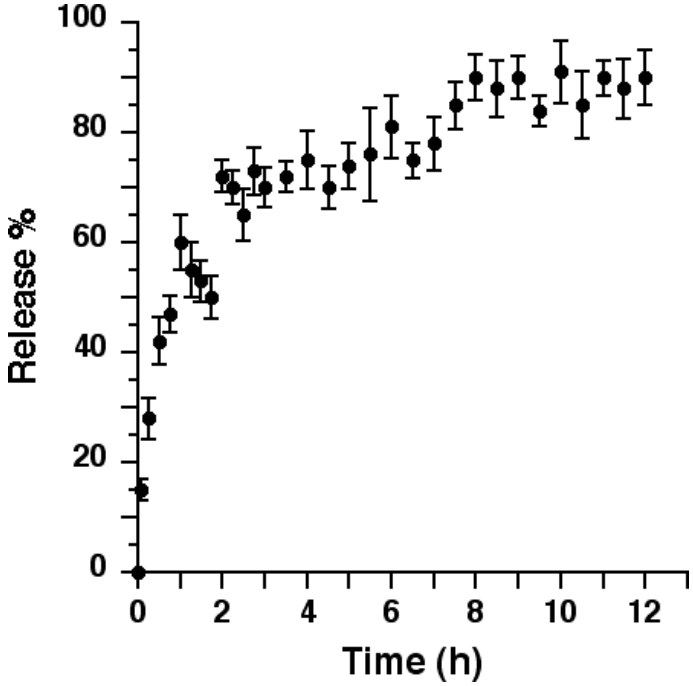

Figure 5-1. Release of atropine from preloaded edsIPN (mean ± standard error). Initial burst release was observed, with 90% released by 8h.

3.2 Ocular dimensions

Vitreous chamber depth for all treatment groups was found to increase at a significantly faster rate than fellow eyes (repeated-measures ANOVA, $p < 0.05$; Figure 5-2A), as expected from negative lens wear. However, comparison of interocular differences in vitreous chamber depth across treatment groups revealed that the treated eyes of the hydrogel-atropine treated group underwent significantly smaller vitreous chamber growth than their contralateral eyes compared to all other groups (repeated-measures ANOVA, $p < 0.01$; Figure 5-2B).

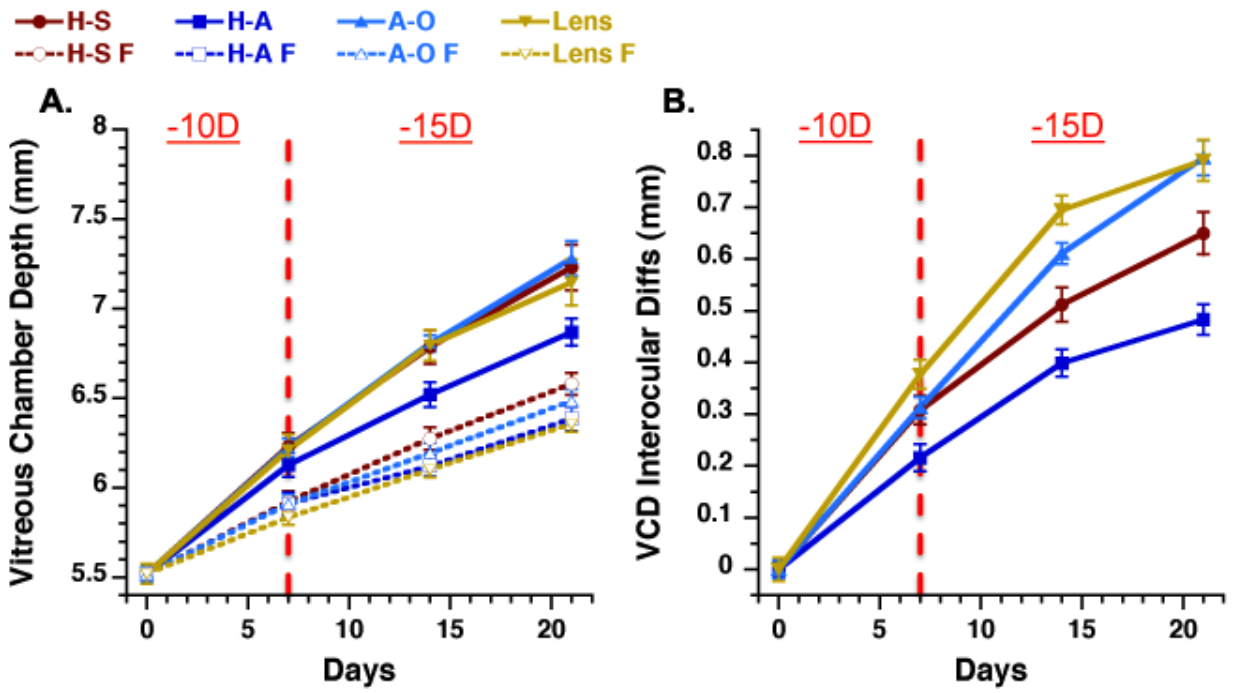

Figure 5-2. Ultrasonography measurements of (A) vitreous chamber depth and (B) vitreous chamber depth interocular differences for all treatment groups over 21 days (mean ± standard error). H-S = hydrogel-saline. H-A = hydrogel-atropine. A-O = atropine ointment. Lens = lens only. F = fellow.

Scleral cup depth was found to be significantly lower in the hydrogel-atropine injection group compared to all other treatment groups (repeated-measures ANOVA, $p < 0.05$; Figure 5-3A). However, the expected decrease with scleral cup depth with atropine ointment treatment was not observed. Comparison of interocular differences in scleral cup depth demonstrated that both hydrogel-saline and hydrogel-atropine treatment groups had significantly reduced scleral cup depth increases compared to the lens only or atropine ointment treatment groups (repeated-measures ANOVA, $p < 0.05$; Figure 5-4A). The scleral cup depth increase for the hydrogel-atropine formulation was approximately 43% less than that of the lens only group, while the increase for the hydrogel-saline group was approximately 27% less than that of lens only group (Figure 5-4A).

For axial lengths, treated eyes were significantly longer than their fellows ($p < 0.05$). No statistically significant differences in axial lengths of treated eyes were found for atropine treatment group compared to the lens only group (Figure 5-3B). The interocular differences demonstrated similar effectiveness profiles for hydrogel-atropine and atropine ointment treatment groups, with interocular axial length differences being significantly lower for these two groups by 21 days compared to that of the lens only group (paired t-test, $p < 0.01$; Figure 5-4B). The interocular differences were similar in the two atropine treated groups, and were approximately 35% less than that of the lens only group after 21 days of treatment.

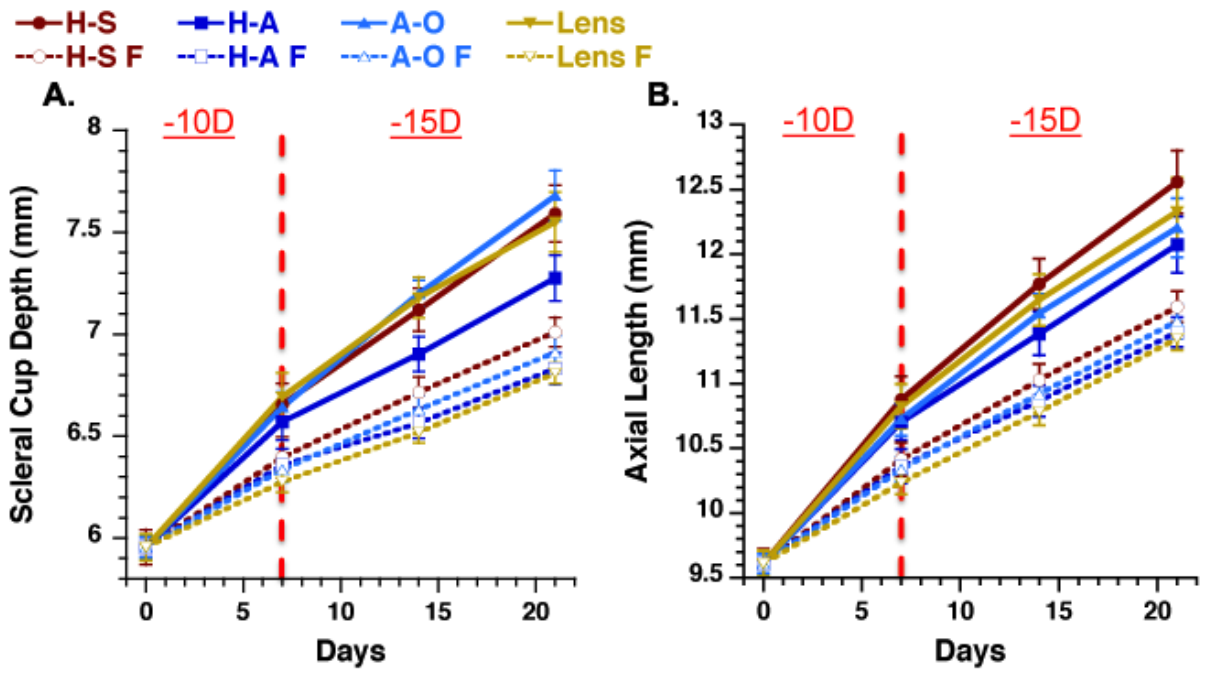

Figure 5-3. Ultrasonography measurements of (A) scleral cup depth and (B) axial length for all treatment groups monitored over 21 days (mean ± standard error). H-S = hydrogel-saline. H-A = hydrogel-atropine. A-O = atropine ointment. Lens = lens only. F = fellow.

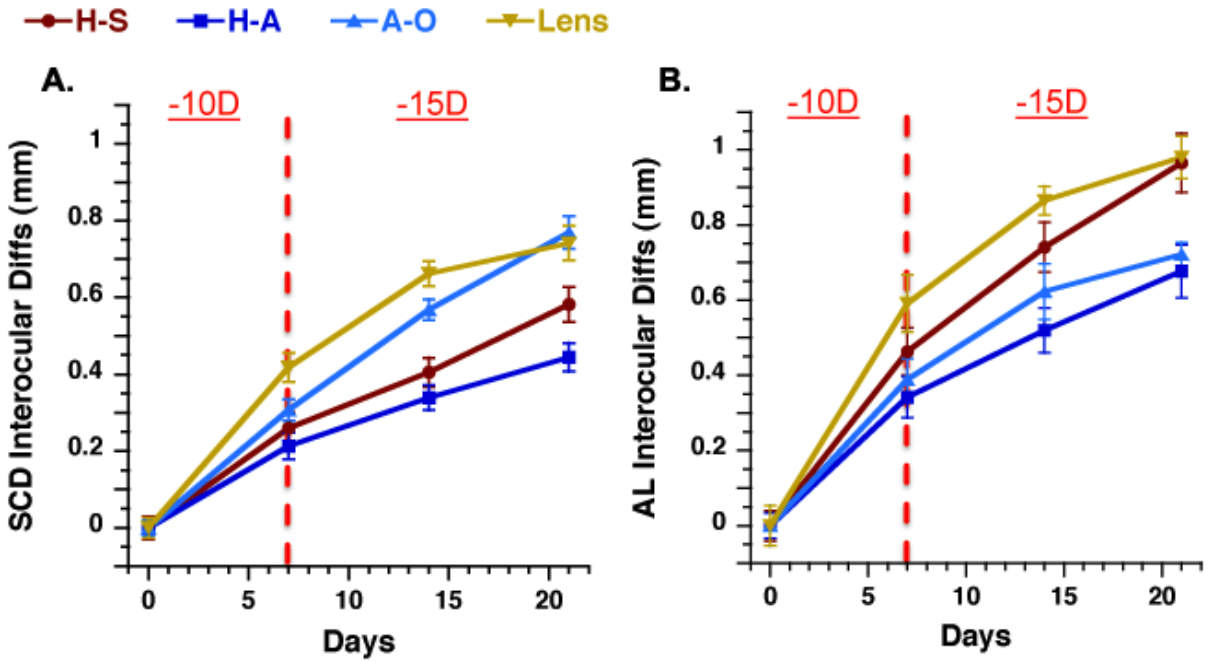

Figure 5-4. Interocular differences (treated – fellow eye) in scleral cup depth (SCD) and axial length (AL) for all treatment groups measured over 21 days (mean ± standard error). H-S = hydrogel-saline. H-A = hydrogel-atropine. A-O = atropine ointment. Lens = lens only.

3.3 Ocular refractions

There was no difference in the refractive errors of the treated eyes between the treatment groups. The endpoint refractions (means ± standard error) in each group were shown in Figure 5-5.

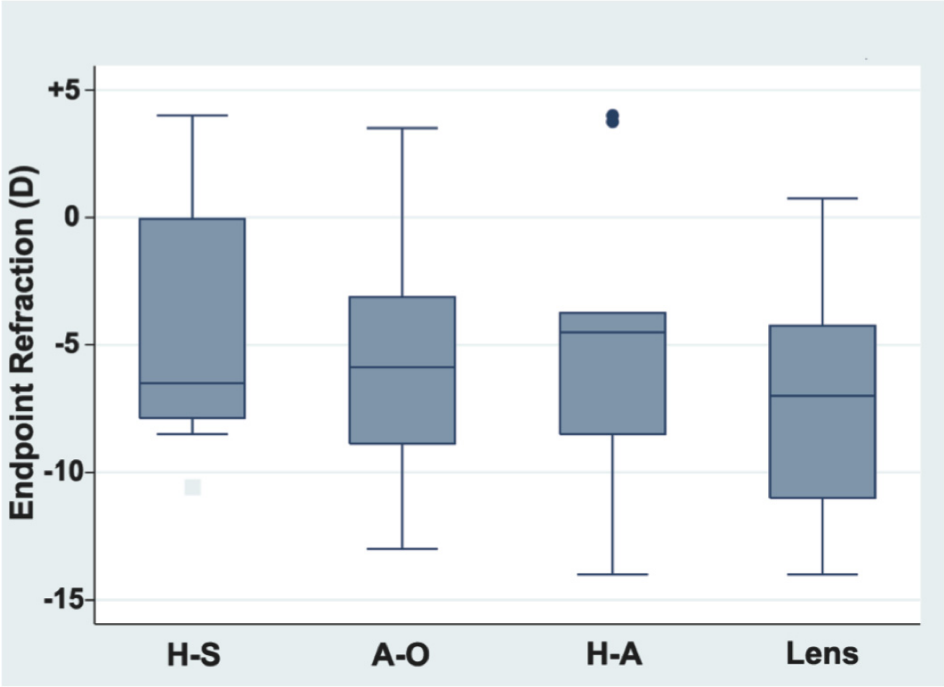

Figure 5-5. Endpoint refractions represented in box plot showing the mean endpoint refractions of each treatment group at 21 days (mean ± standard error). H-S = hydrogel-saline. A-O = atropine ointment. H-A = hydrogel-atropine. Lens = lens only.

Based on comparisons of within-eye changes of refraction M_{diff}, all treatments significantly affected refractions, although the atropine ointment treated eyes were less myopic ($p = 0.011$; Table 5-2) compared to all other treated eyes.

Table 5-2. Summary of within-eye change of refraction (M_{diff}) data collected for all treatment groups at 21 days. H-S = hydrogel-saline. A-O = atropine ointment. H-A = hydrogel-atropine.

	H-S	A-O	H-A	Lens Only
M_{diff}	-8.92±1.82	-7.11±1.69	-9.89±3.95	-0.03±1.12

In looking at the relationship between endpoint refractions and vitreous chamber depths (Figure 5-6), a high correlation between induced myopia and vitreous chamber depth of treated eyes was found. This result confirmed the axial nature of the induced myopia.

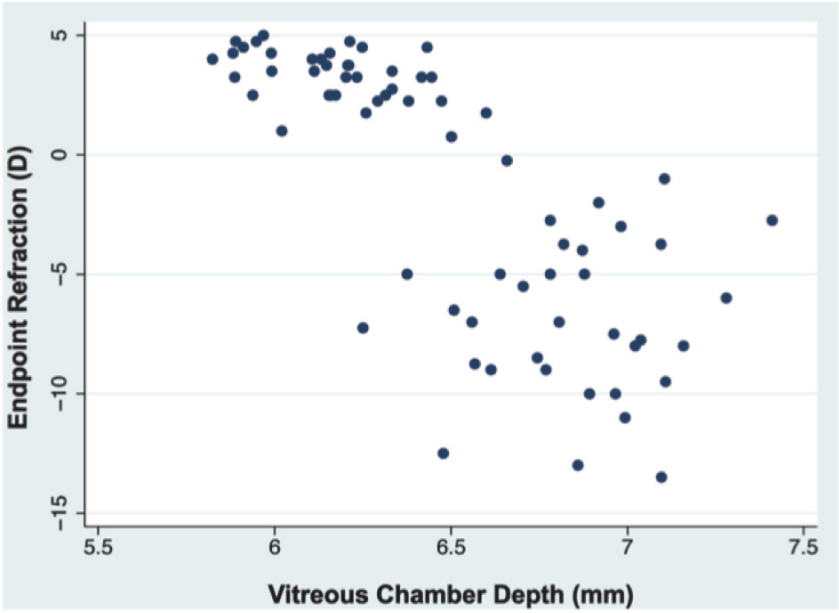

Figure 5-6. Endpoint refraction versus vitreous chamber depth for all data demonstrated high correlation between increasing myopia and higher vitreous chamber depth.

4. Discussion

This study aimed to investigate the potential of using edsIPNs loaded with atropine to deliver this drug to the posterior sclera for the purpose of inhibiting myopia development in chicks wearing negative lenses. Previously, the cytocompatibility of a biomimetic edsIPN with ocular scleral cells and its ocular effects *in vivo* when applied to the outer scleral surface of the posterior pole were studied in the chick, and it showed promising potential as scleral tissue scaffolds (Su et al., 2009b). As a class of materials, edsIPNs are mechanically and biologically tunable, and degrade when exposed to local endogenous matrix metalloproteinases (Kim and Healy, 2003; Kim et al., 2005). The edsIPN preserved the phenotypes of the scleral cells *in vitro*, and the injected edsIPN increased the thickness of the outer wall of the eye by promoting cellular infiltration and subsequent deposition of collagen into the edsIPN. In addition, normal eye growth rate was not affected by the injected edsIPN. These findings supported further investigation of edsIPNs as a drug delivery vehicle for delivering atropine to the posterior sclera.

The edsIPNs could be an ideal platform to deliver atropine for treating high myopia by directly targeting the sclera, and in doing so minimizing ocular complications. The main benefits of this approach include achieving immediate inhibition of myopia progression through the pharmacological action of atropine, and providing long-term scleral stability through the thickening of the fibrous sclera. We had expected atropine to be released within a relatively short time frame from the edsIPN, due to the hydrophilic and loose structure of the synthetic matrix. This expectation was confirmed by measured *in vitro* release kinetics, where approximately 90% of the drug was found to have eluted from the edsIPN by 8h. However, if these *in vitro* data translate to the *in vivo* conditions, this very fast release rate is impractical, limiting the delivery of atropine to within a couple of days at most. Our application required that the edsIPN to be

sufficiently fluid as to be injectable but to stiffen in the body, to facilitate its retention at the injection site for drug delivery. However, this requirement limits the use of higher crosslinking density that could be employed to retain the drug longer within the edsIPN. The intraorbital space is composed of mainly fatty connective tissue, and thus fluid exchange rate is expected to be quite low. As the *in vivo* release rate could be much reduced due to low fluid exchange rate, we proceeded to test the atropine-loaded edsIPN in lens-induced myopic chick eyes to investigate its effects on slowing myopic eye growth.

Even though the *in vitro* release was relatively rapid, we expected to observe some inhibition of myopia progression in the lens-induced chick myopia model due to the early inhibitory action of atropine. This was indeed the case as the increase in vitreous chamber depth was significantly reduced upon the start of hydrogel-atropine treatment compared lens only treatments, and this inhibitory effect was maintained up to two weeks after. Interestingly, the treated eyes in sham group also showed significantly reduced vitreous chamber depth from 1 to 3 weeks compared to the eyes wearing only lenses, although no atropine was present. The reasons could be that the volume of injected hydrogel at the outer posterior scleral surface was mechanically restraining the vitreous chamber depth, or that the hydrogel injections triggered a response in the sclera, slowing its growth. However, our previous findings tends to rule out the latter (Su et al., 2009b), as normal eye growth response was shown after edsIPN injections. However, this earlier biocompatibility test was conducted in normal eyes, raising the further possibility that myopic scleras interact differently with edsIPNs than normal scleras.

Our finding provides additional support for an inhibitory action of atropine on myopia progression with the observation that interocular differences in axial length were similarly decreased in the hydrogel-atropine and atropine ointment treatment groups compared to hydrogel-saline and lens only treatment groups. However, this was not the case for scleral cup depth, as the hydrogel-atropine and hydrogel-saline groups had significantly decreased interocular differences in scleral cup depth compared to the atropine ointment and lens only treatments. The reason for this disparity is that axial length includes anterior segment dimensions, and atropine treatments decreased the thickness of anterior components to slow overall axial length increase (data not shown). On the other hand, the scleral cup depth could be affected by the injected volume of the hydrogel, which was 100 μl, with the observed effect of smaller increase in elongation of both the scleral cup depth and vitreous chamber depth. The injection volume may need to be decreased in further studies to rule out the mechanical shape-changing effects at the posterior sclera.

We did not find significant changes in the endpoint refractions of the chicks in atropine treated eyes, although there appears to be a trend towards lower myopia progression compared to eyes treated with lenses only. The fact that there were no significant intergroup differences observed after starting atropine treatment may indicate that the amount of atropine being applied could have been too low, and that future studies should increase the amount of atropine loaded into the edsIPN and use the atropine ointment more than once daily. The applied atropine ointment at the anterior chamber may experience fast washout due to rapid tear fluid exchange. Although the refraction data correlates highly with the vitreous chamber depth, a greater variation in vitreous chamber depth was observed with increasing refractive error, implying contributions of other ocular components to the induced myopia.

Another possibility to prolong therapeutic duration of atropine is to embed drug-loaded nanoparticles, such as polylactide-*b*-methoxypolyethylene glycol that have previously been reported to enable sustained drug delivery (Park and Healy, 2003; Yamamoto et al., 2002). In an effort to reduce the ocular complications and to study the site of action for atropine, we proposed to deliver our treatment by an intraorbital injection at the posterior pole of the eye. For such treatments, it is important to limit the required frequency of treatments as much as possible to avoid injection pain and potential complications from frequent injections. Thus, to extend atropine's residence time in the sIPNs, we could aim to develop a nanoparticle formulation showing that nontoxic nanoparticles (e.g. < 100 nm) can be made from the diblock copolymer polylactide-*b*-methoxypolyethylene glycol (pLL-*b*-mpEG), and loaded with atropine in a single-step process while achieving both high loading content and efficiency (Gref et al., 1995; Park and Healy, 2004; Tobío et al., 1998; Yamamoto et al., 2002). By varying parameters such as % drug incorporation, copolymer M_w, and particle size, drug loading and drug release dynamics of the nanoparticles can be manipulated. These nanoparticles can be loaded into the developed edsIPNs to create a slow drug delivery platform. Previous efforts investigating nanoparticle release kinetics have achieved promising results, with a nanoparticle formulation showing zero order release kinetics maintained over 6 weeks (Park and Healy, 2004). However, there have been few studies investigating the dual release mechanism from drugs encapsulated within both nanoparticles and edsIPNs, with nanoparticles themselves embedded inside the edsIPNs. The main advantage of this system is the ability to provide a highly tunable control release platform that can produce constant atropine release rate at the ocular site of action, and which could also avoid the need for repeat injections.

5. Conclusion

In summary, we have designed and synthesized an enzymatically-degradable semi-interpenetrating polymer network for the application of delivering atropine to the posterior outer scleral surface. The atropine-loaded edsIPN was found to effectively lower vitreous chamber depth, scleral cup depth, and interocular difference in axial lengths, which are all indicators of slowed ocular growth. However, the finding that no significant changes were found for endpoint refractions points to further complications arising from changes in anterior chamber depth or that the presence of the edsIPNs in the posterior pole induced direct mechanical changes to the posterior eye shape. Future work should explore variations in the design parameters of the edsIPN, such as crosslinking density, modulus, and use of other polymers for effective delivery of atropine to the posterior sclera. The potential to include nanoparticles in the edsIPNs should be explored, as a dual release mechanism that could effectively prolong the release rate beyond what is possible using the edsIPNs alone.

Chapter VI

Dissertation Summary and Discussion

1. Major Findings of the Dissertation

The prevalence of myopia has steadily climbed worldwide in recent decades with the most dramatic impact in East Asian countries. Treatments such as eyeglasses, contact lenses, and laser surgery for the refractive error are widely available, but none of these treatments cure the underlying cause. There has been generally little attention paid to the use of biomaterials as an anti-myopia treatment. In progressive high myopia, invasive surgical procedures using a scleral buckle for mechanical support are performed since the patient is at risk of becoming blind. Treatment outcomes are highly dependent on the surgeon's skills and the patient's myopia progression rate, with limited choices in buckling materials. This dissertation work, with four main studies, represents efforts directed at combating high myopia progression through the exploration and development of biomaterials that slow scleral growth, as an alternative approach.

Two different materials, polyvinylpyrrolidone delivered as injectable gels and poly(2-hydroxyethyl methacrylate) as solid strips, were implanted in chicks to demonstrate the concept of posterior pole scleral reinforcements. The purpose of this study was to investigate whether polymeric hydrogels, either implanted or injected adjacent to the outer scleral surface at the posterior pole, could slow ocular elongation. The pHEMA implant significantly increased scleral thickness by the third week, and the implant became encapsulated with fibrous tissue. The PVP-injected eyes left otherwise untreated, showed a significant increase in scleral thickness, due to increased chondrocyte proliferation and extracellular matrix deposition. However, the PVP injection had no effect on the rate of ocular elongation. In eyes wearing optical devices to induce myopia, there was no effect on either scleral thickness or ocular elongation. These therapies did not work well for the inhibition of myopia progression. However, these results support the idea that scleral growth can be manipulated without adverse inflammatory responses. Since neither approach slowed ocular elongation, additional factors must influence scleral surface area expansion in the avian eye.

The mRNA expression levels of the chick scleral matrix metalloproteinase-2, -13, tissue-inhibitor of metalloproteinase-2, and transforming growth factor-beta 2 were assessed for influences of treatment duration and defocus power. Results for the fibrous and cartilaginous layers of chick sclera showed opposite trends, as did the responses to positive and negative lenses. Expression levels in the fellow eyes of positive and negative lens groups were not significantly different, indicating that there was no interocular yoking. TGF-β2 expression showed an early transient increase with positive lenses in both scleral layers, similar to previously reported finding in the chick retinal pigment epithelium after 48h lens wear, and consistent with a role for TGF-β2 as an inhibitory growth modulator. However, the transient nature of its up-regulation in sclera suggests additional growth modulatory influences on the latter. The scleral cartilage expression patterns for MMP-2 and MMP-13 were consistent with the opposite directions of growth induced by positive and negative lenses. TIMP-2 expression showed robust expression changes, mostly confined to the fibrous sclera. The suitability of

exploiting native scleral MMP activity to degrade biomaterials will depend on there being equivalent changes in MMP activity with long-term myopia.

These findings led to the exploration of biomimetic hydrogels comprising enzymatically-degradable semi-interpenetrating polymer networks (edsIPNs) to determine their biocompatibility and effects on the posterior wall of the chick eye, as a means of reinforcement. The edsIPNs comprised thermo-responsive poly(*N*-isopropylacrylamide-*co*-acrylic acid), customizable peptide crosslinkers cleavable by matrix metalloproteinases, and interpenetrating linear poly(acrylic acid)-*graft*-peptide chains to engage with cell-surface receptors. Rheological studies revealed an increase in stiffness at body temperature; the complex shear modulus $|G^*|$ was 14.13 ± 6.13 Pa at 22 ºC and 63.18 ± 12.24 Pa at 37 ºC, compatible with injection at room temperature. Primary chick scleral fibroblasts and chondrocytes cultured on edsIPN increased by 15.1 and 11.1 fold respectively over 11 days; both cell types exhibited delayed onset of exponential growth compared to cells plated on tissue-culture polystyrene. While edsIPN injections did not affect the rate of ocular elongation, the outer fibrous sclera showed significant thickening. The demonstration that this injectable biomimetic edsIPN stimulate scleral fibrous tissue growth represents proof-of-principle for a novel approach for scleral reinforcement, and a potential therapy for high myopia.

The muscarinic antagonist, atropine, was encapsulated within the edsIPNs and delivered to the posterior pole of the chick eye posterior pole to evaluate the effect of atropine release. Initial burst release *in vitro* showed approximately 47% of atropine to be released within the first 30 min, while 90% of atropine was released by 8h. Lens treated eyes were significantly longer than their fellows. There were significantly lower axial length interocular differences by 21 days for hydrogel-atropine compared to lens only treatment groups. Endpoint refractions (mean spherical equivalent) of treated eyes in each group were not significantly different from each other; although atropine treated eyes tended to have lower refractive error. This study demonstrated the feasibility of using a synthetic extracellular matrix to deliver atropine to the posterior sclera for myopia control and further supports the sclera as a potential site of action of atropine for myopia inhibition.

2. Discussion

The major findings of this dissertation support the ongoing development of bioinspired materials for the treatment of high axial myopia. Currently, there are no effective treatments for this condition. Optical appliances intended to correct near focusing errors have limited application (targeting low-to-moderate myopia), and the only drug currently being explored, atropine, is available only as topical ophthalmic drops, used on a daily basis, with a poorly understood mechanism of action and many ocular side effects. For high myopia, donor scleral tissue implants are currently the only option. With continued development, the biomaterial proposed and used in this dissertation work could potentially revolutionize the way myopia is managed, and drastically lower the economic and social costs of high myopia. The improved understanding of the complex interactions between polymer materials and the sclera has applications for retinal detachment surgery as well as myopia control, and would be a major contribution to the greater scientific and clinical communities.

The production of the complete dissertation work was not the sole effort of the author, but involved many members of the scientific and clinical communities coming together to solve a practical scientific problem: scleral weakening in highly myopic eyes. During this dissertation work, an interdisciplinary collaborative environment was strongly promoted and utilized with scientists, faculty researchers, and doctors contributing from various disciplines including bioengineering, materials science & engineering, and ophthalmology. This large interdisciplinary effort has also increased the awareness of myopia treatment options for the community at large, and serves as a model for approaching other clinical problems as well. On-going and further work derived from this dissertation work continues to utilize this interdisciplinary approach, with goals of enhancing the design of biomaterials specific for myopia treatment, and adding novel insights into scleral tissue engineering.

3. Future work

There are multiple paths to follow and potential materials that could be utilized in devising strategies for scleral reinforcement against high axial myopia progression. For success in this endeavor, one needs to be sufficiently flexible to allow for not only rigorous analytical work but also highly creative thought. Three strategies considered as high priority in the development of biomaterials for high axial myopia based on this dissertation work are:

1) The development of biomaterials for the slow release of atropine (and other pharmaceutical agents as discovered) for the inhibition of myopia progression. This strategy takes advantage of the known inhibitory action of atropine. Another benefit of this strategy is that the process of testing different delivery locations and drugs could help elucidate further the site of action for drugs known to inhibit myopia progression.

2) The development of biomaterials that can be injected at the sclera to attract host scleral cells to migrate into and remodel the biomimetic scaffold, while not losing the normal cellular phenotype and behavior within the scaffold environment. This strategy aims for effective integration of the scaffold with the native fibrous sclera by promoting native scleral cell migration, growth, and proliferation within the developed biomaterial. Such biomimetic scaffolds must degrade in a controlled manner over time to allow for tissue remodeling and integration. This process could effectively strengthen the eye wall by increasing scleral wall thickness, essentially reversing the scleral changes observed in highly myopic eyes.

3) The development of biomaterials to encapsulate an allogeneic or syngeneic population of cells (e.g. scleral fibroblasts or limbal stem cells) that can be injected to promote integration with the host sclera. This strategy would obviate the need to design a way to attract host scleral cells, but must be able to maintain the introduced cell population. The main benefit of this approach would be that less time may be required to remodel the scaffold into host-like tissue compared to the second strategy described in (2) above, although a potential disadvantage is that these cells, away

from their native environment, may not be able to maintain their normal phenotype. However, with creative design of the biomaterials, this problem should be avoidable.

There are, of course, other possible strategies to pursue for the reinforcement of the sclera, such as the use of collagen crosslinking treatments or mechanically reinforcing the sclera by using synthetic scleral bands. As typical in the world of research, the choice of strategy to pursue may change, depending on findings from newer studies. Nonetheless, the field of biomaterials as applied to regenerative medicine has grown so much that there is a great opportunity for the development of biomaterials that are responsive to the different environmental stimuli in the sclera arising from the ocular changes underlying myopia progression. In particular, the use of MMPs, both MMP-2 and MMP-13, incorporated into the design for biomaterials should be pursued in future work as both were modulated in the sclera during myopia progression. The findings from this dissertation work represent the initial proof of principle and feasibility that "smart" biomaterials have a potential role in the treatment of myopia.

Bibliography

1. Abramoff MD, Magelhaes PJ, Ram SJ, 2004. Image processing with Image-J. *Biophotonics Int* 11: 36-42.
2. Ashby R, McCarthy CS, Maleszka R, Megaw P, Morgan IG, 2007. A muscarinic cholinergic antagonist and a dopamine agonist rapidly increase ZENK mRNA expression in the form-deprived chicken retina. *Exp Eye Res* 85: 15-22.
3. Avetisov ES, Savitskaya NF, Vinetskaya MI, Iomdina EN, 1983. A study of biochemical and biomechanical qualities of normal and myopic eye sclera in humans of different age groups. *Metab Pediatr Syst Ophthalmol* 7: 183-8.
4. Avetisov ES, Tarutta EP, Iomdina EN, Vinetskaya MI, Andreyeva LD, 1997. Nonsurgical and surgical methods of sclera reinforcement in progressive myopia. *Acta Ophthalmol Scand* 75: 618-23.
5. Bailey AJ, Paul RG, Knott L, 1998. Mechanisms of maturation and ageing of collagen. *Mech Ageing Dev* 106: 1-56.
6. Barber TA, Harbers GM, Park S, Gilbert M, Healy KE, 2005. Ligand density characterization of peptide-modified biomaterials. *Biomaterials* 26: 6897-6905.
7. Barocas VH, Balachandran RK, 2008. Sustained transscleral drug delivery. *Expert Opin Drug Deliv* 5: 1-10.
8. Bartlett JD, Niemann K, Houde B, Allred T, Edmondson MJ, Crockett RS, 2003. A tolerability study of pirenzepine ophthalmic gel in myopic children. *J Ocul Pharmacol Ther* 19: 271-279.
9. Bartmann M, Schaeffel F, Hagel G, Zrenner E, 1994. Constant light affects retinal dopamine levels and blocks deprivation myopia but not lens-induced refractive errors in chickens. *Vis Neurosci* 11: 199-208.
10. Battaglioli JL, Kamm RD, 1984. Measurements of the compressive properties of scleral tissue. *Invest Ophthalmol Vis Sci* 25: 59-65.
11. Bedrossian RH, 1971. The effect of atropine on myopia. *Ann Ophthalmol* 3: 891-897.
12. Bedrossian RH, 1985. The treatment of myopia with atropine and bifocals: a long-term prospective study. *Ophthalmology* 92: 716.
13. Bellahcene A, Bonjean K, Fohr B, Fedarko NS, Robey FA, Young MF, Fisher LW, Castronovo V, 2000. Bone sialoprotein mediates human endothelial cell attachment and migration and promotes angiogenesis. *Circ Res* 86: 885-891.
14. Berne RM, Levy MN, 2001. *Cardiovascular Physiology*, 8th ed. Mosby. St. Louis, MO.
15. Bill A, 1985. Some aspects of the ocular circulation. Friedenwald lecture. *Invest Ophthalmol Vis Sci* 26: 410-424.
16. Bitzer M, Feldkaemper M, Schaeffel F, 2000. Visually induced changes in components of the retinoic acid system in fundal layers of the chick. *Exp Eye Res* 70: 97-106.
17. Bitzer M, Kovacs B, Feldkaemper M, Schaeffel F, 2006. Effects of muscarinic antagonists on ZENK expression in the chicken retina. *Exp Eye Res* 82: 379-388.
18. Borley WE, Snyder AA, 1958. Surgical treatment of high myopia; the combined lamellar scleral resection with scleral reinforcement using donor eye. *Trans Am Acad Ophthalmol Otolaryngol* 62: 791-801.
19. Buck C, Schaeffel F, Simon P, Feldkaemper M, 2004. Effects of positive and negative lens treatment on retinal and choroidal glucagon and glucagon receptor mRNA levels in the chicken. *Invest Ophthalmol Vis Sci* 45: 402-409.

20. Casanova M, Furlán C, Sterin-Borda L, Borda ES, 2006. Muscarinic cholinoceptor activation modulates DNA synthesis and CD40 expression in fibroblast cells. *Auton Autacoid Pharmacol* 26: 293-301.
21. Ceyhan T, Kartal M, Altun ML, Tülemis F, Cevheroglu S, 2001. LC determination of atropine sulfate and scopolamine hydrobromide in pharmaceuticals. *J Pharm Biomed Anal* 25: 399-406.
22. Chapman SA, Ayad S, O'Donoghue E, Bonshek RE, 1998. Glycoproteins of trabecular meshwork, cornea and sclera. *Eye* 12: 440-448.
23. Choh V, Lew MY, Nadel MW, Wildsoet CF, 2006. Effects of interchanging hyperopic defocus and form deprivation stimuli in normal and optic nerve-sectioned chicks. *Vision Res* 46: 1070-1079.
24. Chou SC, Yang CH, Lee CH, Yang CM, Ho TC, Huang JS, Lin CP, Chen MS, Shih YF, 2006. Characteristics of primary rhegmatogenous retinal detachment in Taiwan. *Eye* 21: 1056-1061.
25. Chua W-H, Balakrishnan V, Chan Y-H, Tong L, Ling Y, Quah B-L, Tan D, 2006. Atropine for the treatment of childhood myopia. *Ophthalmology* 113: 2285-2291.
26. Chung EH, Gilbert M, Virdi AS, Sena K, Sumner DR, Healy KE, 2006. Biomimetic artificial ECMs stimulate bone regeneration. *J Biomed Mater Res A* 79A: 815-826.
27. Colthurst MJ, Williams RL, Hiscott PS, Grierson I, 2000. Biomaterials used in the posterior segment of the eye. *Biomaterials* 21: 649-665.
28. Cottriall C, McBrien N, 1996. The M1 muscarinic antagonist pirenzepine reduces myopia and eye enlargement in the tree shrew. *Invest Ophthalmol Vis Sci* 37: 1368-1379.
29. Curtin B, 1985. *The Myopias. Basic Science and Clinical Management*, Harper & Row. Philadelphia.
30. Curtin BJ, Iwamoto T, Renaldo DP, 1979. Normal and staphylomatous sclera of high myopia: an electron microscopic study. *Arch Ophthalmol* 97: 912-5.
31. Curtin BJ, Whitmore WG, 1987. Long-term results of scleral reinforcement surgery. *Am J Ophthalmol* 103: 544-8.
32. D'Hermies F, Korobelnik J, Savoldelli M, Chauvaud D, Pouliquen Y, 1995. Miragel versus silastic used as episcleral implants in rabbits. An experimental histopathologic comparative study. *Retina* 15: 62-67.
33. D'Hermies F, Korobelnik J-F, Caputo G, Mashhour B, Chauvaud D, Pouliquen Y, Renard G, 1998. Encapsulation of scleral buckling materials: A study of sixty specimens. *Ophthalmology* 105: 1079-1086.
34. Davanger M, 1971. Descemetocele and the law of Laplace. *Acta Ophthalmol* 49: 715-718.
35. De Feo F, Bagnis A, Bricola G, Scotto R, Traverso CE, 2009. Efficacy and safety of a steel drainage device implanted under a scleral flap. *Can J Ophthalmol* 44: 457-462.
36. De Stefano M, Mugnaini E, 1997. Fine structure of the choroidal coat of the avian eye. Lymphatic vessels. *Invest Ophthalmol Vis Sci* 38: 1241-1260.
37. DeCroos FC, Ahmad S, Kondo Y, Chow J, Mordes D, Lee MR, Asrani S, Allingham RR, Olbrich KC, Klitzman B, 2009. Expanded polytetrafluoroethylene membrane alters tissue response to implanted Ahmed glaucoma valve. *Curr Eye Res* 34: 562-567.
38. Diether S, Schaeffel F, 1999. Long-term changes in retinal contrast sensitivity in chicks from frosted occluders and drugs: relations to myopia? *Vision Res* 39: 2499-2510.

39. Ding Q, Gladson CL, Wu H, Hayasaka H, Olman MA, 2008. FAK-related non-kinase inhibits myofibroblast differentiation through differential MAPK activation in a FAK-dependent manner. *J Biol Chem* 283: 26839-26849.
40. Dirani M, Chamberlain M, Shekar SN, Islam AFM, Garoufalis P, Chen CY, Guymer RH, Baird PN, 2006. Heritability of refractive error and ocular biometrics: the genes in myopia (GEM) twin study. *Invest Ophthalmol Vis Sci* 47: 4756-4761.
41. Eckes B, Zigrino P, Kessler D, Holtkotter O, Shephard P, Mauch C, Krieg T, 2000. Fibroblast-matrix interactions in wound healing and fibrosis. *Matrix Biol* 19: 325-332.
42. Edelhauser HF, Ubels JL, 2003. The cornea and the sclera, In: *Adler's physiology of the eye, Clinical applications*, (Eds.), St. Louis, Missouri, Mosby,
43. Engler AJ, Sen S, Sweeney HL, Discher DE, 2006. Matrix elasticity directs stem cell lineage specification. *Cell* 126: 677-689.
44. Fan DSP, Lam DSC, Chan CKM, Fan AH, Cheung EYY, Rao SK, 2007. Topical atropine in retarding myopic progression and axial length growth in children with moderate to severe myopia: a pilot study. *Jpn J Ophthalmol* 51: 27-33.
45. Feldkaemper MP, Schaeffel F, 2002. Evidence for a potential role of glucagon during eye growth regulation in chicks. *Vis Neurosci* 19: 755-766.
46. Fischer AJ, McKinnon LA, Nathanson NM, Stell WK, 1998a. Identification and localization of muscarinic acetylcholine receptors in the ocular tissues of the chick. *J Comp Neurol* 392: 273-284.
47. Fischer AJ, Miethke P, Morgan IG, Stell WK, 1998b. Cholinergic amacrine cells are not required for the progression and atropine-mediated suppression of form-deprivation myopia. *Brain Res* 794: 48-60.
48. Fischer AJ, Seltner RLP, Poon J, Stell WK, 1998c. Immunocytochemical characterization of quisqualic acid- and N-methyl-D-aspartate-induced excitotoxicity in the retina of chicks. *J Comp Neurol* 393: 1-15.
49. Fischer AJ, McGuire JJ, Schaeffel F, Stell WK, 1999a. Light and focus-dependent expression of the transcription factor ZENK in the chick retina. *Nat Neurosci* 2: 706-12.
50. Fischer AJ, Wallman J, Mertz JR, Stell WK, 1999b. Localization of retinoid binding proteins, retinoid receptors, and retinaldehyde dehydrogenase in the chick eye. *J Neurocytol* 28: 597-609.
51. Fitzgerald MEC, Wildsoet CF, Reiner A, 2002. Temporal relationship of choroidal blood flow and thickness changes during recovery from form deprivation myopia in chicks. *Exp Eye Res* 74: 561-570.
52. Friberg TR, Lace JW, 1988. A comparison of the elastic properties of human choroid and sclera. *Exp Eye Res* 47: 429-436.
53. Frick KD, Rein DB, 2007. Economic Impact of Vision Problems, Prevent Blindness America, Chicago, IL.
54. Friedman B, 1966. Stress upon the ocular coats: effects of scleral curvature, scleral thickness, and intraocular pressure. *Eye Ear Nose Throat Mon* 45: 59-66.
55. Geever LM, Cooney CC, Lyons JG, Kennedy JE, Nugent MJD, Devery S, Higginbotham CL, 2008. Characterisation and controlled drug release from novel drug-loaded hydrogels. *Eur J Pharm Biopharm* 69: 1147-1159.
56. Gerinec A, Slezakova G, 2001. Posterior scleroplasty in children with severe myopia. *Bratisl Lek Listy* 102: 73-8.

57. Ghosh K, Pan Z, Guan E, Ge S, Liu Y, Nakamura T, Ren X-D, Rafailovich M, Clark RAF, 2007. Cell adaptation to a physiologically relevant ECM mimic with different viscoelastic properties. *Biomaterials* 28: 671-679.
58. Gilmartin B, 2004. Myopia: precedents for research in the twenty-first century. *Clin Experiment Ophthalmol* 32: 305-324.
59. Girard MJ, Suh JK, Bottlang M, Burgoyne CF, Downs JC, 2009. Scleral biomechanics in the aging monkey eye. *Invest Ophthalmol Vis Sci* 50: 5226-37.
60. Gottlieb MD, Joshi HB, Nickla DL, 1990. Scleral changes in chicks with form-deprivation myopia. *Curr Eye Res* 9: 1157-65.
61. Goureau O, Amiot F, Dautry F, Courtois Y, 1997. Control of nitric oxide production by endogenous TNF-alpha in mouse retinal pigmented epithelial and Müller glial cells. *Biochem Biophys Res Commun* 240: 132-135.
62. Graham B, Judge SJ, 1999. The effects of spectacle wear in infancy on eye growth and refractive error in the marmoset (Callithrix jacchus). *Vision Res* 39: 189-206.
63. Gref R, Domb A, Quellec P, Blunk T, Muller RH, Verbavatz JM, Langer R, 1995. The controlled intravenous delivery of drugs using PEG-coated sterically stabilized nanospheres. *Adv Drug Delivery Rev* 16: 215-233.
64. Grotendorst GR, Duncan MR, 2005. Individual domains of connective tissue growth factor regulate fibroblast proliferation and myofibroblast differentiation. *FASEB* 19: 729-738.
65. Guggenheim J, McBrien N, 1996. Form-deprivation myopia induces activation of scleral matrix metalloproteinase-2 in tree shrew. *Invest Ophthalmol Vis Sci* 37: 1380-1395.
66. Guo SS, Sivak JG, Callender MG, Diehl-Jones B, 1995. Retinal dopamine and lens-induced refractive errors in chicks. *Curr Eye Res* 14: 385 - 389.
67. Hainfeld JF, Powell RD, 2000. New frontiers in gold labeling. *J Histochem Cytochem* 48: 471-480.
68. Harbers GM, Healy KE, 2005. The effect of ligand type and density on osteoblast adhesion, proliferation, and matrix mineralization. *J Biomed Mater Res A* 75A: 855-869.
69. Hardman JG, Limbird LE, Gilman AG, 2001. *Goodman & Gilman's The Pharmacological Basis of Therapeutics*, 10th ed. McGraw-Hill.
70. Hayes AJ, MacPherson S, Morrison H, Dowthwaite G, Archer CW, 2001. The development of articular cartilage: evidence for an appositional growth mechanism. *Anat Embryol* 203: 469-479.
71. Healy KE, Rezania A, Stile RA, 1999. Designing biomaterials to direct biological responses. *Ann N Y Acad Sci* 875: 24-35.
72. Ho P, Chan I, Refojo M, Tolentino F, 1984. The MAI hydrophilic implant for scleral buckling: a review. *Ophthalmic Surg* 15: 511-5.
73. Hornbeak DM, Young TL, 2009. Myopia genetics: a review of current research and emerging trends. *Curr Opin Ophthalmol* 20: 356-362.
74. Howlett MHC, McFadden SA, 2006. Form-deprivation myopia in the guinea pig (Cavia porcellus). *Vision Res* 46: 267-283.
75. Hsiong SX, Huebsch N, Fischbach C, Kong HJ, Mooney DJ, 2008. Integrin-adhesion ligand bond formation of preosteoblasts and stem cells in three-dimensional RGD presenting matrices. *Biomacromolecules* 9: 1843-51.
76. Hubbell J, 1995. Biomaterials in tissue engineering. *Biotechnology* 13: 565-76.

77. Huebsch N, Gilbert M, Healy KE, 2005. Analysis of sterilization protocols for peptide-modified hydrogels. *J Biomed Mater Res B Appl Biomater* 74B: 440-447.
78. Ihanamaki T, Pelliniemi LJ, Vuorio E, 2004. Collagens and collagen-related matrix components in the human and mouse eye. *Prog Retin Eye Res* 23: 403-434.
79. Irwin EF, Saha K, Rosenbluth M, Gamble LJ, Castner DG, Healy KE, 2008. Modulus-dependent macrophage adhesion and behavior. *J Biomater Sci Polym Ed* 19: 1363-1382.
80. Iuvone P, Tigges M, Stone R, Lambert S, Laties A, 1991. Effects of apomorphine, a dopamine receptor agonist, on ocular refraction and axial elongation in a primate model of myopia. *Invest Ophthalmol Vis Sci* 32: 1674-1677.
81. Iuvone PM, Tigges M, Fernandes A, Tigges J, 1989. Dopamine synthesis and metabolism in rhesus monkey retina: development, aging, and the effects of monocular visual deprivation. *Vis Neurosci* 2: 465-71.
82. Jacob JT, Gebhardt BM, Lewando J, 1996. Synthetic scleral reinforcement materials. II. Collagen types in the fibrous capsule. *J Biomed Mater Res* 32: 181-6.
83. Jacob JT, Lin JJ, Mikal SP, 1997. Synthetic scleral reinforcement materials. III. Changes in surface and bulk physical properties. *J Biomed Mater Res* 37: 525-533.
84. Jacob-LaBarre JT, Assouline M, Byrd T, McDonald M, 1994. Synthetic scleral reinforcement materias: I. Development and in vivo tissue biocompatibility response. *J Biomed Mater Res* 28: 699-712.
85. Jobling AI, Nguyen M, Gentle A, McBrien NA, 2004. Isoform-specific changes in scleral transforming growth factor-beta expression and the regulation of collagen synthesis during myopia progression. *J Biol Chem* 279: 18121-18126.
86. Jobling AI, Gentle A, Metlapally R, McGowan BJ, McBrien NA, 2009. Regulation of scleral cell contraction by transforming growth factor-beta and stress: competing roles in myopic eye growth. *J Biol Chem* 284: 2072-2079.
87. Jones BE, Thompson EW, Hodos W, Waldbillig R, Chader GJ, 1996. Scleral matrix metalloproteinases, serine proteinase activity and hydrational capacity are increased in myopia induced by retinal image degradation. *Exp Eye Res* 63: 369-381.
88. Kee C-S, Marzani D, Wallman J, 2001. Differences in time course and visual requirements of ocular responses to lenses and diffusers. *Invest Ophthalmol Vis Sci* 42: 575-583.
89. Kermis HR, Rao G, Barbari TA, 2003. Transport properties of pHEMA membranes for optical glucose affinity sensors. *J Memb Sci* 212: 75-86.
90. Kidane A, Szabocsik JM, Park K, 1998. Accelerated study on lysozyme deposition on poly(HEMA) contact lenses. *Biomaterials* 19: 2051-2055.
91. Kim S, Healy KE, 2003. Synthesis and characterization of injectable poly(*N*-isopropylacrylamide-*co*-acrylic acid) hydrogels with proteolytically degradable cross-links. *Biomacromolecules* 4: 1214-1223.
92. Kim S, Chung EH, Gilbert M, Healy KE, 2005. Synthetic MMP-13 degradable ECMs based on poly(*N*-isopropylacrylamide-*co*-acrylic acid) semi-interpenetrating polymer networks. I. Degradation and cell migration. *J Biomed Mater Res A* 75A: 73-88.
93. Klein AP, Duggal P, Lee KE, Klein R, Bailey-Wilson JE, Klein BEK, 2005. Support for polygenic influences on ocular refractive error. *Invest Ophthalmol Vis Sci* 46: 442-446.
94. Koh SW, Chader GJ, 1984. Elevation of intracellular cyclic AMP and stimulation of adenylate cyclase activity by vasoactive intestinal peptide and glucagon in the retinal pigment epithelium. *J Neurochem* 43: 1522-1526.

95. Kohane DS, Langer R, 2008. Polymeric biomaterials in tissue engineering. *Pediatr Res* 63: 487-491.
96. Kolodsick JE, Peters-Golden M, Larios J, Toews GB, Thannickal VJ, Moore BB, 2003. Prostaglandin E2 inhibits fibroblast to myofibroblast transition via E. prostanoid receptor 2 signaling and cyclic adenosine monophosphate elevation. *Am J Respir Cell Mol Biol* 29: 537-544.
97. Kusakari T, Sato T, Tokoro T, 1997. Regional scleral changes in form-deprivation myopia in chicks. *Exp Eye Res* 64: 465-476.
98. Kusakari T, Sato T, Tokoro T, 2001. Visual deprivation stimulates the exchange of the fibrous sclera into the cartilaginous sclera in chicks. *Exp Eye Res* 73: 533-546.
99. Kutty JK, Cho E, Soo Lee J, Vyavahare NR, Webb K, 2007. The effect of hyaluronic acid incorporation on fibroblast spreading and proliferation within PEG-diacrylate based semi-interpenetrating networks. *Biomaterials* 28: 4928-4938.
100. Lee J-J, Fang P-C, Yang IH, Chen C-H, Lin P-W, Lin S-A, Kuo H-K, Wu P-C, 2006. Prevention of myopia progression with 0.05% atropine solution. *J Ocul Pharmacol Ther* 22: 41-46.
101. Li J, Gallemore R, Dmitriev A, Steinberg R, 1994. Light-dependent hydration of the space surrounding photoreceptors in chick retina. *Invest Ophthalmol Vis Sci* 35: 2700-2711.
102. Li XX, Schaeffel F, Kohler K, Zrenner E, 1992. Dose-dependent effects of 6-hydroxy dopamine on deprivation myopia, eletroretinograms, and dopaminergic amacrine cells in chickens. *Vis Neurosci* 9: 483-492.
103. Li YJ, Chung EH, Rodriguez RT, Firpo MT, Healy KE, 2006. Hydrogels as artificial matrices for human embryonic stem cell self-renewal. *J Biomed Mater Res A* 79A: 1-5.
104. Liang H, Crewther SG, Crewther DP, Junghans BM, 2004. Structural and elemental evidence for edema in the retina, retinal pigment epithelium, and choroid during recovery from experimentally induced myopia. *Invest Ophthalmol Vis Sci* 45: 2463-2474.
105. Lin L, Shih Y, Tsai C, Chen C, Lee L, Hung P, Hou P, 1999. Epidemiologic study of ocular refraction among schoolchildren in Taiwan in 1995. *Optom Vis Sci* 76: 275-81.
106. Lin T, Grimes PA, Stone RA, 1993. Expansion of the retinal pigment epithelium in experimental myopia. *Vision Res* 33: 1881-1885.
107. Lind GJ, Chew SJ, Marzani D, Wallman J, 1998. Muscarinic acetylcholine receptor antagonists inhibit chick scleral chondrocytes. *Invest Ophthalmol Vis Sci* 39: 2217-2231.
108. Liu Q, Wu J, Wang X, Zeng J, 2007. Changes in muscarinic acetylcholine receptor expression in form deprivation myopia in guinea pigs. *Mol Vis* 13: 1234-44.
109. Liu S-J, Kau Y-C, Liaw C-W, Peng Y-J, 2009. In vitro elution of vancomycin/amikacin/steroid from solvent-free biodegradable scleral plugs. *Int J Pharm* 370: 75-80.
110. Lloyd AW, Faragher RGA, Denyer SP, 2001. Ocular biomaterials and implants. *Biomaterials* 22: 769-785.
111. Lodish H, Berk A, Zipursky SL, Matsudaira P, Baltimore D, Darnell JE, 2000. *Molecular Cell Biology*, 4th ed. W. H. Freeman and Company. New York, NY.
112. Luft WA, Ming Y, Stell WK, 2003. Variable effects of previously untested muscarinic receptor antagonists on experimental myopia. *Invest Ophthalmol Vis Sci* 44: 1330-1338.
113. Marshall GE, 1995. Human scleral elastic system: an immunoelectron microscopic study. *Br J Ophthalmol* 79: 57-64.

114. Marzani D, Wallman J, 1997. Growth of the two layers of the chick sclera is modulated reciprocally by visual conditions. *Invest Ophthalmol Vis Sci* 38: 1726-1739.
115. Mathis U, Schaeffel F, 2007. Glucagon-related peptides in the mouse retina and the effects of deprivation of form vision. *Graefes Arch Clin Exp Ophthalmol* 245: 267-275.
116. McBrien NA, Moghaddam HO, Reeder AP, 1993. Atropine reduces experimental myopia and eye enlargement via a nonaccommodative mechanism. *Invest Ophthalmol Vis Sci* 34: 205-215.
117. McBrien NA, Norton TT, 1994. Prevention of collagen crosslinking increases form-deprivation myopia in tree shrew. *Exp Eye Res* 59: 475-486.
118. McBrien NA, Lawlor P, Gentle A, 2000. Scleral remodeling during the development of and recovery from axial myopia in the tree shrew. *Invest Ophthalmol Vis Sci* 41: 3713-3719.
119. McBrien NA, Cornell LM, Gentle A, 2001a. Structural and ultrastructural changes to the sclera in a mammalian model of high myopia. *Invest Ophthalmol Vis Sci* 42: 2179-2187.
120. McBrien NA, Cottriall CL, Annies R, 2001b. Retinal acetylcholine content in normal and myopic eyes: a role in ocular growth control? *Vis Neurosci* 18: 571-580.
121. McBrien NA, Gentle A, 2003. Role of the sclera in the development and pathological complications of myopia. *Prog Retin Eye Res* 22: 307-338.
122. McBrien NA, Jobling AI, Gentle A, 2009a. Biomechanics of the sclera in myopia: extracellular and cellular factors. *Optom Vis Sci* 86: E23-30.
123. McBrien NA, Jobling AI, Truong HT, Cottriall CL, Gentle A, 2009b. Expression of muscarinic receptor subtypes in tree shrew ocular tissues and their regulation during the development of myopia. *Mol Vis* 15: 464-75.
124. McCarty CA, Taylor HR, 2000. Myopia and vision 2020. *Am J Ophthalmol* 129: 525-527.
125. McFadden SA, Howlett MHC, Mertz JR, 2004. Retinoic acid signals the direction of ocular elongation in the guinea pig eye. *Vision Res* 44: 643-653.
126. Merrett K, Griffith CM, Deslandes Y, Pleizier G, Sheardown H, 2001. Adhesion of corneal epithelial cells to cell adhesion peptide modified pHEMA surfaces. *J Biomater Sci Polym Ed* 12: 647-671.
127. Mertz JR, Wallman J, 2000. Choroidal retinoic acid synthesis: a possible mediator between refractive error and compensatory eye growth. *Exp Eye Res* 70: 519-527.
128. Metlapally R, Jobling AI, Gentle A, McBrien NA, 2006. Characterization of the integrin receptor subunit profile in the mammalian sclera. *Mol Vis* 6: 725-34.
129. Morgan I, Rose K, 2005. How genetic is school myopia? *Prog Retin Eye Res* 24: 1-38.
130. Morgan IG, 2003. The biological basis of myopic refractive error. *Clin Exp Optom* 86: 276-288.
131. Moring AG, Baker JR, Norton TT, 2007. Modulation of glycosaminoglycan levels in tree shrew sclera during lens-induced myopia development and recovery. *Invest Ophthalmol Vis Sci* 48: 2947-2956.
132. Mutti D, Zadnik K, Adams A, 1996. Myopia. The nature versus nurture debate goes on. *Invest Ophthalmol Vis Sci* 37: 952-957.
133. Nakagawa S, Pawelek P, Grinnell F, 1989. Extracellular matrix organization modulates fibroblast growth and growth factor responsiveness. *Exp Cell Res* 182: 572-82.

134. Nickla D, Rada J, Wallman J, 1999a. Isolated chick sclera shows a circadian rhythm in proteoglycan synthesis perhaps associated with the rhythm in ocular elongation. *J Comp Physiol A* 185: 81-90.
135. Nickla DL, Wildsoet C, Wallman J, 1998. Visual influences on diurnal rhythms in ocular length and choroidal thickness in chick eyes. *Exp Eye Res* 66: 163-181.
136. Nickla DL, Wildsoet CF, Troilo D, 1999b. Nitric oxide may mediate the compensatory choroidal expansion seen in response to experimentally-induced myopia in chicks. *Invest Ophthalmol Vis Sci* 40: S451.
137. Nickla DL, Wildsoet CF, 2004. The effect of the nonspecific nitric oxide synthase inhibitor N^G-nitro-L-arginine methyl ester on the choroidal compensatory response to myopic defocus in chickens. *Optom Vis Sci* 81: 111-118.
138. Nickla DL, Damyanova P, Lytle G, 2009. Inhibiting the neuronal isoform of nitric oxide synthase has similar effects on the compensatory choroidal and axial responses to myopic defocus in chicks as does the non-specific inhibitor l-NAME. *Exp Eye Res* 88: 1092-1099.
139. Norman RE, Flanagan JG, Rausch SMK, Sigal IA, Tertinegg I, Eilaghi A, Portnoy S, Sled JG, Ethier CR, 2009. Dimensions of the human sclera: Thickness measurement and regional changes with axial length. *Exp Eye Res* Ahead of print. doi: 10.1016/j.exer.2009.11.001.
140. Norton, 1999. Animal models of myopia: learning how vision controls the size of the eye. *ILAR J* 40: 59-77.
141. Norton TT, Rada JA, 1995. Reduced extracellular matrix in mammalian sclera with induced myopia. *Vision Res* 35: 1271-1281.
142. Okano T, Bae YH, Jacobs H, Kim SW, 1990. Thermally on-off switching polymers for drug permeation and release. *J Control Release* 11: 255-265.
143. Olsen TW, Aaberg SY, Geroski DH, Edelhauser HF, 1998. Human sclera: thickness and surface area. *Am J Ophthalmol* 125: 237-41.
144. Overall CM, Wrana JL, Sodek J, 1989. Independent regulation of collagenase, 72-kDa progelatinase, and metalloendoproteinase inhibitor expression in human fibroblasts by transforming growth factor-beta. *J Biol Chem* 264: 1860-1869.
145. Paik DC, Wen Q, Airiani S, Braunstein RE, Trokel SL, 2008. Aliphatic beta-nitro alcohols for non-enzymatic collagen cross-linking of scleral tissue. *Exp Eye Res* 87: 279-285.
146. Park D, Congdon N, 2004. Evidence for an "epidemic" of myopia. *Ann Acad Med Singapore* 33: 21-26.
147. Park S, Healy KE, 2003. Nanoparticulate DNA packaging using terpolymers of poly(lysine-g-(lactide-b-ethylene glycol)). *Bioconjugate Chem* 14: 311-319.
148. Park S, Healy KE, 2004. Compositional regulation of poly(lysine-g-(lactide-*b*-ethylene glycol))-DNA complexation and stability. *J Control Release* 95: 639-651.
149. Park TG, 1999. Temperature modulated protein release from pH/temperature-sensitive hydrogels. *Biomaterials* 20: 517-521.
150. Parver LM, Auker C, Carpenter DO, 1980. Choroidal blood flow as a heat dissipating mechanism in the macula. *Am J Ophthalmol* 89: 641-646.
151. Peppas NA, Langer R, 1994. New challenges in biomaterials. *Science* 263: 1715-1720.
152. Peppas NA, Bures P, Leobandung W, Ichikawa H, 2000. Hydrogels in pharmaceutical formulations. *Eur J Pharm Biopharm* 50: 27-46.

153. Phillips JR, McBrien NA, 1995. Form deprivation myopia: elastic properties of sclera. *Ophthal Physiol Opt* 15: 357-362.
154. Phillips JR, Khalaj M, McBrien NA, 2000. Induced myopia associated with increased scleral creep in chick and tree shrew eyes. *Invest Ophthalmol Vis Sci* 41: 2028-2034.
155. Phillips JR, McBrien NA, 2004. Pressure-induced changes in axial eye length of chick and tree shrew: significance of myofibroblasts in the sclera. *Invest Ophthalmol Vis Sci* 45: 758-763.
156. Pijls RT, Cruysberg LPJ, Nuijts RMMA, Dias AA, Koole LH, 2007. Capacity and tolerance of a new device for ocular drug delivery. *Int J Pharm* 341: 152-161.
157. Poukens V, Glasgow BJ, Demer JL, 1998. Nonvascular contractile cells in sclera and choroid of humans and monkeys. *Invest Ophthalmol Vis Sci* 39: 1765-1774.
158. Qiu Y, Park K, 2001. Environment-sensitive hydrogels for drug delivery. *Adv Drug Deliv Rev* 53: 321-339.
159. Qu J, Zhou X, Xie R, Zhang L, Hu D, Li H, Lu F, 2006. The presence of m1 to m5 receptors in human sclera: evidence of the sclera as a potential site of action for muscarinic receptor antagonists. *Curr Eye Res* 31: 587 - 597.
160. Rada J, Brenza H, 1995. Increased latent gelatinase activity in the sclera of visually deprived chicks. *Invest Ophthalmol Vis Sci* 36: 1555-1565.
161. Rada JA, Matthews AL, Brenza H, 1994. Regional proteoglycan synthesis in the sclera of experimentally myopic chicks. *Exp Eye Res* 59: 747-760.
162. Rada JA, Achen VR, Rada KG, 1998. Proteoglycan turnover in the sclera of normal and experimentally myopic chick eyes. *Invest Ophthalmol Vis Sci* 39: 1990-2002.
163. Rada JA, Perry CA, Slover ML, Achen VR, 1999. Gelatinase A and TIMP-2 expression in the fibrous sclera of myopic and recovering chick eyes. *Invest Ophthalmol Vis Sci* 40: 3091-3099.
164. Rada JA, Nickla DL, Troilo D, 2000. Decreased proteoglycan synthesis associated with form deprivation myopia in mature primate eyes. *Invest Ophthalmol Vis Sci* 41: 2050-2058.
165. Rasmussen R, Meuer S, Wittwer C, Nakagawara K, 2001. *Quantification on the lightcycler. Rapid Cycle Real-Time PCR, Methods and Applications*, Springer Press. Heidelberg.
166. Rezania A, Healy KE, 1999. Integrin subunits responsible for adhesion of human osteoblast-like cells to biomimetic peptide surfaces. *J Orthop Res* 17: 615-623.
167. Rezania A, Healy KE, 2000. The effect of peptide surface density on mineralization of a matrix deposited by osteogenic cells. *J Biomed Mater Res* 52: 595-600.
168. Rohrer B, Spira AW, Stell WK, 1993. Apomorphine blocks form-deprivation myopia in chickens by a dopamine D2-receptor mechanism acting in retina or pigmented epithelium. *Vis Neurosci* 10: 447-453.
169. Rosenfield M, Gilmartin B, 1998. *Myopia & Nearwork*, Butterworth-Heinemann. Boston, Massachusetts.
170. Rozen S, Skaletsky HJ, 2000. Primer3 on the WWW for general users and for biologist programmers, In: *Bioinformatics Methods and Protocols: Methods in Molecular Biology*, Krawetz, S., Misener, S. (Eds.), Totowa, NJ, Humana Press, 365-386.
171. Rymer J, Wildsoet CF, 2005. The role of the retinal pigment epithelium in eye growth regulation and myopia: A review. *Vis Neurosci* 22: 251-261.

172. Saha K, Keung AJ, Irwin EF, Li Y, Little L, Schaffer DV, Healy KE, 2008. Substrate modulus directs neural stem cell behavior. *Biophys J* 95: 4426-4438.
173. Sall JW, Klisovic DD, O'Dorisio MS, Katz SE, 2004. Somatostatin inhibits IGF-1 mediated induction of VEGF in human retinal pigment epithelial cells. *Exp Eye Res* 79: 465-476.
174. Sampson WG, 1979. Role of cycloplegia in the management of functional myopia. *Ophthalmology* 86: 695-697.
175. Saw S, 2003. A synopsis of the prevalence rates and environmental risk factors for myopia. *Clin Exp Optom* 86: 289-94.
176. Saw S-M, Katz J, Schein OD, Chew S-J, Chan T-K, 1996. Epidemiology of Myopia. *Epidemiol Rev* 18: 175-187.
177. Saw S-M, Gazzard G, Shih-Yen EC, Chua W-H, 2005. Myopia and associated pathological complications. *Ophthalmic Physiol Opt* 25: 381-391.
178. Schaeffel F, Hagel G, Bartmann M, Kohler K, Zrenner E, 1994. 6-Hydroxy dopamine does not affect lens-induced refractive errors but suppresses deprivation myopia. *Vision Res* 34: 143-149.
179. Schaeffel F, Bartmann M, Hagel G, Zrenner E, 1995. Studies on the role of the retinal dopamine/melatonin system in experimental refractive errors in chickens. *Vision Res* 35: 1247-1264.
180. Schepens CL, Acosta F, 1991. Scleral implants: an historical perspective. *Surv Ophthalmol* 35: 447-453.
181. Schippert R, Brand C, Schaeffel F, Feldkaemper MP, 2006. Changes in scleral MMP-2, TIMP-2 and TGFβ-2 mRNA expression after imposed myopic and hyperopic defocus in chickens. *Exp Eye Res* 82: 710-719.
182. Schippert R, Burkhardt E, Feldkaemper M, Schaeffel F, 2007. Relative axial myopia in Egr-1 (ZENK) knockout mice. *Invest Ophthalmol Vis Sci* 48: 11-17.
183. Schmid GF, Papastergiou GI, Nickla DL, Riva CE, Lin T, Stone RA, Laties AM, 1996. Validation of laser Doppler interferometric measurements in vivo of axial eye length and thickness of fundus layers in chicks. *Curr Eye Res* 15: 691-6.
184. Schmid K, Wildsoet C, 2004. Inhibitory effects of apomorphine and atropine and their combination on myopia in chicks. *Optom Vis Sci* 81: 137-147.
185. Schrödl F, 2009. Intrinsic choroidal neurons, In: *Neuropeptides in the Eye*, Troger, J., Kieselbach, G. (Eds.), Kerala, India, Research Signpost, 169-197.
186. Schwahn HN, Kaymak H, Schaeffel F, 2000. Effects of atropine on refractive development, dopamine release, and slow retinal potentials in the chick. *Vis Neurosci* 17: 165-76.
187. Seko Y, Tanaka Y, Tokoro T, 1997. Apomorphine inhibits the growth-stimulating effect of retinal pigment epithelium on scleral cells *in vitro*. *Cell Biochem Funct* 15: 191-196.
188. Shaikh AW, Siegwart Jr JT, Norton TT, 1999. Effect of interrupted lens wear on compensation for a minus lens in tree shrews. *Optom Vis Sci* 76: 308-315.
189. Shelton L, Rada JS, 2007. Effects of cyclic mechanical stretch on extracellular matrix synthesis by human scleral fibroblasts. *Exp Eye Res* 84: 314-322.
190. Shieh AC, Athanasiou KA, 2003. Principles of cell mechanics for cartilage tissue engineering. *Ann Biomed Eng* 31: 1-11.

191. Shih Y-F, Hsiao CK, Chen C-J, Chang C-W, Hung PT, Lin LLK, 2001. An intervention trial on efficacy of atropine and multi-focal glasses in controlling myopic progression. *Acta Ophthalmol Scand* 79: 233-236.
192. Short BG, 2008. Safety evaluation of ocular drug delivery formulations: techniques and practical considerations. *Toxicol Pathol* 36: 49-62.
193. Siatkowski RM, Cotter SA, Crockett RS, Miller JM, Novack GD, Zadnik K, 2008. Two-year multicenter, randomized, double-masked, placebo-controlled, parallel safety and efficacy study of 2% pirenzepine ophthalmic gel in children with myopia. *J AAPOS* 12: 332-339.
194. Siegwart Jr JT, Strang CE, 2007. Selective modulation of scleral proteoglycan mRNA levels during minus lens compensation and recovery. *Mol Vis* 13: 1878-1886.
195. Siegwart JT, Norton TT, 1999. Regulation of the mechanical properties of tree shrew sclera by the visual environment. *Vision Res* 39: 387-407.
196. Siegwart JT, Jr., Norton TT, 2002. The time course of changes in mRNA levels in tree shrew sclera during induced myopia and recovery. *Invest Ophthalmol Vis Sci* 43: 2067-2075.
197. Siegwart JT, Jr., Norton TT, 2005. Selective regulation of MMP and TIMP mRNA levels in tree shrew sclera during minus lens compensation and recovery. *Invest Ophthalmol Vis Sci* 46: 3484-3492.
198. Simon P, 2003. Q-Gene: processing quantitative real-time RT-PCR data. *Bioinformatics* 19: 1439-1440.
199. Simon P, Feldkaemper M, Bitzer M, Ohngemach S, Schaeffel F, 2004. Early transcriptional changes of retinal and choroidal TGFβ-2, RALDH-2, and ZENK following imposed positive and negative defocus in chickens. *Mol Vis* 10: 588-597.
200. Sivak JG, Barrie DL, Callender MG, Doughty MJ, Seltner RL, West JA, 1990. Optical causes of experimental myopia. *Ciba Found Symp* 155: 160-177.
201. Smith EL, Bradley DV, Fernandes A, Boothe RG, 1999. Form deprivation myopia in adolescent monkeys. *Optom Vis Sci* 76: 428-32.
202. Somerman MJ, Fisher LW, Foster RA, Sauk JJ, 1988. Human bone sialoprotein I and II enhance fibroblast attachment in vitro. *Calcif Tissue Int* 43: 50-53.
203. Song J, Saiz E, Bertozzi CR, 2003. A new approach to mineralization of biocompatible hydrogel scaffolds: an efficient process toward 3-dimensional bonelike composites. *J Am Chem Soc* 125: 1236-1243.
204. Song J, Malathong V, Bertozzi CR, 2005. Mineralization of synthetic polymer scaffolds: a bottom-up approach for the development of artificial bone. *J Am Chem Soc* 127: 3366-3372.
205. Stile RA, Burghardt WR, Healy KE, 1999. Synthesis and characterization of injectable poly(*N*-isopropylacrylamide)-based hydrogels that support tissue formation in vitro. *Macromolecules* 32: 7370-7379.
206. Stile RA, Chung E, Burghardt WR, Healy KE, 2004. Poly(*N*-isopropylacrylamide)-based semi-interpenetrating polymer networks for tissue engineering applications. Effects of linear poly(acrylic acid) chains on rheology. *J Biomater Sci Polym Ed* 15: 865-878.
207. Stone RA, Lin T, Laties AM, Iuvone PM, 1989. Retinal dopamine and form-deprivation myopia. *Proc Natl Acad Sci* 86: 704-706.
208. Strauss O, 2005. The retinal pigment epithelium in visual function. *Physiol Rev* 85: 845-881.

209. Su J, Iomdina E, Tarutta E, Ward B, Song J, Wildsoet CF, 2009a. Effects of poly(2-hydroxyethyl methacrylate) and poly(vinyl-pyrrolidone) hydrogel implants on myopic and normal chick sclera. *Exp Eye Res* 88: 445-457.
210. Su J, Wall ST, Healy KE, Wildsoet CF, 2009b. Scleral reinforcement through host tissue integration with biomimetic enzymatically-degradable semi-interpenetrating polymer network. *Tissue Engineering Part A* Ahead of print. doi:10.1089/ ten.TEA.2009.0488.
211. Tamm E, Koch T, Mayer B, Stefani F, Lutjen-Drecoll E, 1995. Innervation of myofibroblast-like scleral spur cells in human monkey eyes. *Invest Ophthalmol Vis Sci* 36: 1633-1644.
212. Tano Y, 2002. Pathologic myopia: where are we now? *Am J Ophthalmol* 134: 645-660.
213. Tarutta EP, Iomdina EN, Shamkhalova ES, Andreeva LD, Maksimova MV, 1992. Scleral fortification in children at high risk of progressive myopia. *Vestn Oftalmol* 108: 14-7.
214. Tarutta EP, Andreeva LD, Markosian GA, Iomdina EN, Lazuk AV, Kruzhkova GV, 1999. Reinforcement of the sclera with new types of synthetic materials in progressive myopia. *Vestn Oftalmol* 115: 8-10.
215. Thieme H, 2003. *Classic models of density-dependent population growth for single species. Mathematics in population biology*, Princeton University Press. Princeton, NJ.
216. Thompson FB, 1978. A simplified scleral reinforcement technique. *Am J Ophthalmol* 86: 782-90.
217. Tobío M, Gref R, Sánchez A, Langer R, Alonso MJ, 1998. Stealth PLA-PEG nanoparticles as protein carriers for nasal administration. *Pharm Res* 15: 270-275.
218. Tong L, Huang XL, Koh ALT, Zhang X, Tan DTH, Chua W-H, 2009. Atropine for the treatment of childhood myopia: effect on myopia progression after cessation of atropine. *Ophthalmology* 116: 572-579.
219. Törnquist P, Alm A, Bill A, 1990. Permeability of ocular vessels and transport across the blood-retinal-barrier. *Eye* 4: 303-309.
220. Tortora GJ, Grabowski SR, 1992. *Principles of Anatomy and Physiology*, 7th ed. HarperCollins College Publishers. New York.
221. Trier K, Olsen EB, Kobayashi T, Ribel-Madsen SM, 1999. Biochemical and ultrastructural changes in rabbit sclera after treatment with 7-methylxanthine, theobromine, acetazolamide, or L-ornithine. *Br J Ophthalmol* 83: 1370-1375.
222. Trier K, 2005. The Sclera, In: *Advances in Organ Biology*, Fischbarg, J. (Eds.), Elsevier, 353-373.
223. Troilo D, Gottlieb MD, Wallman J, 1987. Visual deprivation causes myopia in chicks with optic nerve section. *Curr Eye Res* 6: 993-9.
224. Urata Y, Nishimura Y, Hirase T, Yokoyama M, 2005. Sphingosine 1-phosphate induces alpha-smooth muscle actin expression in lung fibroblasts via Rho-kinase. *Kobe J Med Sci* 51: 17-27.
225. Vacanti FX, 2004. PHEMA as a fibrous capsule-resistant breast prosthesis. *Plast Reconstr Surg* 113: 949-952.
226. Vandesompele J, De Preter K, Pattyn F, Poppe B, Van Roy N, De Paepe A, Speleman F, 2002. Accurate normalization of real-time quantitative RT-PCR data by geometric averaging of multiple internal control genes. *Genome Biol* 3: research0034.1-0034.11.
227. Vernon B, Sung Wan K, You Han B, 1999. Insulin release from islets of Langerhans entrapped in a poly(N-isopropylacrylamide-co-acrylic acid) polymer gel. *J Biomater Sci Polymer Edn* 10: 183-198.

228. Vessey KA, Lencses KA, Rushforth DA, Hruby VJ, Stell WK, 2005. Glucagon receptor agonists and antagonists affect the growth of the chick eye: a role for glucagonergic regulation of emmetropization? *Invest Ophthalmol Vis Sci* 46: 3922-3931.
229. Waldbillig RJ, Schoen TJ, Chader GJ, Pfeffer BA, 1992. Monkey retinal pigment epithelial cells in vitro synthesize, secrete, and degrade insulin-like growth factor binding proteins. *J Cell Physiol* 150: 76-83.
230. Wall S, 2008. Bioactive polymers for cardiac tissue engineering. Bioengineering, University of California - Berkeley and the University of California - San Francisco; Ph.D. Dissertation; Berkeley, CA.
231. Wall ST, Yeh C-C, Tu RYK, Mann MJ, Healy KE, 2009. Biomimetic matrices for myocardial stabilization and stem cell transplantation. *J Biomed Mater Res A* Manuscript accepted for publication.
232. Wallman J, 1993. Retinal control of eye growth and refraction, In: *Progress in Retinal Research*, Osborne, N. N., Chader, G. J. (Eds.), New York, Pergamon Press, 133-153.
233. Wallman J, 1994. Nature and nurture of myopia. *Nature* 371: 201-202.
234. Wallman J, Wildsoet C, Xu A, Gottlieb MD, Nickla DL, Marran L, Krebs W, Christensen AM, 1995. Moving the retina: choroidal modulation of refractive state. *Vision Res* 35: 37-50.
235. Ward B, Tarutta EP, Mayer MJ, 2009. The efficacy and safety of posterior pole buckles in the control of progressive high myopia. *Eye* Ahead of print. doi: 10.1038/eye.2008.433.
236. Watson PG, Young RD, 2004. Scleral structure, organisation and disease. A review. *Exp Eye Res* 78: 609-623.
237. Wildsoet C, Wallman J, 1995. Choroidal and scleral mechanisms of compensation for spectacle lenses in chicks. *Vision Res* 35: 1175-1194.
238. Wildsoet C, 2003. Neural pathways subserving negative lens-induced emmetropization in chicks- insights from selective lesions of the optic nerve and ciliary nerve. *Curr Eye Res* 27: 371-85.
239. Wildsoet CF, Pettigrew JD, 1988. Experimental myopia and anomalous eye growth patterns unaffected by optic nerve section in chickens: evidence for local control of eye growth. *Clin Vision Sci* 3: 99-107.
240. Wildsoet CF, 1997. Active emmetropization - evidence for its existence and ramifications for clinical practice. *Ophthalmic Physiol Opt* 17: 279-290.
241. Wollensak G, Spoerl E, 2004. Collagen crosslinking of human and porcine sclera. *J Cataract Refract Surg* 30: 689-695.
242. Wollensak G, Iomdina E, Dittert D-D, Salamatina O, Stoltenburg G, 2005. Cross-linking of scleral collagen in the rabbit using riboflavin and UVA. *Acta Ophthalmol Scand* 83: 477-482.
243. Yamamoto Y, Yasugi K, Harada A, Nagasaki Y, Kataoka K, 2002. Temperature-related change in the properties relevant to drug delivery of poly(ethylene glycol)-poly(-lactide) block copolymer micelles in aqueous milieu. *J Control Release* 82: 359-371.
244. Yamaoka A, Matsuo T, Shiraga F, Ohtsuki H, 2001. TIMP-1 production by human scleral fibroblast decreases in response to cyclic mechanical stretching. *Ophthalmic Res* 33: 98-101.
245. Yasuda H, 2006. Biocompatibility of nanofilm-encapsulated silicone and silicone-hydrogel contact lenses. *Macromol Biosci* 6: 121-138.

246. Yasukawa T, Kimura H, Tabata Y, Ogura Y, 2001. Biodegradable scleral plugs for vitreoretinal drug delivery. *Adv Drug Deliv Rev* 52: 25-36.
247. Yew K-L, 2004. Is lens-induced myopia another type of form-deprivation myopia? Evidence from chicks using optical, lighting, and surgical manipulations. Vision Science, School of Optometry, University of California, Berkeley; M.S. Thesis; Berkeley, CA.
248. Zhan Z, Geller S, Su J, Flannery J, Wildsoet C, 2008. Effects of imposed defocus on th expression of IGF1R, SSTR2, TGF-b2 and TGF-bR1 genes in chick RPE and implications for ocular growth regulation. *Molecular Vision, in submission.*
249. Zhang Y, Maminishkis A, Zhi C, Li R, Agarwal R, Miller SS, Wildsoet CF, 2009. Apomorphine regulates TGF-beta1 and TGF-beta2 expression in human fetal retinal pigment epithelial cells. *Invest Ophthalmol Vis Sci* 50: E-Abstract 3845.
250. Zhang ZM, Song ZM, Shen LM, Qu JM, 2008. A new scleral plug with shouldered-stop for use during vitrectomy. *Retina* 28: 908-909.
251. Zhu X, Park TW, Winawer J, Wallman J, 2005. In a matter of minutes, the eye can know which way to grow. *Invest Ophthalmol Vis Sci* 46: 2238-2241.